AD-A181 512 CLOSING DEVELOPMENTS IN AERODYNAMIC SIMULATION WITH DISJOINT PATCHED MESHES(U) PEDA CORP PALO ALTO CA C K LOMBARD ET AL. 28 NOV 86 AFOSR-TR-87-0702 1/1

UNCLASSIFIED F49620-85-C-0081 F/G 20/4 NL

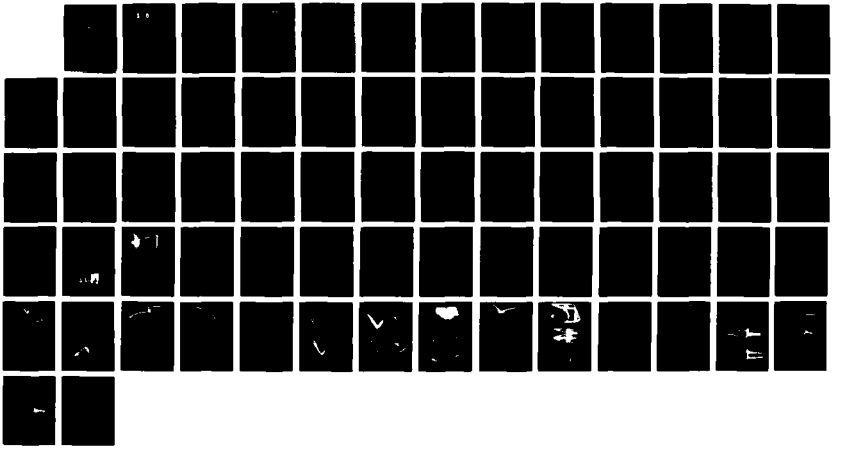

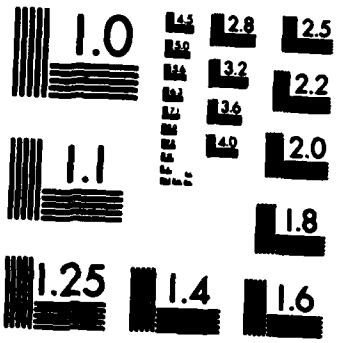

UNCLASSIFIED

DTIC FILE COPY (2)

AD-A181 512

DTIC ELECTE JUN 11 1987 D

REPORT DOCUMENTATION PAGE

UNCLASSIFIED	1b. RESTRICTIVE MARKINGS
2a. SECURITY CLASSIFICATION AUTHORITY	3. DISTRIBUTION/AVAILABILITY OF REPORT: Approved for public release; distribution unlimited.
2b. DECLASSIFICATION/DOWNGRADING SCHEDULE	
4. PERFORMING ORGANIZATION REPORT NUMBER(S)	5. MONITORING ORGANIZATION REPORT NUMBER(S): AFOSR-TR- 87-0782
6a. NAME OF PERFORMING ORGANIZATION: PEDA Corporation	6b. OFFICE SYMBOL (If applicable):
7a. NAME OF MONITORING ORGANIZATION: Air Force Office of Scientific Research	
6c. ADDRESS (City, State and ZIP Code): 4151 Middlefield Road, Suite 7, Palo Alto, CA 94303	7b. ADDRESS (City, State and ZIP Code): BLG 410 Directorate of Mathematical & Information Sciences, Bolling AFB DC 20332-6448
8a. NAME OF FUNDING/SPONSORING ORGANIZATION: AFOSR	8b. OFFICE SYMBOL (If applicable): NM
9. PROCUREMENT INSTRUMENT IDENTIFICATION NUMBER: F49620-85-C-0081	
8c. ADDRESS (City, State and ZIP Code): BLG 410 Bolling AFB DC 20332-6448	10. SOURCE OF FUNDING NOS.

PROGRAM ELEMENT NO.	PROJECT NO.	TASK NO.	WORK UNIT NO.
61102F	2304	A3	

11. TITLE (Include Security Classification): CLOSING DEVELOPMENTS IN AERODYNAMIC SIMULATION WITH DISJOINT PATCHED MESHES

12. PERSONAL AUTHOR(S): C. K. Lombard, E. Venkatapathy, J. Bardina, N. Nagaraj, J. Y. Yang, R.C.-C. Luh & J. Oliger

13a. TYPE OF REPORT	13b. TIME COVERED	14. DATE OF REPORT (Yr., Mo., Day)	15. PAGE COUNT
Annual	FROM 01 Jun 85 TO 31 Aug 86	86 11 28	

16. SUPPLEMENTARY NOTATION

17. COSATI CODES		
FIELD	GROUP	SUB. GR.

18. SUBJECT TERMS (Continue on reverse if necessary and identify by block number): Algebraic Grid Generation, Upwind Methods, Relaxation, Approximate Factorization, Euler, Navier-Stokes, TVD Limiters

19. ABSTRACT (Continue on reverse if necessary and identify by block number)

In the first three years of a continuing program the research ~~has~~ aimed at providing computational tools and procedures as the building blocks ~~for a system~~ to permit efficient solution and high resolution capture of flow structure in gasdynamic problems of realistically complex geometries. ~~The research~~ has yielded a comparatively simple algebraic procedure for constructing two and three dimensional geometry fitted base level composite meshes in quadrilateral patches. The method provides complete control of coordinate distribution and gradient on all patch boundaries which may include slope discontinuities. A robust upwind implicit method (CSCM) was the basis to solve the multidimensional pseudo time dependent Euler or compressible Navier-Stokes equations. Research into solution algorithms for that upwind method has yielded a more robust diagonally dominant (DDADI) approximate factorization that subsequently led to a family of rapidly convergent and data storage and management efficient relaxation schemes in two and three space dimensions. Those operationally explicit and unconditionally

20. DISTRIBUTION/AVAILABILITY OF ABSTRACT	21. ABSTRACT SECURITY CLASSIFICATION
UNCLASSIFIED/UNLIMITED ☒ SAME AS RPT. ☐ DTIC USERS ☐	UNCLASSIFIED

22a. NAME OF RESPONSIBLE INDIVIDUAL	22b. TELEPHONE NUMBER (Include Area Code)	22c. OFFICE SYMBOL
Capt. John P. Thomas, Jr., USAF	(202) 767-5026	NM

DD FORM 1473, 83 APR — EDITION OF 1 JAN 73 IS OBSOLETE

UNCLASSIFIED
SECURITY CLASSIFICATION OF THIS PAGE

19. Abstract cont.

stable upwind algorithms have led to a simple robust boundary procedure based on interpolation of conservative variable data from adjacent patches overlying interior patch boundaries where coordinates are discontinuous. Results of tests with reflecting shock capture on overset adaptively refined mesh patches in a 2-D supersonic inlet problem show for comparable accuracy a savings of about an order of magnitude in mesh points relative to uniform mesh refinement. A simple algorithm has been created to construct continuous contour plots of solutions on global domains covered by such a system of multiple meshes. The 3-D symmetric Gauss-Seidel implicit method of planes space marching relaxation algorithm has been implemented on a system of composite patched meshes and applied in the solution of a multi rocket engine shrouded exhaust problem that features large pockets of separated base flow.

The methodology of the flux difference split upwind schemes has been extended with new locally one dimensional total variation diminishing (TVD) schemes that provide robust second or third order spatial accuracy. One of the latter schemes has been implemented in a consistent second order method in both time and space and applied in a problem of unsteady strong shock diffraction around a model aeroassisted orbital transfer vehicle (AOTV). Finally in a study of the impact of mesh topology and refinement on solution accuracy we have shown how local patches of refined overset mesh can be used to tie a system of overlapping composite mesh together to give a hybrid topology with superior balance in flow resolution.

Closing Developments in Aerodynamic Simulation with Disjoint Patched Meshes

Annual Report
F49620-85-C-0081
01 Jun 1985 through 31 Aug 1986

Charles K. Lombard
Principal Investigator
PEDA Corporation

Closing Developments in Aerodynamic Simulation with Disjoint Patched Meshes

Charles K. Lombard, Ethiraj Venkatapathy, Jorge Bardina,
N. Nagaraj, Jaw Yen Yang and Raymond C.-C. Luh
PEDA Corporation

Joseph Oliger
Stanford University

1. Introduction

Recent and projected developments in supercomputers, numerical grid generation techniques and computational algorithms for the compressible Euler and Navier-Stokes equations portend a major revolution in the manner, pace, cost of design and the resulting performance of aerodynamic systems. To realize these potential benefits, certain closing developments in computational technique must be made in order to effect a highly accurate, reliable, efficient and productive simulation environment for aerodynamic design analysis.

A primary need of the developments is to achieve the capability for a user to easily, rapidly and accurately perform flowfield calculations among problems of disparate and realistically complex geometries. The natural approach to realizing this objective with comparatively straightforward extensions of existing finite difference computational technology is through the use of systems of quadrilateral patched meshes.

Such systems can be either/both composite (joined) or overset (disjoint). In the former case adjacent patches share a common boundary, or at least parallel boundaries in the case of mesh patch overlap for purposes of applying numerical boundary conditions. With composite meshes, patch boundaries are piecewise fitted to segments of physical or computational boundaries or embedded flow structures. As shown by Lombard, et al[1], composite mesh systems, that may have numerically useful properties of geometric continuity across patch boundaries, admit topologically singular global meshes that have the capability to connect computational regions of great (really any) geometric complexity. However, situations exist where multiple mesh topologies, each naturally related to some different piece of geometry or flow structure, offer greater flexibility and accuracy than composite meshing alone. Examples involve multiple bodies that may have relative motion or weak shocks that bear little geometric relationship to boundaries of the flow domain. In such cases systems of disparately oriented and at least partially overset grids as proposed by Berger and Oliger[2] allow arbitrarily high resolution of all features of the flowfield.

To make efficient, productive use of patched meshing strategies requires a body of new computational tools and methodology that are the objectives of the present research. The needed factors are: (1) a simple procedure for generating patched

computational meshes with freedom of point and gradient specification on all patch boundaries; (2) improved upwind algorithm/numerical boundary condition procedures for semi-autonomous implicit but unconditionally stable conservative coupling of solutions on a system of multiple patched meshes; and (3) computer graphics, particularly a simple algorithm for constructing contour plots on systems of overset patched meshes. The glue that is to bind these tools together in a simulation requiring minimum human intervention to adapt to new configurations is a flexible parameter controlled multiple mesh data structure. An important objective of the program is to test the evolving techniques in appropriate problems.

2. Research Accomplishments

This annual report, the first under contract F49620-85-C-0081, summarizes the research accomplishments of the first three years of a continuing program. In the first year of the program the emphasis was placed on the most crucial and challenging objectives – patched grid generation and robust upwind algorithm/boundary procedures for rapid relaxation on multiple meshes. The first year's effort[3] sufficed to create some needed tools of algebraic grid generation and to establish an operationally explicit but unconditionally stable upwind algorithm/numerical boundary condition procedure for systems of patched meshes. The techniques were tested in comparatively simple problems.

In the second year's effort[4] the techniques were implemented in 2-D and tested against internal aerodynamics problems of moderate geometric complexity. The upwind algorithm was extended from two to three spatial dimensions. A simple, effective algorithm for contour plotting on domains covered by multiple patched meshes was created to exhibit results.

In the third year the 3-D upwind implicit relaxation algorithm was implemented on a system of composite patched grids. The techniques in two and three space dimensions were tested against realistic internal/external aerodynamics problems of challenging geometric complexity. Within the framework of one of the problems, a continuing study of alternate composite and overset patched meshing topologies demonstrated a strategy of superior balance in mesh point utilization for overall resolution of flow structures on the domain.

Also in the third year, new implicit TVD schemes were constructed to improve the nonlinear stability of second and third order accurate spatial differencing. One of the latter was implemented in a consistent second order method in both time and space and applied in an unsteady strong shock diffraction problem around a model hypersonic space transportation vehicle (AOTV).

Algebraic Grid Generation

The concept of patched meshing in which complex domains are broken up into many geometrically regular and topologically rectangular subdomains leads naturally to the use of efficient algebraic techniques for the construction of the individual

mesh patches. To obtain the desired smoothness properties over the global mesh in the vicinity of patch boundaries, a technique that permits specification of point distribution and gradient on all boundaries was devised. The technique – termed generalized transfinite interpolation[5] – makes use of a parameterized general cubic polynomial for the coordinate curves. Regularity of the mesh is obtained by employing continuous distributions of the parameters of the curves within judiciously chosen bounds based on analysis. Stretching functions such as that of Vinokur[6] are used to distribute points and blending functions are used to distribute parameters of the curves between lateral boundaries.

A novel feature of the technique is the introduction of the corner singularity from analysis to govern distribution of points and parameters in the vicinity of boundary slope singularities. At such points, the method thus obtains the desired properties of mesh smoothness to the interior. A global mesh solution obtained with the method for a backward step problem is shown in Figure 1. Here the solution was generated in two patches, one containing the exterior corner and the other the interior corner. The solution was matched analytically at the patch interface.

Early in the second year, in the process of attempting to apply the generalized transfinite interpolation technique in a variety of 2-D problems, it became evident the method was too sensitive to parameter selection among too many options, was confusing and ultimately required too much artistry to meet the objectives of simplicity and user friendliness set for the products of the research. Further, the lack of an analytical solution to corner problems blocked the straightforward extention of the technique to 3-D.

With some reflection it became evident to us that the difficulty lay in trying to accomplish too much in a single step process. Rather, borrowing the tools of the algebraic technique and redefining the process in multiple steps with interactive computer graphics sets, we could define a straightforward procedure to meet the desired ends.

The approach that has been implemented is in the realm of two boundary methods, in that one pair of opposite sides of a patch is regarded as prescribed and often includes a portion of a physical boundary. The other pair of sides is formed of the left and right limiting members of the family of generalized cubic coordinate curves joining the initially given two boundaries. In either 2-D or 3-D the general cubic coordinate curve has the simple form

$$\underline{r} = \underline{r}_1 + (\underline{r}_2 - \underline{r}_1) f(u) + \underline{\sigma}_1 g(u) + \underline{\sigma}_2 h(u) \tag{1}$$

where

$$f(u) = u^2(3 - 2u)$$

$$g(u) = u(1 - u)^2$$

$$h(u) = u^2(u - 1)$$

Equation (1) is a hermite interpolation of value ($\underline{r}$) and gradient ($\underline{\sigma}$) on the two boundaries and is parameterized in terms of u which varies from zero to unity. The scalings of $\underline{\sigma_1}$ and $\underline{\sigma_2}$ influence the shape (curvature) of the curve between any pair of end points. The specification of a discrete set of u values using a generalized distribution function such as that of reference 5 defines the nodal intersections with the other family of coordinate curves.

In our implementation, the left and right limiting (lateral bounding) coordinate curves are developed interactively on a graphics terminal or workstation to have the desired configurations. The parameters of these lateral bounding curves are then blended with polynomial weighting functions to describe the general cubic coordinate curve over the intervening also discretized interval.

The lateral patch boundaries are essentially control devices that specify shape and distribution to surrounding regions. As such they are placed where needed – at breaks in body surface geometry and as terminators or transition guides from regions of strong shape variation to regions of very regular mesh. In fact the mesh generation problem, particularly for geometries with any substantial complexity, is a problem of multiple length scales. The purpose of multiple patching is to isolate regions of comparable scales and on which subdomains the solution is comparatively regular and can be conveniently fit by simple functions.

Once a primary grid is generated by the technique described above it can be interactively improved by modifying parameter blending and point distribution including point redistribution along the alternate family of coordinate lines implicitly defined by the nodes on the cubic coordinate curves. The latter operation is in the spirit, if not the detailed implementation, of a two step generalized transfinite interpolation.

Another secondary operation that we employ is the modification of coordinate lines in the vicinity of a boundary to smoothly enforce local normality. The latter operation like all the procedures has been programmed as a convenient tool requiring minimal input to apply at a boundary. Finally, a parameterized tension spline that provides an analytical description of a curve amongst discrete data is a tool that has proved useful in the latter operation, in effecting redistribution of points along coordinate curves of either family and for fitting numerically specified boundary data. In Figures 2 and 3 are shown respectively typical examples of 2-D and 3-D mesh planes generated with the simplified technique.

Upwind Implicit Relaxation Algorithm/Boundary Procedures

Under the contract we have devised a new single level operationally explicit but effectively implicit algorithm for gasdynamics. The algorithm is particularly appropriate for multiple patch mesh systems because each solution sweep operation on any patch is decoupled from any other. Thus the method is not only very storage efficient and simple to program including the coupling at patch boundaries but, also, can make excellent use of parallel computing in several straightforward ways.

Previously the Beam-Warming factored implicit algorithm[7] with the Baldwin-Lomax thin layer viscous approximation[8] has provided the basis for two similar space marching (PNS) procedures[9,10] for the compressible Navier-Stokes equations. These PNS methods which are highly efficient – requiring half the data storage and a small fraction of the computer time of two level time dependent methods – have proven effective for flows[11,12] with favorable streamwise pressure gradient or with relatively small adverse pressure gradients. However, in the presence of a strong adverse pressure gradient such as occurs in a wing or fin root regions the contemporary PNS methods suffer numerical stability problems and may infer streamwise separation even where separation doesn't occur[13]. In such unseparated (perhaps weakly separated) regions, numerical stability has been maintained at the price of employing large amounts of artificial viscosity with a resulting loss in predictive accuracy and knowledge of the actual state of the flow. Where strong streamwise separation occurs the methods are unstable and cannot proceed. Particularly for the increasingly relevant laminar flow situation that will be encountered at very high altitude by aerodynamic systems such as orbital transfer vehicles (OTV's) and space shuttles, streamwise separation becomes a likely occurrence[14] in compression corners associated with canopies, pods, flared bodies, wing or fin roots and deflected control surfaces. Thus a more general technique is needed that is inherently stable for all types of upstream influence. At a minimum the mixed elliptic-hyperbolic problem requires global iteration, preferably with type dependent differencing. More background on this problem area is given in the first annual report[3].

New Universal Single Level Scheme CSCM-S

The CSCM flux difference eigenvector split upwind implicit method[15,16,17] for the inviscid terms of the compressible Navier-Stokes equations provides the natural basis for an unconditionally stable space marching technique through regions of subsonic and streamwise separated flow. In such regions the split method can be likened to stable marching of each scalar characteristic wave system in the direction of its associated eigenvalue (simple wave velocity). In supersonic flow, where all eigenvalues have the same sign, the method automatically becomes equivalent to the referenced PNS techniques based on the Beam-Warming factored implicit method with the Baldwin-Lomax thin layer viscous approximation.

Compared to contemporary central difference methods, the CSCM characteristics based upwind difference approximation with its inherent numerical stability leads to greatly reduced oscillation and greater accuracy in the presence of captured discontinuities such as shocks, contacts and physical or computational boundaries. The correct mathematical domains of dependence that correspond with physical directions of wave propagation are coupled with well posed characteristic boundary approximations[16] naturally consistent with the interior point scheme. The result is a faster sorting out of transient disturbances and substantially more rapid convergence to the steady state. The splitting and the associated time dependent implicit method have been described in detail in references (15) and (17) for quasi 1-D and

2-D planar or axisymmetric flow.

In the following, we will sketch the differences between the time dependent method and the new space marching technique which we designate CSCM-S. The discussion will begin with the quasi 1-D inviscid formulation, present some results elucidating the properties and performance of the method, then give additional details entering into multidimensional inviscid and thin layer viscous procedures and present some 2-D solutions obtained with the new single level scheme in problems solved previously[17] with the time dependent method. Lastly we sketch a 3-D implicit method of planes algorithm and give some results for an axisymmetric nozzle flow over a backward facing step.

Quasi 1-D Formulation

The general jth interior point difference equations for the time dependent CSCM upwind implicit method for the inviscid advection terms is

$$(I + \tilde{A}^{+}\nabla + \tilde{A}^{-}\Delta)\delta q_j = -\tilde{A}^{+}\Delta q)^{n}_{j-1} - \tilde{A}^{-}\Delta q)^{n}_{j} \tag{2}$$

where ∇ and Δ are backward and forward spatial difference operators. Here q is the conservative dependent variable vector and F is the associated flux vector. In the notation the interval averaged matrices between node points j and $j+1$ are indexed j. For simplicity, the right hand side of equation (2) is written for the first order method. Higher order methods in space are given with results in references 15 and 17. In equation (2) the CSCM flux difference splitting is

$$(\tilde{A}^{+} + \tilde{A}^{-})\Delta q \equiv \Delta F^{+} + \Delta F^{-} = \Delta F \tag{3a}$$

with

$$\tilde{A}^{\pm} = (\overline{MT}I^{\pm}\overline{T}^{-1}\overline{M}^{-1})\tilde{A} \equiv \hat{A}^{\pm}\tilde{A} \tag{3b}$$

and

$$I^{\pm} = \frac{1}{2}(I \pm \mathrm{sgn}(\overline{\Lambda})) \tag{3c}$$

exhibiting the similarity transformation that diagonalizes the constructed[15,17] flux difference Jacobian $\tilde{A}$. Here $\overline{\Lambda}$ is a diagonal matrix of the interval averaged eigenvalues that through the truth function diagonal matrices $I^{\pm}$ make the decisions about directions of characteristic wave propagation and whether or not to send signal to the solution point. Thus in equation (2) the piece of the flux difference splitting $\tilde{A}^{+}\Delta q)_{j-1}$ represents the convection of characteristic wave contributions in the positive coordinate direction from grid point $j-1$ to solution point j and $\tilde{A}^{-}$, in the negative direction from $j+1$ to j. As the result of incorporating multiplicatively the (local) time step (for pseudo time relaxation) and the spatial (divided) differences in the matrices, the numerical eigenvalues are Courant numbers for the characteristic waves whose speeds are u, $u+c$ and $u-c$, with c the sound speed.

Central to its accurate shock capturing capability, the CSCM conservative flux difference splitting has the Roe[18] "property U" embodied in equation 3a.

With $\delta q = q^{n+1} - q^n$, equation (2) defines a two level linearized coupled block matrix implicit scheme that can be solved by a block tridiagonal procedure. In reference (17) a new (DDADI) approximately factored alternating sweep bidiagonal solution procedure for equation (2) is presented that is shown to be very robust and is operationally explicit, i.e. requires only a decoupled sequence of local block matrix inversions rather than the solution of the coupled set. For the forward sweep the bidiagonal solution procedure can be written

$$(I + \tilde{A}^+ - \tilde{A}^-)\delta q^*{}_j = RHS + \tilde{A}^+ \delta q^*{}_{j-1} \tag{4}$$

For the linear problem, i.e. constant coefficient case of stability analysis, equation (4) is equivalent to the single level space marching procedure

$$(I + \tilde{A}^+ - \tilde{A}^-)\delta q^*{}_j = \tilde{A}^+ q^*{}_{j-1} - \tilde{A}^+ q^n_j - \tilde{A}^- \Delta q)^n_j \tag{5}$$

Nonlinearity enters in the single level space marching form (5) in that at each step of the forward sweep the matrices $\tilde{A}^+$ are averaged between $q^*{}_{j-1}$ and q^n_j rather than homogeneously at the old iteration level n. Similarly, a companion backward space marching sweep that is symmetric to equation (5) and that is intimately related to the backward sweep of the alternating bidiagonal algorithm of reference (17) is

$$(I + \tilde{A}^+ - \tilde{A}^-)\delta q_j = -\tilde{A}^+ \Delta q^*)_{j-1} + \tilde{A}^- q^*_j - \tilde{A}^- q^{n+1}_{j+1} \tag{6}$$

The method given by equations (5) and (6) is von Neumann unconditionally stable for the scalar wave equation. The analysis shows the significance of DDADI approximate factorization in rendering both the forward and backward sweeps separately stable regardless of eigenvalue sign. Consequently as the local Courant number becomes very large, the robust method becomes a very effective (symmetric Gauss-Seidel) relaxation scheme for the steady equations, a fact which substantially contributes to the very fast performance that will be demonstrated.

At a right computational boundary on the forward sweep we solve the characteristic boundary point approximation[17]

$$(\widetilde{\tilde{A}}^+ + \tilde{A}^+)\delta q^*_N = \tilde{A}^+ q^*_{N-1} - \tilde{A}^+ q^n_N \tag{7}$$

$q^{n+1}_N = q^*_N$ and at a left, on the backward sweep

$$(\widetilde{\tilde{A}}^- - \tilde{A}^-)\delta q_1 = \tilde{A}^- q^n_1 - \tilde{A}^- q^{n+1}_2 \tag{8}$$

Following the solution of equations (7) and (8) the conservative state vector is iteratively corrected[16] to maintain the accuracy of prescribed boundary conditions while not disrupting the representation of the computed characteristic variables running to the boundary from the interior. Analysis of a model system with upwind differenced scalar equations and coupled boundary conditions was related to the linearized bidiagonal scheme[17] by Oliger and Lombard[19]; the analysis also strongly supports the numerically confirmed robust stability of the present nonlinear method for gasdynamics. A useful result of reference 19 that simplifies the procedure of reference 17 is that on the forward sweep there is no need for a predictor step at the left boundary $J = 1$; thus, the solution sweep begins at $J = 2$. Similarly, the backward sweep begins at $J = N - 1$.

With the updating at each step, where in equation (6) $\delta q_j = q_j^{n+1} - q_j^*$, it is clear that the symmetric pair of equations (5) and (6) serve to advance the solution two pseudo time (iteration) levels; whereas, the linear alternating bidiagonal sweep algorithm of reference (17) advances the solution only one level. To maintain conservation to a very high degree, in single sweep marching in supersonic zones we iterate (at least) once locally at each space marching step. The local iteration serves to make the eigenvectors in the coefficient matrices consistent with the advanced state and thus provides improved accuracy for the nonlinear system. It appears effective to do this inner iteration everywhere, i.e. in both subsonic and supersonic regions, as the number of global iteration steps to convergence with two inner iterations has been found reduced by a factor of three to four. Since the computational work per two steps is about the same for the single level and two level schemes, and beyond the fact that one saves a level of storage in the space marching algorithm, the question arises: Can one get solutions in less computational work through faster convergence with the nonlinear space marching algorithm?

One Dimensional Results

First, we present results for supersonic flow with no shock in Shubin's diverging nozzle. In purely supersonic zones, the experience with the present method is that the solution can be marched accurately in one global iteration, as ought to be the case. Figure 4 shows the exact solution (in solid line) and the computed result from the first forward sweep. It is evident that the method correctly predicts the solution to plotting accuracy in one forward sweep. With subsequent sweeps the error (the difference between the exact and the computed solution) reduces to machine accuracy in less than three global iterations. In fact, by increasing (from two) the number of inner iterations on the solution procedure at each space marching step, convergence to prescribed accuracy can be guaranteed in one forward sweep. This is also true of contemporary locally linearized unsplit methods in supersonic flow.

With the globally iterative nonlinear space marching formulation, early experience in two quasi 1-D nozzle problems with mixed supersonic-subsonic zones is that solutions are obtained in roughly an order of magnitude fewer iteration steps

than had been required with the previously fast pseudo time dependent technique and block tridiagonal solving.

The two nozzle problems which are described and solved by Yee, Beam and Warming[20] and solved with the CSCM time dependent technique in references (15) and (16) are Shubin's diverging nozzle flow and Blottner's converging-diverging nozzle flow. Both problems involve unmatched overpressures at the outflow which result in internal shock terminated supersonic zones and subsonic outflow. For the experiments involving flow of mixed type the same initial data given by Yee, Beam and Warming – a linear interpolation between inflow and outflow values for effectively exact solutions of the problems – is used that was used previously with the time dependent approach.

For flows of mixed type, in Figures 5 and 6 respectively, results are shown for successive forward and backward sweeps for five global iteration steps with Shubin's and Blottner's nozzle flows. In both cases, the exact solution as given by Yee, Beam and Warming is shown in solid line and the present computational results solved on a 51 point mesh, in boxes. Blottner's nozzle flow is shown converged after 10 global iteration steps. There is substantial evidence in other results not shown that with further work the number of global iterations required to compute flows such as Blottner's can be reduced by a factor of two, to about five.

In Figure 7, we show a subcritical, i.e. completely subsonic, flow solution computed in only two global iteration steps for the Blottner nozzle geometry with different inflow conditions. Here the exact analytical solution derived by Venkatapathy is shown in solid line and our computed results in boxes.

The alternating direction sweeps in our method have been derived directly out of theory for solving the implicit set of difference equations. However, one can see mechanistically (numerically speaking) that omitting the backward sweep from the pair and globally iterating only with the forward sweep equation (5) will result in permitting the influence of a subsonic outflow boundary (or interior disturbance) to propagate upstream only one grid point per global iteration. In such a case, which relates to other global iteration methods found in the literature and that also sweep only in the main flow direction, the rate of convergence is greatly inhibited relative to symmetric sweeping by a factor of order roughly the number of grid points in the subsonic zone. Mathematically, this inhibition is the result of the failure to include in the implicit process the effect of the eigenvectors governing upstream influence but instead treating these waves explicitly with effective CFL unity.

In Figure 8 we illustrate the progress of the transient solution to the subcritical nozzle problem after 15 forward sweeps, with the backward sweeps omitted. One can clearly see that the wave influence of the outflow boundary has progressed only 15 mesh points forward of the outflow boundary. In Figure 9 the transient solution is shown after 60 steps which is beyond one characteristic transit time (equivalent to 50 mesh intervals) for the upwind wave to reach the inflow boundary. In Figure

10 we show the history of the RMS error in the primitive variables. The solution is found to converge to roughly the same RMS error after three characteristic times (150 steps) as the solution obtained with the symmetric alternating sweep sequence after only 3 global iterations.

Blottner's supercritical nozzle problem which involves subsonic inflow accelerating through a sonic point to a supersonic zone terminated by a shock to subsonic outflow is the most computationally demanding of the test cases and indicates the capability for the method to compute simply and consistently over the subsonic forebody and base regions of blunt bodies in supersonic flow. Thus the need for separate time dependent codes will be obviated by this new method.

Finally, in Figures 11 and 12, we present the convergence history for the present nonlinear scheme and the linearized time dependent scheme for completely subsonic and supersonic nozzle flows. The x-axis shows the number of iterations each scheme requires to reduce the exact error to five orders of magnitude for various Courant numbers. It is evident that the present scheme converges extremely fast at all CFL numbers compared with the method based on the linearized block tridiagonal solver.

Two Dimensional Formulation

For two dimensional flow, assuming a marching coordinate ξ, inviscid terms

$$B^+\nabla_\eta + B^-\Delta_\eta \tag{9a}$$

and

$$-B^+\Delta_\eta q)_{k-1} - B^-\Delta_\eta q)_k \tag{9b}$$

are added to the left and right hand sides respectively of both the forward and backward sweep equations (5) and (6). For viscous flow, second centrally differenced, thin layer viscous terms are also added in the η direction as is conventionally practiced, e.g. Steger[21]. With the terms for the η cross marching coordinate direction, the technique now becomes an implicit method of lines. Along each η coordinate line, one can solve the equations coupled with a block tridiagonal procedure. Alternatively, a further DDADI bidiagonal approximate factorization can be employed in the η direction and solved either linearly as in reference (17) or nonlinearly as here in the ξ direction. As shown in the quasi 2-D numerical experiments of reference (17), DDADI bidiagonal approximate factorization is stable for viscous as well as inviscid terms. Finally in reference (17) there is a relevant discussion of the reduced approximate factorization error that attends using DDADI in one or more space directions.

Two Dimensional Results

We present results for a 45° - 15° axisymmetric transonic nozzle flow previously studied experimentally by Cuffel, Back and Massier[22] and computationally by Cline, Prozan, Serra and Shelton (all referenced in (22)) and ourselves[17]. In Figure 13 we show results after 10 steps of an early computation run at a local CFL number of

14 with the present first order single level scheme. Except for the addition of an error correction procedure[16] to counter numerical inflow boundary condition drift, a factor which has improved the present solution in the vicinity of the axis, the effectively converged results found here are the same as those given for the two level scheme in reference 17. (As long as the problem has a unique solution, the two schemes must give equivalent results since the right hand side difference equation sets, including boundary approximations, are the same.)

For the solution given in Figure 13, we noted a very rapid rate of reduction in residual, three orders of magnitude in ten steps. This compares with 60 steps given in reference (17) for the solution obtained with the two level scheme. The rapid convergence found in this transonic problem for the CSCM-S method with viscous terms provides the reasonable expectation of similar fast results to be obtained without viscous effects. Thus the method in multidimensions appears to have attractive potential for an improved transonic Euler solver as well as Navier-Stokes solver.

Next, we present first order inviscid and viscous results for an inlet problem shown in Figure 14. The pressure contours for the first order inviscid solutions are shown in Figure 15. Figure 16 shows the first order viscous results. The viscous computation shows the presence of the leading edge shock. The flow structure compares very well with the theoretical (for the inviscid case) and other computational results. In Figure 17, the inviscid and viscous wall pressure are compared with the exact solution (inviscid). Figure 18 shows the convergence history of the RMS residual of all the conservative flow variables for the inviscid problem solved at CFL = 100 with 4 inner iterations at every axial location. For the inviscid case, only forward marching was carried out and backward marching was omitted. The solution has converged for practical purposes at the end of the first sweep. The residual reaches machine accuracy in 10 iterations. In reference 23, we show the residual reduction versus inner iteration number in single sweep solutions for supersonic flow and compare results with contemporary PNS procedures. Finally in work described in reference 24 we have applied the single level scheme to the solution of the coupled forebody captured shock layer and massively separated wake flow of a hypersonic axisymmetric AOTV.

Three Dimensional Method of Planes Algorithm

In reference 23 we presented a symbolic algebra for DDADI approximate factorization and derived single level relaxation schemes. The algebra is based on the implicit difference stencil of the implicit method. Here we will show how the approach can be used to derive an symmetric Gauss-Seidel implicit method of planes relaxation algorithm.

The unfactored three dimensional linearized implicit method can be represented

by the symbolic matrix expression

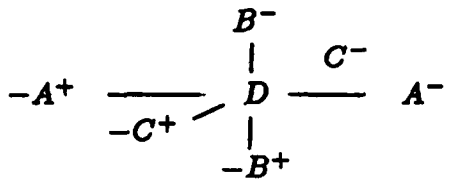

On the block diagonal the matrix $D = I + A^+ - A^- + B^+ - B^- + C^+ - C^-$. A once DDADI approximate factorization in the ξ coordinate direction leads to the expression

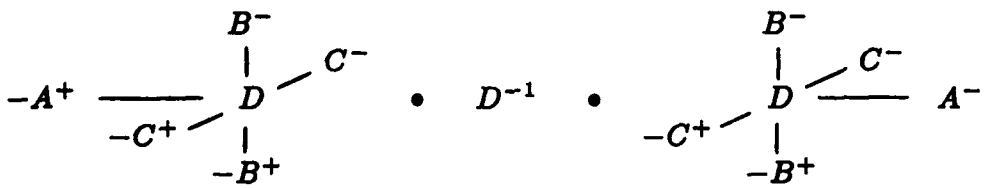

By analogy with the derivation of the single level scheme for quasi 1-D flow from DDADI bidiagonal approximate factorization we identify the above expression with the alternate space marching implicit method of planes algorithm

Forward Sweep

$$\begin{bmatrix} & B^- & \\ -C^+ & D & C^- \\ & -B^+ & \end{bmatrix} \delta q_j^n = RHS[\, q_{j-1}^{n+1} \,,\, q_j^n \,]$$

Backward Sweep

$$\begin{bmatrix} & B^- & \\ -C^+ & D & C^- \\ & -B^+ & \end{bmatrix} \delta q_j^{n+1} = RHS[\, q_j^{n+1} \,,\, q_{j+1}^{n+2} \,]$$

In the planes the coupled block matrix problem can be further simplified by the approximate factorization

$$[\, -C^+ \,,\, D \,,\, C^- \,]\, D^{-1}\, [\, -B^+ \;\; D \;\; B^- \,]\delta q = RHS \qquad (10a)$$

which leads directly to the block tridiagonal solution sequence

$$[\, -C^+ \;\; D \;\; C^- \,]\delta q^* = RHS \qquad (10b)$$

$$[\, -B^+ \;\; D \;\; B^- \,]\delta q = D\delta q^* \qquad (10c)$$

Three Dimensional Results

This 3-D space marching algorithm has been tested against an axisymmetric viscous flow problem of a supersonic RL-10 nozzle exhausting over a backward facing step into a cylindrical shroud.

In Figure 19 we show a 3-D perspective view of the wall surface mesh in the quarter sector for which we solved. A section of computational mesh in a longitudinal plane through the axis is shown in Figure 20. For such planes, Figures 21 and 22 show pressure contour and velocity vector plots that exhibit the expected flow structures – a weak shock in the nozzle diffuser, a strong expansion at the nozzle exit with subsequent recompression shock off the shroud wall and, lastly, a substantial region of streamwise separated flow under the backward facing step. The Mach contour plot of Figure 23 for a cross flow data plane in the shroud shows the excellence with which the method and, in particular the lateral boundary conditions, numerically maintain the axisymmetry of the solution.

Patched Mesh Boundary Procedures

In previous work Lombard, et al[16,17] and Oliger and Lombard[19] gave stable implicit procedures for computing the solution at external boundaries of a computational domain. Those procedures generalized the work of Kenzer to matrix coupled linearized boundary conditions complementing a set of advective difference equations (associated with well posed characteristics) to the boundary.

Under the present contract we have explored the problem of implicitly coupling at interior patch boundaries the global solution on a system of multiple patch meshes. The approach we have taken in this research is numerical experimentation among a number of boundary treatment approximations to the solution of the continuous domain problem. For comparison purposes with previous single mesh results, numerical experiments were performed with the well tested two level pseudo time relaxation CSCM scheme at the interior points of the mesh patches.

Quasi 2-D Studies

Our first experiments, to be described here, dealt with breaking a single coordinate line into segments and solving sequentially on each the equations for a quasi 2-D viscous compressible flow. The model problem, with which we experimented in reference 17 for an uninterrupted mesh, is a transient pipe flow resulting from an initially nonequilibrated pressure between the axis and wall boundaries. Three kinds of cases were run with the two-level linearized implicit procedure; all featured sequential solving on patches with at least one point of overlap. Case 1 had frozen boundary data, obtained from the solution on neighboring meshes in an operationally explicit manner. Specifically at left and right first computed interior points of a patch, we solved the bidiagonal equations respectively

$$(I + \tilde{A}^+ - \tilde{A}^- \Delta)\delta q_2 = \tilde{A}^+ q_1^n - (\tilde{A}^+ - \tilde{A}^-) q_2^n - \tilde{A}^- q_3^n \qquad (11a)$$

and

$$(I - \tilde{A}^- + \tilde{A}^+\nabla)\delta q_{N-1} = \tilde{A}^+ q^{\,n}_{N-2} - (\tilde{A}^+ - \tilde{A}^-) q^{\,n}_{N-1} - \tilde{A}^- q^{\,n}_{N} \qquad (11b)$$

Here the symbols n indicate the "frozen" boundary data coming from the solution on the interior of an adjoining and partially overlying patch which was at the old iteration level in the global procedure. In Case 1 the solution on all the grids was effectively updated at the same time.

Case 2 featured reverse sequential cycling of the two level time dependent solution procedure through the grids on alternate global steps. In the forward sequence the right interior patch boundaries were (a) frozen or (b) computed with one-sided characteristic boundary conditions obviating any change in the characteristic data from outside (to the right of) a patch. The left interior patch boundaries inherited implicit data (δq) from the solution on the computed patch to the left. In the backward sequence all the roles were reversed including the directions of forward elimination and back substitution in the tridiagonal matrix inversion procedure.

Case 3 featured cycling through the patches in the predictor (forward elimination) step of the solution procedure, inheriting implicit left boundary data as in Case 2. Then the patches were cycled through in reverse order on the corrector (back substitution) step. The result (save for interpolation if data points of the grids were interlaced) is identically equivalent to solving on an uninterrupted single patch mesh.

The results of the three sets of experiments were comparable for local time steps based on constant CFL number up to about 50. Beyond that the rate of convergence of the solutions for Cases 1 and 2 diminished and at sufficiently high CFL number failed to converge. The effort involved in Case 2 with the two level scheme was not rewarded relative to the simple procedure of Case 1. Within the framework of the single-level symmetric Gauss-Seidel implicit relaxation scheme, which is linearly equivalent to the bidiagonal scheme employed at the boundary, Case 2a is operationally no more difficult than Case 1 and more closely approximates Case 3. Case 2b has a consistency problem that inhibits firm convergence.

Figure 24 compares RMS residual (density) convergence history for Cases 1 and 3 with three mesh segments with two cells of overlap and run at CFL 25. As one might expect, the effectively uninterrupted mesh procedure is found to converge (two to three times) faster for about the first 50 steps through the major transient. After that the performance is comparable. The performance of the frozen boundary treatment Case 1 with five segments at CFL 25 was found to be not materially worse than with three segments, but the performance degradation with increasing CFL was found to proceed faster with increasing number of patches.

From the results of the quasi 2-D experiments and extrapolation from experience with the single level scheme, we observe that the simple boundary procedure

with frozen conservative variable data taken from the solutions at either iteration level n or $n+1$ on adjacent meshes and coupled implicitly by alternating direction sequential solving through the patches has robust stability to sufficiently high CFL number to yield a rate of convergence meeting our needs.

Two Dimensional Patch Boundary Treatment

In earlier work solving the Euler equations on multiple patch meshes Benek, et al.[26] employed linear interpolation of the conservative variables from the interior solution of one mesh to give Dirichlet boundary data for the other. With several points of mesh overlap at the mesh boundaries, transonic solutions obtained with central differencing exhibited considerable oscillation in the vicinity of shocks propagating through the boundary region. Eberhardt[27] with the code of Benek, et al.[26] attempted to reduce the oscillation and attendant stability problems encountered in the vicinity of a bluff body shock intersecting an embedded patch boundary by introducing a characteristic computed boundary point approximation with scalar upwind difference equations in Riemann variables. In his procedure, interpolation was performed only on the variables whose characteristics ran to the patch boundary from outside the computational domain. Eberhardt based the decision about domain of dependence of the characteristics on eigenvalues computed within the patch domain. When this decision was compatible with the flow, then the characteristics boundary procedure gave markedly superior results compared to interpolation of conservative variable data, which leads to solution overspecification in subsonic zones. In other cases where incorrect domain of dependence was inferred, the characteristic boundary procedure was unstable.

Here, based on our quasi 2-D studies described above, we give a simple, robustly stable implicit approach to computing solutions of the conservative equations of gasdynamics on either composite or overset meshes. Without requiring special flux conservative operators, but rather, interpolating conservative variable data at mesh boundaries, the implicit upwind method is accurate and relatively free of oscillation where shocks intersect interior patch boundaries. In a supersonic inlet problem with an expansion and reflected shocks, we exhibit the capability to conveniently carry out with rapidly convergent implicit methods for systems of equations the adaptive refined meshing strategy in overset patches proposed by Berger and Oliger[2]. Further, the test case shows concretely in a realistic aerodynamic problem the savings in mesh points (about an order of magnitude here in two dimensions) for similar accuracy that flow structure aligned adaptive patched meshing affords compared to uniform grid refinement.

The factors in our approach are supported by previous research by ourselves and generically by others cited in reference 28 and are proven in numerical experiments reported here and elsewhere[29]. We employ an implicit conservative upwind scheme CSCM[17] with which in the present work we can solve to either first or second order spatial accuracy the Euler or compressible Navier-Stokes equations in two-

dimensional planar or axisymmetric flows. The flux difference split upwind schemes of generalized Roe form such as CSCM have a number of qualities that make them ideal for the purpose of solving on discontinuous patched mesh systems.

First, conservative schemes in the Roe form satisfy Roe's property U that guarantees the correct speed for captured shocks. The CSCM scheme has been tested in a wide variety of internal and external transonic and hypersonic flows[17,23] and has been found to capture strong and weak shocks accurately in location and with little oscillation. The shock transition is particularly sharp, about two mesh cells wide, on an aligned grid; and this factor will be accommodated as much as possible in our adaptive patched mesh strategy.

Second, in the Roe form, the difference operators on conservative variable data represent the effects of differencing to characteristic data only for disturbances propagating toward the given node and reject the mathematically unstable contribution from disturbances that may be propagating downwind of the node. The one sided upwind difference operation represents identically[30] the (split) conservative partial flux difference between the nodes. To the extent that the data from an adjacent mesh is consistent with the solution, the associated upwind partial flux difference to that data will serve to provide at convergence consistency of the partial flux convective into the given mesh from its neighbor, and vice versa for signals of the other eigenvalue sign. Thus the method acts within truncation error to provide the similar continuity of the flux tensor among patched grids that exists in the physical solution across shocks and that would obtain on a single grid alone. The correct domain of dependence coupled with the well posed characteristic boundary point approximations[17] tend not to support oscillatory disturbances but convect them out of the flow domain.

Third, one sided difference interval averaged eigenvalues let majority rule determine the direction of local signal propagation. When applied, as we do, to a difference operator between boundary data obtained from an adjacent mesh and the local mesh solution point, the data of both meshes participate in making the decision as to whether an incoming signal is being sent. Both in concept and from our experience, this factor seems to overcome the inter-mesh communication difficulty experienced by Eberhardt[27] with his characteristic boundary procedure.

Lastly, with the CSCM difference equations, with diagonally dominant approximate factorization[17,23] that retains on the diagonal the contributions from both sets of eigenvalues in what is effectively an absolute value Jacobian matrix, we can solve the equations either with two data level linearized block implicit methods[17] or with a single data level relaxation technique[23] that is substantially more rapidly convergent than the linearized implicit procedures. As can be inferred from the theory and numerical experiments of reference 23, the use of DDADI on the solution point while differencing effectively explicitly to data obtained from an adjoining mesh (which may be at either the old (n) or new (n+1) level) is unconditionally stable. When the solutions on the patched meshes are alternately updated using either

the linearized implicit or relaxation methods the global procedure is implicit. As will be shown here, the robust stability of the global procedure has been confirmed to approximately coarse mesh CFL 100.

One point that has not been touched on is the form of interpolation that we use. Differencing to interpolated data is equivalent to a weighted sum of differences operating on the interpolants. It is intuitive that for robust stability each of these assumed upwind differences ought to be well posed. This implies that the interpolation weights should all be positive and the domains of dependence of all the interpolants should be outside (i.e. on the assumed side) of the solution point with respect to its mesh interior. Neither of these properties was shared by the data interpolation schemes used by Benek, et al.[26] or Eberhardt[27].

Finally, extending a direction of Benek, et al.[26], we do not compute on sections of coarser meshes underlying patches of overset refinement. Our data structure and automated procedures for the consequent partitioning of meshes are described in reference 31. The partitioning concept in which coordinate lines of a patch have differing (index) lengths in computational space also leads to useful possibilities including, as will be shown here, fitting mesh patches obliquely to boundaries, e.g. to sharply capture reflecting shocks.

Interior Boundary Treatment – First Computed Point Formulation

In Equations (2) - (8) we sketched the development of the single level relaxation algorithm and the treatment at external boundaries of the global computational domain. Here we describe the treatment of an interior patch boundary. The left hand side of equation (2) has the tridiagonal structure

$$\tilde{A}^+ \quad , \quad I + \tilde{A}^+ - \tilde{A}^- \quad , \quad \tilde{A}^- \tag{12}$$

In relation (12), the central block which we call D can be seen to contain the absolute values of the eigenvalues for signals propagating to the solution point from either left or right. Indeed, the simplified approximation to equation (2)

$$D\delta q_j = \tilde{A}^+ q^{n,n+1}_{j-1} - (\tilde{A}^+ - \tilde{A}^-) q^{n}_{j} - \tilde{A}^- q^{n,n+1}_{j+1} \tag{13}$$

leads to an operationally explicit implicit relaxation procedure[23] that is unconditionally stable either as a computed interior patch boundary point or general interior point relation. Here $n, n+1$ means data from either time level. If the interior point implicit solution procedure is two level, then the term of equation (12) at the interior point $j-1$ or $j+1$ will be linearized (assumed at the $n+1$ level) as in equations (11a) or (11b).

For left or right boundary points, the frozen (i.e. not computed on the patch) data at $j-1$ or $j+1$ in equation (13) is gotten from adjacent patch mesh data. If the mesh system is composite and mesh lines cross the boundary to the solution

point, then the frozen boundary data is the solution point data of the adjoining mesh. For the case of nodes on lines ending at the patch boundary, which relates equally to composite mesh with lines of either patch ending at the boundary or to overset meshes, the frozen data is got by interpolation of adjacent mesh patch data to the boundary point location.

Linear interpolation to an included point on a coordinate line or within a polygonal cell involves only positive weights on the interpolant data. In most of the numerical experiments made to date with overset grids we have employed a bilinear interpolation[31] based on the four corner points of the overlapping mesh cell enclosing the frozen boundary point. However, with less data processing a linear interpolation involving the three corner points on the including triangle (Figure 25a) generalizes to the use of the four corner points of the enclosing tetrahedron in three dimensions.

In the composite mesh case, Figure 25b, interpolation is naturally along an interior coordinate line paralleling the zonal boundary. Such interpolation is one-dimensional for a two-dimensional problem and two-dimensional for a three-dimensional problem. The generic composite grid problem just described and which we have tested among the numerical experiments to be reported in the next section also serves as a *gedanken* model problem for the overset mesh case. Possible solutions that come to mind by analogy are shown in Figure 25c and Figure 25d. In both figures the interpolation is along two point coordinate line segments (or three point triangular surfaces in 3-D) of the adjacent mesh and thus is a direct analog with the attendant data requirements of the composite mesh case.

We use stable and consistent first order differencing and interpolation at the boundaries regardless of the order of accuracy of the difference approximation in the patch interiors. Since the divided differences of the computed boundary point approximation are of the same accuracy as the interpolation, the approaches sketched in Figures 25c and 25d may be regarded as letting the difference operator perform the interpolation (to uniformly spaced data Figure 25a) in the direction away from the computed boundary. Thus, to the extent that the solution is locally well represented by a linear function the approaches sketched in Figures 25a and 25c and 25d are equivalent. The treatment shown in Figure 25a, however, requires the same dimensionality of the (triangular) interpolation procedure as that of the problem and one higher than for the (linear) treatment of Figures 25c and 25d.

As a final theoretical point regarding data exchange at patch mesh boundaries, we note here that equations (11) imply[30]

$$\Delta F^{\pm} = \hat{A}^{\pm} \Delta F \tag{14}$$

Hence we may equivalently write the right hand side difference operators of equation (13) directly in terms of flux components. An advantage of this approach is that the flux components normal to the shock discontinuity are continuous across the

discontinuity. Thus interpolating flux data from one grid to serve as needed boundary data of another can be a smoother more accurate procedure than interpolating conservative variable data.

We close this section by noting that, consistent with the 2-D interior point schemes,[17,23] we difference along the computed boundary coordinate line with operators written for the boundary aligned coordinate. In the diagonally dominant approximate factorizations that we employ in multidimensions, the convective matrices with absolute values of the eigenvalues for both coordinate directions are retained in the diagonal block.

Two Dimensional Numerical Experiments

To achieve both accuracy and robust stability in this difficult problem area, particularly with overset meshes, theory can provide insight into what to attempt, but the acid test of numerical methods is performance in relevant numerical experiments.

We present here some sample results with major findings from a substantial number of experiments[28] designed to test various aspects of the accuracy and stability question for the conservative system of equations for gasdynamics solved on patched meshes.

The numerical experiments to be discussed here involve solution of an inviscid flow in a Mach 5 inlet with 10° compression ramp that we have employed in previous experiments with first and second order upwind methods on uniform meshes[17]. The problem involves two of the generic kinds of flow structure, shock and expansion fan, which are not possible to resolve both efficiently and to the extent desired on uniform mesh. As the result of interaction of the expansion fan with the compression corner and reflected shocks, they curve in non simple regions for which the exact solution is not known analytically. The coarse base level grid of the experiments has 26×26 points.

Composite Grid with Boundary Overlap

As a simple test of employing frozen interpolated boundary data, we show in Figure 26a and 26b the grid and density contours for a patched mesh with two full cell overlap and refinement with twice as many mesh points in the streamwise direction in the lower patch. Thus every other mesh point at the upper interior boundary of the lower patch is interpolated between computed conservative variable data of the upper patch along the common streamwise coordinate line. This test case solving sequentially on the patches with the first order method is numerically stable with local time steps based on CFL 100. There is no oscillation in the solution in the vicinity of the patch boundary (shown) and refinement in the lower patch has served to sharpen the solution in that region, though high gradient regions of the solution are very smeared on the coarse, nonaligned meshes.

Solutions on Uniformly Refined Mesh

As a standard for comparison with results from overset patched refinement, we show in Figures 27a and 27b pressure contours for first and second order upwind methods on 101 × 101 point uniform grids, i.e. 4 times refined in each coordinate direction.

Adaptive Refinement in Overset Grids

Based on a uniform coarse mesh solution similar to Figure 26b, the coarse mesh was overlaid with two refined mesh patches (Figure 28a) aligned with the compression corner and reflected shocks. Note in the reflection region, the two overset patches have been constructed to share the same coordinate lines for superior grid communication. The coarse grid is segmented (broken) under the overset patches and the refinement is segmented to terminate at the reflecting boundary (symmetry plane). In Figures 28b and 28c respectively, we show pressure contours for the first and second order upwind methods on the overset grid.

Discussion

While the adaptive refinement about doubled the coarse mesh, the shock structures treated are better resolved than with the uniformly refined mesh in 16 times the points. Thus the results demonstrate an order of magnitude improvement in data efficiency to be gained by overset refinement. We sketch in Figure 28d a strategy of refinement for the as yet untreated expansions of the problem.

Graphics for Patched Grids

Graphics is an important tool to develop and debug numerical codes and analyze numerical results. In some problems, contour plots of certain flow quantities such as pressure and Mach number are sufficient to look at; in other problems, one may need to look at velocity vectors to understand the solution better. In the case of multiple grids, complication arises due to the fact that solutions in more than one grid are available in some regions of the flow domain and the global solution needs to be composed from solutions on individual grids.

Graphics for Single Grid Solution

Before we deal with multiple grid graphics, we outline how we analyze the single grid solutions. Since multiple grid solutions are made up of single grid solutions, insight into the single grid graphics will help to understand the multiple grid graphics plotting strategy. In the process of solving problems there are three roles for graphics. First, the grid and the starting solution can be checked. Second, as the solution evolves, graphics can be used as a tool to debug and understand the time evolution of the solution process. Third, the converged or the final solution is plotted to study the physics and compare the present solution with other solutions. Most of the above tasks can be grouped into three categories of plotting: 1) Grid plotting; 2) Contour plotting of various scalar flow quantities and velocity vector plotting; 3) Comparison plotting. Here we deal with the first two.

Grid Plotting

Single grid plotting is done by essentially drawing straight line segments. We use the commercial macro plotting package DISSPLA* for all plotting purposes. Our plot program links the macro DISSPLA program. Only higher level commands need to be defined on the plotting program and all the lower level commands are defined in the DISSPLA program and are transparent to the users. Given the ordered set of grid points, the grid plotting routine calls the line segment drawing command for every line segment and plots the grid. Since only discrete grid values are used in all the finite difference calculations, the representation of the grid by linear elements is most appropriate and no interpolation or smoothing is necessary.

The same philosophy is adhered to in plotting contour curves of flow quantities. Independent of the order of the scheme and the solution accuracy, the solution is available only at discrete node points and any attempt to represent the solution in a smoother sense can only corrupt the solution. With this in mind, we use a fast, simple and robust contour plotting routine.

Contour Plotting

Contour plots for the two dimensional problems are very useful to show how accurately shock and other flow structures have been captured. Any scalar flow quantity, such as pressure, density, Mach number, temperature, stream function or vorticity can be plotted for various constant contour levels. The general method for plotting contour levels are given in the following section. First, the desired flow quantities are calculated from the dependent variable solution vector at all grid points and the contour subroutine is called with the set of contour values. The contour subroutine computes and plots the various contour curves, usually in the physical domain.

Since any finite difference/finite volume formulation solves the flow field in an ordered set of grid points/cells, the construction and the execution of the contour program is structured on the basic grid cell. We draw all contour curves cell by cell as we sweep through the complete grid. At the corners of a cell, flow function F has values $F1$, $F2$, $F3$, $F4$. It is desired that the contour curve for function level FC need to be plotted. Then along each side of the base grid cell, where cross over points of the contour curve FC occur, they can be found through linear interpolation. By connecting sequentially the cross-over points encountered among the sides, one obtains the part of the contour curve or curves in a given cell corresponding to the contour value FC. By repeating this process for all cells, the complete set of contour curves for the whole domain can be found.

Since the interpolation used to find the contour curve in the base cell is only linear, the accuracy of the contour curve inside the cells is also linear. This does

* DISSPLA is a trademark of ISSCO.

not mean that the solution represented by the contour curves is first order. The discrete solution at the nodes is at as high an order as the solution technique. If one used higher order interpolation to represent the discrete data, then the contour curves represent not just the solution but non-physical/extra smoothing. Higher order interpolations to represent discrete data can also result in an oscillatory solution representation when such is not the case.

Velocity Vector Plotting

Apart from the contours, at times it is also desirable or necessary to look at velocity vectors. This may be to study the location of separation and reattachment points and to see the size of the separation zone. The development of the boundary layer and shear layer can also best be shown by velocity vector plots. The present graphics code provides the option of plotting velocity vectors. To plot the velocity vectors, at every grid point, a line vector with or without an arrow head proportional in length to the absolute value of the velocity at the given grid point is drawn. Instead of the velocity vectors, an option is provided to plot just the velocity direction. In problems where the magnitude of the velocities may change drastically, it has been found convenient to plot the velocity direction.

Graphics for the Multiple Grids

The multiple grid graphics code is based on the single grid graphics code. In the multiple patched grid solution procedure grids are constructed to overlap. When more than one grid is used to solve the flow problem, the major question that arises is what to do in regions where the grids overlap. The solution is obtained in all of the grids and so there are regions in the flow field where multiple solutions are available. The accuracy of the solution on each grid is influenced by grid fineness and grid topology, among overlapping grids the solution accuracy can be quite different. Since the solutions in overlapping regions do not have the same function values or accuracy, any attempt to represent them there will exhibit some non-smoothness.

Though it is true that the solution in the overlapping region is multivalued, if the solution procedure assures smoothness and continuity to the interface boundary, then any one of the solutions in the overlapping region could be used to represent the global solution. In the solution procedure, we order the grids with assigned indices in some sequence. The graphics plotting is done in the reverse sequence. In general, the coarsest grid is the first grid, and any finer grid interior to it will have a higher index value. To plot the solution in the global domain, the grid with a highest number (finest grid) and most accurate solution will be plotted first. Next the solution in the lower grids will be plotted sequentially. In regions of overlap, only the finer grid with higher index values is used. It is of interest to note that the base grid is subdivided by the higher level grids and solution in the finer grid regions (except for minimal necessary overlap) are available only from the finer grid solutions and not from the coarse grid.

In Figure 28a we have shown an example of overlapping grids for a supersonic

inlet problem. Figure 28b shows the pressure contour in the global domain. To obtain this plot, the pressure contours in the refined and shock aligned grid were plotted first (with the single grid contour plot). Before the contours in the base grid were plotted, the previously plotted refined grid region was "blanked out" so that no contour lines of the coarse grid solution could subsequently be plotted inside the region. Blanking a curve bounded region is accomplished without special effort using a feature of the DISSPLA graphics program. Finally, the base grid solution is plotted only in the non-blanked regions. For all partitioned grids, like the base grid in this case, we have a special subroutine that plots the contour curves on the integrable cells of the base grid. The part of a contour line outside of a blanked region for a cell partially overlapping such a region is plotted up to the blanking boundary.

The above choice of solution representation does not guarantee smoothness and continuity of contours along the boundaries of overlapping grids. The available discrete solution itself is nonsmooth due to the spatial discretization error being different in each grid. Without adding additional smoothing, it is not possible to represent the multiple grid solution with smoothness and continuity. We have chosen not to add any smoothing but to represent the best available solution. The technique has a virtue of exhibiting the extent of truncation errors between grids and making evident places where more refinement may be needed. In our numerical studies, the above choice of contour plotting in multiple grids seems to represent the solution very well.

Implicit Upwind TVD Schemes with DDADI Approximate Factorization

Methods of higher than first order accuracy in the spatial difference approximations are not monotonicity preserving, i.e. lead to oscillation and nonlinear instability, particularly in the vicinity of shock and contact discontinuities. This problem can be overcome by a local reduction to first order based on a change in eigenvalue sign[15,17] or with greater generality (and effectiveness in multidimensions) by the use of flux limiters. Locally one dimensionally monotonicity preserving or total variation diminishing (TVD) limiters have been given by van Leer[32,33] for the scalar equation with Fromm's method. The first of these, now operating on conservative split partial flux differences, has been extended to systems of equations by Yang[34,35]. A second limiter has been given by Harten[36] for an (unlimited) Lax-Wendroff central difference method. Harten's limiter switches to upwind differencing in expansions. Similar to the limiter of reference 33 for Fromm's scheme, but written for the scalar characteristics representation embedded in the splitting of systems of equations, are limiters given by Chakravarthy and Osher[37]. They have given, in a simple one parameter format, the general class of spatially second order biased upwind schemes that are linear combinations of central and upwind differencing. The above three limiters were extended in partial flux difference split pieces to systems of equations and adapted to implicit methods in reference 38.

Unconditionally stable linearized block implicit schemes in delta form can be constructed, e.g. Warming and Beam[39], with first order upwind differencing on the left hand side (LHS) of the difference equations and second order biased upwind (flux limited) differencing on the right hand side (RHS). Approximate factorizations of the LHS block matrix lead to labor and storage efficient, locally one dimensional solution procedures that may be block tridiagonal, block bidiagonal, or approximately scalar[17,40,41].

Implicit schemes with LU decompositions for hyperbolic equations were constructed by Jameson and Turkel[42]. One of their important findings is that the resulting three-dimensional alternating direction algorithm is unconditionally stable in the linear case and also yields a steady-state solution which is independent of time step so long as each factor of the L and U decompositions is diagonally dominant.

For upwind schemes, Lombard, et. al.[17] have given a simple diagonally dominant approximate factorization (DDADI) that retains the contributions (absolute values of the eigenvalues) for all coordinate directions on the diagonal block in each factor. The approach leads to ADI block tridiagonal and block bidiagonal schemes that have been found in numerical experiments to be more robust than approximate factorizations[7,43] in which eigenvalue contributions are separated among the factors. The DDADI approximate factorization has also led to a class of significantly more rapidly convergent single data level algorithms[23] that use symmetric Gauss-Seidel relaxation.

In the present study, following the DDADI approach, we describe new upwind second-order TVD implicit algorithms for the Euler and Navier-Stokes equations.

Some preliminary computational results are presented for 2-D and axisymmetric flows.

Numerical Algorithms

We consider the 2-D Euler equations of gasdynamics in general curvilinear coordinate system

$$\partial_\tau Q + \partial_\xi F + \partial_\eta G = 0 \tag{15}$$

where $Q = \hat{Q}/J$ and $F = (\xi_x \hat{F} + \xi_y \hat{G})/J$, $G = (\eta_x \hat{F} + \eta_y \hat{G})/J$, and $J = \xi_x \eta_y - \xi_y \eta_x$, the metric Jacobian. Where $\hat{Q} = (\rho, \rho u, \rho v, e)^T$ is the conservative variables, $\hat{F} = (\rho u, \rho u^2 + p, \rho uv, u(e+p))^T$ and $\hat{G} = (\rho v, \rho vu, \rho v^2 + p, v(e+p))^T$ are the flux vectors in Cartesian coordinates. Here ρ is the gas density, u, v are the gas velocity components, p the pressure and the total energy $e = p/(\gamma - 1) + \frac{1}{2}\rho(u^2 + v^2)$.

We employ splittings of the adjacent two point conservative flux difference in the Lombard-Yang generalized Roe forms[44,45]

$$\Delta F^{\pm} \equiv \hat{A}^{\pm} \tilde{A} \Delta Q \equiv \tilde{A}^{\pm} \Delta Q \tag{16a}$$

$$\equiv \hat{A}^{\pm} \Delta F = \hat{A}^{\pm} \Delta A Q \tag{16b}$$

with the projection operators $\hat{A}^{\pm} = (\overline{M}\ \overline{T}\ I^{\pm}\ \overline{T}^{-1}\ \overline{M}^{-1})$ providing partitioning according to the signs of the eigenvalues by $I^{\pm} = \frac{1}{2}(I \pm \mathrm{sgn}(\Lambda))$. Here the matrices $\overline{M}^{-1}$ and $\overline{T}^{-1}$ give the discrete difference transformations between conservative and primitive, and primitive and characteristic variable representations respectively.

With two splittings CSCM[17] and CFDS[35] we can construct implicit upwind schemes, respectively, linearizing the flux differences in the forms (16a) and (16b).

The first-order upwind implicit scheme using backward Euler time differencing and linearization based on the form 16b, for example, can be given as

$$[I + h\hat{A}^{+}_{j-\frac{1}{2},k}\Delta_{j-\frac{1}{2},k}A + h\hat{A}^{-}_{j+\frac{1}{2},k}\Delta_{j+\frac{1}{2},k}A + h\hat{B}^{+}_{j,k-\frac{1}{2}}\Delta_{j,k-\frac{1}{2}}B + h\hat{B}^{-}_{j,k+\frac{1}{2}}\Delta_{j,k+\frac{1}{2}}B]\delta Q^{n}_{j,k}$$
$$= \mathrm{RHS}_{\xi} \quad + \quad \mathrm{RHS}_{\eta} = \mathrm{RHS} \tag{17}$$

where

$$\mathrm{RHS}_{\xi} = -h\hat{A}^{+}_{j-\frac{1}{2},k}\Delta_{j-\frac{1}{2},k}F - h\hat{A}^{-}_{j+\frac{1}{2},k}\Delta_{j+\frac{1}{2},k}F$$

and

$$\mathrm{RHS}_{\eta} = -h\hat{B}^{+}_{j,k-\frac{1}{2}}\Delta_{j,k-\frac{1}{2}}G - h\hat{B}^{-}_{j,k+\frac{1}{2}}\Delta_{j,k+\frac{1}{2}}G$$

Here h is the time step, and

$$\delta Q^{n}_{j,k} = Q^{n+1}_{j,k} - Q^{n}_{j,k}$$

$$\Delta_{j-\frac{1}{2},k}F = F_{j,k} - F_{j-1,k}, \quad \Delta_{j,k+\frac{1}{2}}G = G_{j,k+1} - G_{j,k}$$

Block Tridiagonal Approximate Factorization for the Implicit LHS

We will couch the remainder of the discussion of some efficient solution procedures in a simplified notation based on the form 16a with obvious correspondence to the form 16b. Then equations (17) can be expressed in the matrix form

$$[-A^{+}\ ,\ -B^{+}\ ;\ I + |A| + |B|\ ;\ B^{-}\ ,\ A^{-}\ ]\delta Q = \mathrm{RHS} \tag{18}$$

The LHS of equation (18) may be approximately factored in the DDADI form

$$[\ -A^{+}\ ,\ D\ ,\ A^{-}\ ]D^{-1}[-B^{+}\ ,\ D\ ,\ B^{-}\ ]\delta Q \tag{19}$$

with $D = I + |A| + |B|$. Equation (19) gives the block tridiagonal solution sequence

$$\begin{aligned} [\ -A^{+}\ ,\ D\ ,\ A^{-}\ ]\delta Q^{*} &= \mathrm{RHS} \\ [\ -B^{+}\ ,\ D\ ,\ B^{-}\ ]\delta Q^{n} &= D\delta Q^{*} \end{aligned} \tag{20}$$

$$Q^{n+1} = Q^{n} + \delta Q^{n}$$

Second Order TVD Schemes

The RHS of the above schemes based on equations (17) is only first-order in time and space, and in general is not sufficient for flow resolution. In this study we further investigate the possibility of replacing the RHS by robust second-order methods and retaining the unconditionally stable LHS to achieve an efficient algorithm for steady-state calculations.

In the following we give two second-order flux limited difference approximations written for the ξ direction. As is common practice, the schemes are written as a first order method with added flux limited correction terms that in the absence of limiting render the method second-order accurate.

Scheme I, Adapted Lax-Wendroff/Harten

First, a modified flux vector is defined for a hyperbolic system of conservation laws based on the characteristic flux difference splitting concept. Then the limited second order method couched as a first order upwind method is

$$\mathrm{RHS}_\xi = -h\hat{A}^+_{j-\frac{1}{2},k}\Delta_{j-\frac{1}{2},k}F^M - h\hat{A}^-_{j+\frac{1}{2},k}\Delta_{j+\frac{1}{2},k}F^M \tag{21}$$

where F^M is the modified flux vectors. The value of F^M at nodal point j,k is given by

$$F^M_{j,k} = F_{j,k} + E_{j,k} \tag{22}$$

where F is the original flux vector and E is an additional vector of second order correction terms remaining to be defined.

The column vector E at nodal point j,k is $E_{j,k} = (e_{1_{j,k}}, e_{2_{j,k}}, ..., e_{4_{j,k}})^T$ with its l components given by

$$e_{l_{j,k}} = s_{l_{j+\frac{1}{2},k}} \min(|\tilde{e}_{l_{j+\frac{1}{2},k}}|, |\tilde{e}_{l_{j-\frac{1}{2},k}}|), \qquad \text{when} \quad \tilde{e}_{l_{j+\frac{1}{2},k}}\tilde{e}_{l_{j-\frac{1}{2},k}} \geq 0,$$

$$= 0, \qquad \text{when} \quad \tilde{e}_{l_{j+\frac{1}{2},k}}\tilde{e}_{l_{j-\frac{1}{2},k}} \leq 0, \tag{23}$$

where $\tilde{e}_{l_{j+\frac{1}{2},k}} (l = 1, 2, ..., 4)$ are components of the following column vector

$$\tilde{E}_{j+\frac{1}{2},k} = \mathrm{sgn}A_{j+\frac{1}{2},k}\Delta_{j+\frac{1}{2},k}F/2 - hA_{j+\frac{1}{2},k}\Delta_{j+\frac{1}{2},k}F/2 \tag{24}$$

and

$$s_{l_{j+\frac{1}{2},k}} = \mathrm{sgn}(\tilde{e}_{l_{j+\frac{1}{2},k}}) \tag{25}$$

The sgn A in equation (24) is given by

$$\mathrm{sgn}\ a = MT_\xi \mathrm{diag}\{\mathrm{sgn}\ a_{l,\xi}\}T_\xi^{-1}M^{-1} \tag{26}$$

In equation (21) with (22) the first order terms

$$\hat{A}^{\pm}\Delta F = \Delta F^{\pm} \tag{27}$$

can be represented alternatively using the flux vector splittings of Steger and Warming[43] or van Leer[46]. The latter introduces numerical dissipation that render solutions in the vicinity of shocks and contacts monotone.

Scheme I can be implemented as an implicit relaxation scheme as in equation (17) or as a second order time accurate time split explicit method given by

$$Q^{n+2}_{j,k} = L_\xi L_\eta L_\eta L_\xi Q^n_{j,k} \tag{28}$$

For the L_ξ operator in the ξ-direction, we have for example the first intermediate result

$$Q'_{j,k} = Q^n_{j,k} + \mathrm{RHS}_\xi \tag{29}$$

with RHS_ξ given by equation (21). Results for Scheme I in an implicit relaxation method applied in transonic flow have been given in reference 38. Here we give results for the explicit scheme with van Leer[46] flux splitting for the first order upwind terms[47] applied[48] to 2-D unsteady strong shock diffraction around a hypersonic orbital transfer vehicle (AOTV) configuration. The unsteady problem has potential relevance both in maneuver and in simulating the effect of nonuniformity in the upper atmospheric flight regime.

Figure 29 shows the body shape in a computational grid generated with the interactive algebraic procedure. In Figures 30a and 30b respectively we show pressure and Mach contour plots at an instant in time for a case run at Mach 30, $\gamma = 1.1$ and 15° angle of attack. Other work[49] has shown important dependencies such as shock standoff distance and temperature on the value of γ. In future work we will introduce aspects of the present accurate and robust numerical methodology into upwind codes incorporating variable γ based in equilibrium and nonequilibrium reacting gas procedures.

Scheme II, Adapted and Extended Fromm/van Leer, Chakravarthy-Osher

The scheme is

$$\begin{aligned}(\mathrm{RHS})_\xi = &-h\Delta F^+_{j-\frac{1}{2}} - h\Delta F^-_{j+\frac{1}{2}} \\ &+ \frac{h}{4}(\widetilde{\widetilde{\Delta F}}^+_{j-\frac{1}{2}} - \widetilde{\Delta F}^+_{j+\frac{1}{2}}) + (\widetilde{\Delta F}^-_{j+\frac{1}{2}} - \widetilde{\widetilde{\Delta F}}^-_{j-\frac{1}{2}})\end{aligned} \tag{30}$$

where the $\widetilde{\Delta F}$ and $\widetilde{\widetilde{\Delta F}}$ are respectively backward and forward limited flux differences. Following reference 37 for example,

$$\widetilde{\Delta F}^+_{j+\frac{1}{2}} = (\overline{M}\,\overline{T})_{j+\frac{1}{2}}\,\mathrm{minmod}\,(\Delta f^+_{j+\frac{1}{2}}, 3\Delta f^+_{j-\frac{1}{2}})$$

and

$$\widetilde{\widetilde{\Delta F}}^+_{j-\frac{1}{2}} = (\overline{M}\,\overline{T})_{j-\frac{1}{2}}\,\mathrm{minmod}\,(\Delta f^+_{j-\frac{1}{2}}, 3\Delta f^+_{j-\frac{1}{2}}). \tag{31}$$

Here the characteristic partial flux differences are

$$\Delta f^{\pm} = I^{\pm}\, \overline{T}^{-1}\, \overline{M}^{-1}\, \Delta F \tag{32}$$

and

$$\text{minmod}(x, y) = \text{sign}(x) \max[0, \min(|x|, y\ \text{sign}(x))].$$

As an alternative to limiting the characteristic partial flux differences we also consider here a new scheme limiting in the conservative split partial flux differences, in conformity with scheme I. Then we replace equation (31) with, for example

$$\widetilde{\Delta F}^{+}_{j+\frac{1}{2}} = \text{minmod}(\Delta F^{+}_{j+\frac{1}{2}}, 3\Delta F^{+}_{j-\frac{1}{2}}) \tag{33}$$

Scheme I can be disected to show that in regions of compression the scheme yields a second order central difference approximation and in regions of expansion, second order upwind. Chakravarthy and Osher[37] gave a one parameter family of flux limited second order schemes that can be seen to be linear combinations of the central and upwind methods. The Fromm scheme given here for illustration is the case of $\frac{1}{2}$ central and $\frac{1}{2}$ upwind methods. Another case with $\frac{2}{3}$ central differencing and $\frac{1}{3}$ upwind, yields a third order accurate method.

Computational experiments with the one parameter family of second order schemes for the advective terms of the compressible Navier-Stokes equations have been performed in the context of a much tested 45° - 15° transonic nozzle problem, Figure 31. Figure 32a shows Mach contours in the vicinity of the throat for the unlimited second order upwind method. Limiting in both the characteristic and conservative partial flux difference pieces has been carried out. Here we show in Figures 32b and 32c Mach contours for the Fromm scheme with the two approaches to limiting. The unlimited upwind scheme captures the weak shock somewhat more sharply but is considerably less robust. Limiting in the conservative flux split pieces is simpler to implement and, taking into account eigenvector variation, may have better nonlinear stability than limiting in the characteristic representation; but the solution also appears less smooth behind the weak shock.

Application of 3-D Single Level Algorithm to Multiple Nozzle Flow on Segmented Composite Mesh

A clustered multi rocket nozzle shrouded exhaust system provides a problem of relevant kind and geometric complexity typical of those needing advanced computational techniques to analyze. Here the symmetric Gauss-Seidel implicit method of planes algorithm described earlier is adapted to a segmented composite grid.

The grid covers a "pie slice" sector bounded by symmetry planes through a circular array of engines around a single engine at the center. The symmetry planes pass through the axis of the center engine and either through or between the nozzles

of the outer engines. Figure 33a shows a 3-D perspective view of the surface mesh of the computational domain. Figure 33b shows a symmetry plane mesh through the center and an outer engine, and Figure 33c, the projection of a cross stream mesh surface in the shrouded exhaust region. Figure 34, which relates to Figure 33c, shows the segmented composite mesh coordinate topology. Where the index L is for the azimuthal coordinate ψ of the outer engine associated mesh patch and, similarly, K is for the radial like coordinate η, the center engine associated mesh patch sector is naturally mapped onto a segment of the outer engine grid topology with continuity of the η coordinate in $K1+1 \leq K \leq KMAX$ and $1 \leq L \leq L1$.

Boundary Conditions

The segmented composite mesh approach requires the facility to impose different boundary condition procedures on limited segments of coordinate curves piecewise fitted to boundaries. Segments of viscous wall boundary are treated with implicit characteristic based procedures as described in reference 17. Boundary segments of inviscid symmetry planes can be treated by differencing to out of domain data obtained by applying symmetry relations operationally and explicitly but with unconditional stability based on DDADI as explained earlier in this report for interior patched mesh boundaries. Alternatively, symmetry boundaries can be treated completely locally like inviscid walls by an implicit matrix procedure involving characteristic relations to the boundaries, augmented by local invariance of the zero normal velocity component as in reference 17, and extrapolations of temperature and tangential velocity components through constructed stable characteristic like relations as described in reference 50.

Singular poles such as at $K = 1$ and $KMAX$ of the grid topology are buried at half cell spacing in the mesh. Operationally explicit DDADI differencing is carried out from first interior points to cross pole data obtained from symmetry conditions as given in Figure 34 for the pole at $K = 1$.

Figure 35 shows Mach contours on a cross flow coordinate surface intersecting the backward facing step outside the exit of the outboard nozzle. This region is impacted by the complicated interaction of a weak shock exiting the nozzle and an expansion fan whose strength at the nozzle exit corner is influenced by the size of the local backward facing step. Figures 36a, b and c show Mach contours for longitudinal mesh surfaces associated with the outer nozzle flow. The surfaces intersect the inter nozzle symmetry plane, respectively, in the $L1$ corner, at the minimum step between outboard nozzles, and at the maximum step in the corner where the shroud intersects. The latter figures show the nozzle weak shock, the base corner expansion and then the recompression shock against the symmetry plane, and finally the extensive flow separations in the corners. The extent of departure from axisymmetry in the plume region caused by the azimuthally varying base step heights can be appreciated. Figure 36d shows Mach contours in the symmetry plane through the inner and outer nozzle centers. Here appears the turbulent viscous wake

of the inter-nozzle exit step as another captured feature of the multi-nozzle plume flow.

Computational Experiments in Patched Mesh Topology and Solution Accuracy

For high Reynolds number viscous flows, particularly for massively separated base flows computed in the efficient Baldwin-Lomax thin layer approximation, mesh topology has a great deal to do with accuracy of the resulting solution. Occurring in numerous aerospace applications, separated base flow is of significant interest to predict for it's impact on drag and moments on aircraft, projectiles and tactical missiles. It is of interest for efficient design of dump combustors and to avoid chemical erosion problems in liquid propellant injector systems. Base flow is also of interest for thermal protection requirements on multi-rocket powered vehicles such as the Space Shuttle and hypersonic reentry bodies such as the Galileo Probe and the Aeroassisted Orbital Transfer Vehicle (AOTV).

In recent years, the evolving computational capability for viscous flows has led to attempts to analyze such base flows numerically. The widely perceived need to assess the accuracy of the techniques particularly for solving the compressible Navier-Stokes equations for turbulent base flows, has led to experiments with broadly participated computational efforts featuring axisymmetric afterbody flows with a centered propulsive jet. The time dependent Navier-Stokes solutions have been computed by Deiwert, Andrews and Nakahashi[51] and Sahu and Nietubicz[52]. A novel feature of that work is the use of flow structure adaptive meshing.

Of particular relevance here are computations of Sahu and Nietubicz[52] and Thomas, Reklis, Roloff and Conti[53] for the MICOM model tactical missile experiment[54] at freestream Mach number 1.4. The axisymmetric flow experiment featured a tangent ogive cylinder body, Figure 37, terminating in a square cylindrical base. A centered nozzle with flush exit occupied only 0.2 base diameters of the model which was 9 diameters long. The nozzle exit Mach number was 2.7 for an underexpanded jet with pressure ratio 2.15 relative to freestream.

Sahu and Nietubicz[52] employed the Beam-Warming[7] central difference algorithm with the Baldwin-Lomax[8] algebraic turbulent eddy viscosity model and the thin layer Navier-Stokes approximations. Since viscous terms were not applied in the streamwise direction, the base wall was treated inviscidly. Thomas, et al.[53], who employed the Thomas and Lombard version of the central difference algorithm, applied the full Navier-Stokes equations with eddy viscosity computed from alternative two equation turbulence models. Both groups of computations were made without knowledge of the experimental results except for data given along a line 1.6 diameters upstream of the base to serve as an inflow computational boundary. Unused data was also given on a lateral boundary 1.6 base radii from the model axis.

Both insight and computational experiments suggest there are two ways that topology influences solution accuracy. The first is through the efficiency of utiliza-

tion of mesh point resources to achieve balanced resolution. The second is through alignment with and natural accurate capture of flow structures on the mesh.

Here we report on the first two parts of a continuing capsule study of the impact of computational meshing strategies on solution accuracy in propulsion base flow. The MICOM model problem with the experimental and previous computational data base was chosen as the vehicle for the study. The first part of the study dealt with two complementary composite mesh topologies. The first is a dual wrap-around composite mesh constructed in two blocks. The second is a composite step mesh constructed in three blocks. Based on the techniques described earlier in this report, the blocks of smooth mesh are generated algebraically in subpatches.

The step mesh, shown in Figure 38b, is similar to those employed in references 52 and 53, and naturally fits and is simple to construct for (near) right angle corners such as occur at the cylinder wall and nozzle exit junctures with the base. The wrap around mesh, Figure 38a, provides a continuity of the thin layer viscous approximation around the base corners and is thought to generally make most sense of locally one dimensional algebraic eddy viscosity modeling (modified Baldwin-Lomax) which we employ here. Details of the turbulence model and the application of the CSCM method are given in reference 55.

Propulsion Base Flow Results

For the two base flow meshes, we present results in Mach number contour plots. The results for the two meshes in comparison with each other and with the results of Sahu and Nietubicz[52] and Thomas, et al.[53] are quite interesting and informative.

In Figures 39a and 39b we show Mach contour plots for the wrap-around and step base flow meshes. The two plots exhibit the same flow structures – expansions at the nozzle and upper base corners, followed by weak turning (recompression) shocks in the outer wake flow and inner jet flows, large stagnant separation bubbles in the base region, Mach disc and reflected shock in the jet flow, and finally wake expansion downstream of the recompression neck behind the turning shocks.

In addition, we see shear layers emanating from the nozzle and upper base corners and turning with the recompressing flow to be carried down the wake. Also evident in the figures is the effects of the structure of the slow recirculating flows in the separated base region. All the above structure is in very good qualitative agreement with that shown in plots in reference 52 and 53.

Considering the contour plots and the associated meshes among our results and those referenced, two observations come to mind. The first is that different solutions obviously express different structures with greater or lesser accuracy. The second is that all the meshes employed here and in the references cited employ locally one dimensional clustering and stretchings that emphasize resolution in certain regions or directions at the expense of others. Where grid points are well distributed relative to resolving a particular flow feature, it is sharp and (presumably) well located. Where not, the converse holds. Another more significant mesh dependent

feature is apparent in the formation region of the shear layers from the nozzle base corner. In the wrap-around mesh case of Figure 38a, the boundary layer separates a short distance around the corner at the base wall, whereas, in the step mesh case the separation appears sharply at the corner. Associated with this mesh topology dependent phenomena are observable differences in the angle and possibly energy of the expansion jet down the near base shear layer. The wrap-around grid has much better resolution near the tail of the separation bubble, and also generally better resolution over shear layers on either side of the bubble.

What one might term simple composite mesh schemes of the type employed in Figures 38a and 38b have the obvious flaw that they are comparatively inflexible with regard to continued grid point clusterings throughout the mesh once clustering has been initiated of necessity somewhere, as for example in boundary layers. The rigidity leads to wasted mesh point resources in some inappropriately clustered regions at the expense of needed resolution in others.

The techniques of multiple patched meshes with overlap to stably exchange data through interpolation at interior patch boundaries as described earlier in this report offer the freedom to utilize mixed topologies and commit mesh resources as appropriate to various zones of the problem. The second part of the study employed the multiple patched grid techniques to effect globally a hybrid topology of the wrap-around and step mesh types.

Figure 40a shows the patched grid in the large where it appears as a step mesh but with less clustering in the base wake region *vis a vis* Figure 38b. The wrap-around feature is incorporated in patches of refined overset mesh that are local to the upper and lower exterior corners at the base. Figure 40b shows a local detail of the overset patch boundary at the lower (nozzle exit) corner. Also shown are the overlapping boundaries of other grid patches that intersect in the vicinity.

Figure 41 shows a Mach contour plot for the solution on the hybrid grid. By comparison with Figures 39a and 39b, all flow structure features of the solution on the multiple patch grid appear more sharply resolved though the total number of points in each global grid is comparable. Finally, Figure 42 provides a comparison of base pressure results among computations and the experiment of Petrie and Walker[54]. Except near the nozzle exit corner, the results for our computation on the step mesh of Figure 38b is quite close to that of Sahu and Nietubicz[52] and to reduce confusion is not plotted. All the computed results show a similar wave pattern in the base associated with the two counter-rotating circulation cells. That this structure is not apparent in the experimental results raises some questions. Further study of this problem as to mesh topology, adaptive refinement and turbulence modeling will prove useful in advancing understanding in the difficult and important area of base flow computation.

3. Professional Personnel

Professional researchers who contributed to this project are
Dr. Charles K. Lombard, Principal Investigator
Professor Joseph Oliger, Consultant
Dr. Marcel Vinokur, Consultant
Dr. Ethiraj Venkatapathy
Dr. Jorge Bardina
Dr. N. Nagaraj
Dr. J. Y. Yang
Dr. R. C.-C. Luh

4. Interactions

The research described in this report has to this point been partially presented in the form of a paper on algebraic grid generation by Vinokur and Lombard (reference 5), a SIAM meeting paper (reference 19) by Oliger and Lombard on boundary procedures for bidiagonal alternating sweep schemes and a Computational Fluid Dynamics Seminar at NASA-Ames Research Center by Lombard on the Universal Single Level Implicit Algorithm. The latter invoked tremendous interest and discussion.

The research has spawned four meeting papers on the single level relaxation algorithm – references 23, 24 and 25 and

Lombard, C.K., Raiszadeh, Farhad and Bardina, Jorge: "Efficient, Vectorizable Upwind Implicit Relaxation Algorithms for Three-Dimensional Gasdynamics," SIAM Spring Meeting, Pittsburg, PA, June 1985.

Six papers have been written on interior patch boundary treatment, data structure and applications of patched mesh systems. These are references 28, 29, 31 and 55 of the present report and

Lombard, C.K. and Venkatapathy, Ethiraj: "Implicit Boundary Treatment for Joined and Disjoint Patched Mesh Systems," Workshop on High Reynolds Flows, Nobeyama, Japan, September 1985.

and

Lombard, C.K., Bardina, J., Venkatapathy, E., Yang, J.Y., Luh, R.C.-C., Nagaraj, N. and Raiszadeh, F.: "Accurate, Efficient and Productive Methodology for Solving Turbulent Viscous Flows in Complex Geometry," Presented at the *10th International Conference on Numerical Methods in Fluid Dynamics*, Beijing, China, June 1986 and soon to be published in a bound volume *Lecture Notes in Physics.*

The research has given rise to two papers on the 3-D CSCM-S relaxation algorithm with application to multi rocket engine exhaust flow, a problem of interest to and partially supported by AFRPL. The papers are

Bardina, Jorge and Lombard, C.K.: "Three Dimensional CSCM Method for the Compressible Navier-Stokes Equations with Application to a Multi-Nozzle Exhaust Flowfield," AIAA 85-1193, June 1985.

and

Lombard, C.K., Bardina, Jorge and Raiszadeh, Farhad: "Shrouded Multi-Rocket Engine Plume Flow by an Efficient Upwind Relaxation Algorithm for the Compressible Navier-Stokes Equations," annual meeting of the JANNAF Exhaust Plume Technology Subcommittee, San Antonio, Texas, May 1985.

5. New Discoveries

The Universal Single Level Algorithm for the compressible Euler or Navier-Stokes equations is a new discovery in numerical methods that promises to result in substantial efficiencies in data storage, programming, machine time and human productivity.

References

1. Lombard, C.K., Davy, W.C. and Green, M.J.: "Forebody and Base Region Real-Gas Flow in Severe Planetary Entry by a Factored Implicit Numerical Method – Part 1 (Computational Fluid Dynamics)," AIAA 80-0065, January, 1980.

2. Berger, Marsha J. and Oliger, Joseph: "Adaptive Mesh Refinement for Hyperbolic Partial Differential Equations," *J. of Computational Physics*, Vol. 53, No. 3, March 1984, pp. 484-512.

3. Lombard, C.K.: "Closing Developments in Aerodynamic Simulation with Disjoint Patched Meshes – First Annual Report", Interim AFOSR Report Contract No. F49620-83-C-0084, 1986.

4. Lombard, C.K.: "Closing Developments in Aerodynamic Simulation with Disjoint Patched Meshes – Final Report", AFOSR Report for Contract No. F49620-83-C-0084, 1986.

5. Vinokur, Marcel and Lombard, C.K.: "Algebraic Grid Generation with Corner Singularities," *Advances in Grid Generation*, Vol. 5, Sponsored by ASME Fluids Engineering Div., Symposium on Grid Generation, 1983, ASME Fluids Engineering Conference, Houston, TX.

6. Vinokur, Marcel: "On One-Dimensional Stretching Functions for Finite-Difference Calculations," *J. Comp. Physics* Vol. 50, No. 2, May 1983.

7. Beam, R.M. and Warming, R.F.: "An Implicit Factored Scheme for the Compressible Navier-Stokes Equations," AIAA Paper 77-645, June, 1977.

8. Baldwin, B.S. and Lomax, H.: "Thin Layer Approximation and Algebraic Model for Separated Turbulent Flows," AIAA 73-257, 1973.

8. Schiff, L.B. and Steger, J.L.: "Numerical Simulation of Steady Supersonic Viscous Flow," AIAA-79-0130, January, 1979.

10. Vigneron, Y.C., Rakich, J.V. and Tannehill, J.C.: "Calculation of Supersonic Viscous Flow over Delta Wings with Sharp Subsonic Leading Edges," NASA TM-78500, 1978.

11. Schiff, L.B. and Sturek, W.B.: "Numerical Simulation of Steady Supersonic Flow Over an Ogive-Cylinder-Boattail Body," AIAA-80-0066, January, 1980.

12. Chaussee, D.S., Patterson, J.L., Kutler, P., Pulliam, T.H. and Steger, J.L.: "A Numerical Simulation of Hypersonic Viscous Flows over Arbitrary Geometries at High Angle of Attack," AIAA Paper 81-0050, Jan. 1981.

13. Rai, M.M., Chaussee, D.S. and Rizk, Y.M.: "Calculation of Viscous Supersonic Flows Over Finned Bodies," AIAA-83-1667, July, 1983.

14. Chaussee, D.S. and Rizk, Y.M.: "Computation of Viscous Hypersonic Flow Over Control Surfaces," AIAA Paper 82-0291, January, 1982.

15. Lombard, C.K., Oliger, J. and Yang, J.Y.: "A Natural Conservative Flux Difference Splitting for the Hyperbolic Systems of Gasdynamics," AIAA Paper 82-0976, 1982.

16. Lombard, C.K., Oliger, J., Yang, J.Y. and Davy, W.C.: "Conservative Supra-Characteristics Method for Splitting the Hyperbolic Systems of Gasdynamics with Computed Boundaries for Real and Perfect Gases," AIAA Paper 82-0837, 1982.

17. Lombard, C.K., Bardina, J., Venkatapathy, E. and Oliger, J.: "Multi-Dimensional Formulation of CSCM - An Upwind Flux Difference Eigenvector Split Method for the Compressible Navier-Stokes Equations," AIAA-83-1895CP, AIAA 6th Computational Fluid Dynamics Conference,, Danvers, Mass.

18. Roe, P.L.: "The Use of the Riemann Problem in Finite- Difference Schemes," Seventh International Conference on Numerical Methods in Fluid Dynamics, *Lecture Note in Physics, 141*, pp. 354-359, 1981.

19. Oliger, Joseph and Lombard, C.K.: "Boundary Approximations for Alternating Sweep Implicit Upwind Methods for Hyperbolic Systems," SIAM 1983 Fall Meeting, Norfolk, VA.

20. Yee, H.C., Beam, R.M. and Warming, R.F.: "Stable Boundary Approximations for a Class of Implicit Schemes for the One-Dimensional Inviscid Equations of Gas Dynamics," AIAA Paper 81-1009-CP, 1981.

21. Steger, J.L.: "Implicit Finite Difference Simulation of Flow About Arbitrary Geometries with Application to Airfoils," AIAA Paper 77-665, 1977.

22. Cuffel, R.F., Back, L.H. and Massier, P.F.: "Transonic Flowfield in a Supersonic Nozzle with Small Throat Radius of Curvature," *AIAA J.*, Vol. 7, no. 7, 1969, pp 1364-1372.

23. Lombard, C.K. and Venkatapathy, Ethiraj: "Universal Single Level Implicit Algorithm for Gasdynamics," AIAA 84-1533, AIAA 17th Fluid Dynamics Conference, Snowmass Colorado, June 25-27, 1984.

24. Lombard, C.K., Bardina, J. and Venkatapathy, E.: "AOTV Bluff Body Flow – Relaxation Algorithm" *Thermal Design of Aeroassisted Orbital Transfer Vehicles*, H.F. Nelson, Ed., Progress in Astronautics and Aeronautics, Vol. 96, 1985, pp 85-112.

25. Venkatapathy, Ethiraj and Lombard, C.K.: "Universal Single Level Implicit Algorithm for Gasdynamics," Ninth International Conference on Numerical Methods in Fluid Dynamics, Saclay, France, June 25-29, 1984.

26. Benek, J.A., Steger, J.L., and Dougherty, F.C.: "A Flexible Grid Embedding Technique with Application to the Euler Equations," AIAA 83-1944, July 1983.

27. Eberhardt, David Scott: *A Study of Multiple Grid Problems on Concurrent Processing Computers*, Ph.D. Dissertation, Stanford University, Sept. 1984.

28. Lombard, C.K. and Venkatapathy, Ethiraj: "Implicit Boundary Treatment for Joined and Disjoint Patched Mesh Systems," AIAA-85-1503, 1985.

29. Venkatapathy, Ethiraj and Lombard, C.K.: "Application of Patched Meshes to Viscous and Inviscid Flows," presented at the Sixth GAMM Conference on Numerical Methods in Fluid Mechanics at Gottingen, West Germany, Sept. 1985.

30. Lombard, C.K., Oliger, J. and Yang, J.Y.: "A Natural Conservative Flux Difference Splitting for the Hyperbolic Systems of Gasdynamics," Presented at the Eighth International Conference on Numerical Methods in Fluid Dynamics, in Aachen, West Germany, 1982.

31. Venkatapathy, Ethiraj, and Lombard, C.K.: "Flow Structure Capturing on Overset Patched Meshes," AIAA-85-1690, July, 1985.

32. van Leer, Bram: "Towards the Ultimate Conservative Difference Scheme. II. Monotonicity and Conservation Combined in a Second-Order Scheme," *J. Comp. Phys.* 14, 361-370, 1974.

33. van Leer, Bram: "Towards the Ultimate Conservative Difference Scheme IV. A New Approach to Numerical Convection," *J. Comp. Phys.* 23, 276-299, 1977.

34. Yang, J.Y.: "Second- and Third-Order Upwind Difference Schemes for Hyperbolic Conservation Laws," NASA-TM-85959, July 1984.

35. Yang, J. Y.: "Numerical Solution of the Two-Dimensional Euler Equations by Second-Order Upwind Difference Schemes," AIAA Paper 85-0292, 1985.

36. Harten, A.: "High Resolution Schemes for Hyperbolic Conservation Laws," *J. Comp. Phys.* 49, 357-393, 1983.

37. Chakravarthy, S.R. and Osher, Stanley: "A New Class of High Accuracy TVD Schemes for Hyperbolic Conservation Laws," AIAA Paper 85-0363, 1985.

38. Yang, J.Y., Lombard, C.K. and Bardina, Jorge: "Implicit Upwind TVD Schemes for the Euler Equations with Bidiagonal Approximate Factorization," Presented at the *International Symposium on Computational Fluid Dynamics-Tokyo*, Sept. 1985.

39. Warming, R.F. and Beam, R. M.: "On Construction and Application of Implicit Factored Schemes for Conservation Laws," SIAM-AMS Proceedings, Vol. II, 1977.

40. Pulliam, T. and Chaussee, D.: "A Diagonal Form of an Implicit Approximate-Factorization Algorithm," *J. Comp. Phys.* 39, No. 2, 347-363, 1981.

41. Coakley, T.J.: "Implicit Upwind Methods for the Compressible Navier-Stokes Equations," AIAA Paper 83-1953, 1983.

42. Jameson, A. and Turkel, E.: "Implicit Schemes and LU Decompositions," *Math. Comp.* 37, No. 156, 385-397, 1981.

43. Steger, J. and Warming, R. F.: "Flux Vector Splitting of the Inviscid Gasdynamics Equations with Application to Finite Difference Methods," NASA TM-78605, July 1979.

44. Lombard, C.K., Oliger, J. and Yang, J. Y.: "A Natural Conservative Flux Difference Splitting for the Hyperbolic Systems of Gasdynamics,"Proc. 8th Int. Conf. on Numerical Methods in Fluid Dynmaics, *Lecture Notes in Physics* 170, Ed. Krause, E., 364-370, 1982.

45. Yang, J.Y., Lombard, C.K. and Bershader, D.: "A Characteristic Flux Difference Splitting for the Hyperbolic Conservation Laws of Inviscid Gasdynamics," AIAA Paper 83-0040, 1983.

46. van Leer, Bram: "Proc. 8th Int. Conf. on Numerical Methods in Fluid Dynamics, *Lecture Notes in Physics*, 170, Ed. Krause, E., 507-512, 1982.

47. Yang, J.Y.: "A Hybrid Upwind Scheme for the Computation of Shock-on-Shock Interaction Around Blunt Bodies," Presented at the 10th Internal Conference on Numerical Methods in Fluid Dynamics, Beijing, China, 1986.

48. Yang. J.Y., Luh, R. C.-C. and Lombard, C.K.: "Computation of Time-Dependent Shock Waves Around AOTV in Hypersonic Chemical Equilibrium," Work in progress, 1986.

49. Yang, J.Y., Lombard, C.K. and Bershader, D.: "Computation of Nonstationary Strong Shock Diffraction by Curved Surfaces," Presented at the 15th International Symposium on Shock Waves and Shock Tubes, 1985.

50. Lombard, C.K., Bardina, J. and Luh, R. C.-C.: "Implicit Numerical Boundary Procedures Applied in the CSCM Upwind Algorithm with Characteristic and Characteristic-Like Extrapolations," To be presented at the 5th International Conference on *Numerical Methods in Laminar and Turbulent Flow*, July 1987.

51. Deiwert, G.S., Andrews, A.E. and Nakahashi, K.: "Theoretical Analysis of Aircraft Afterbody Flow," AIAA-84-1659, 1984.

52. Sahu, J. and Nietubicz, C.J.: "Numerical Computation of Base Flow for a Missile in the Presence of a Centered Jet," AIAA-84-0527, 1984.

53. Thomas, P.D., Reklis, R.P., Roloff, R.R. and Conti, R.J.: "Numerical Simulation of Axisymmetric Base Flow on Tactical Missiles with Propulsive Jet," AIAA-84-1658, 1984.

54. Petrie, H.L. and Walker, B.J.: "Comparison of Experiment and Computation for a Missile Base Region Flowfield with a Centered Propulsive Jet," AIAA-85-1618, 1985.

55. Lombard, C.K., Luh, R. C.-C., Nagaraj, N., Bardina, J. and Venkatapathy, E.: "Numerical Simulation of Backward Step and Jet Exhaust Flows," AIAA-86-0432, 1986.

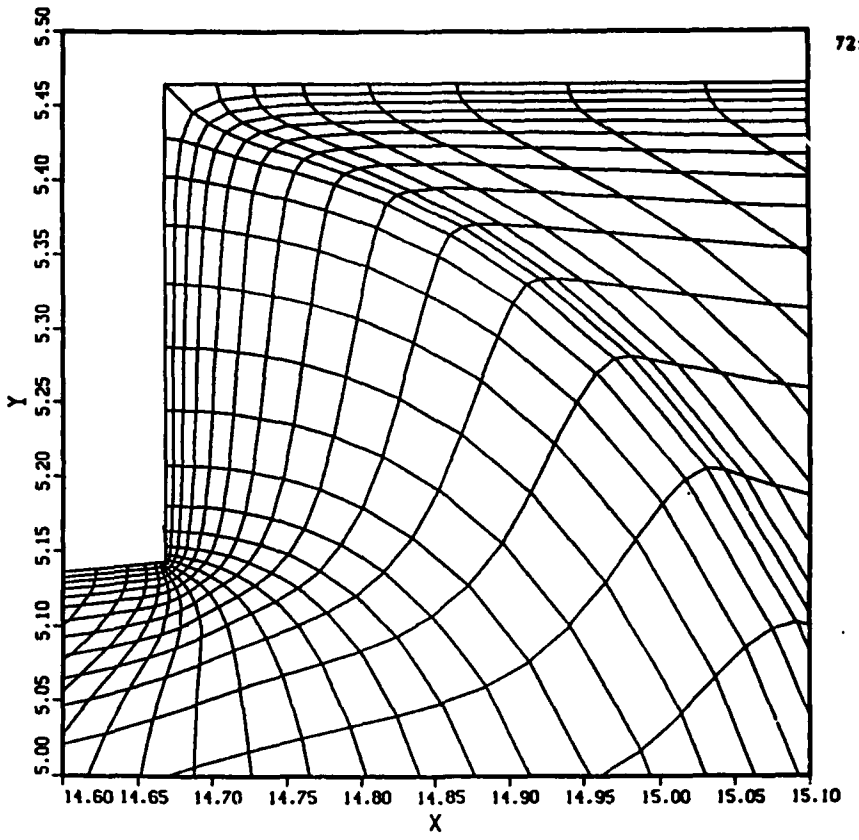

Figure 1. Portion of an algebraically generated computational mesh for a flow domain containing an external and an internal corner.

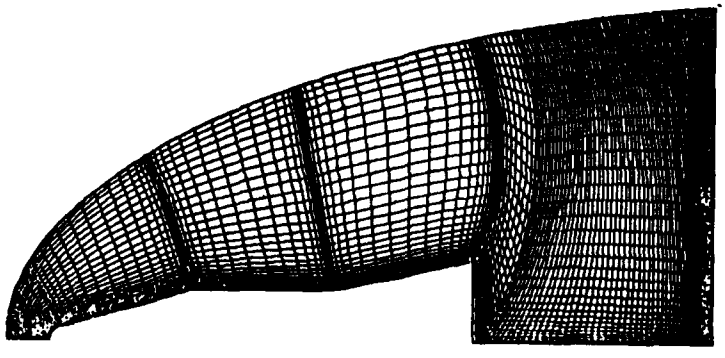

Figure 2. Representative 2-D mesh generated with simplified interactive algebraic procedure.

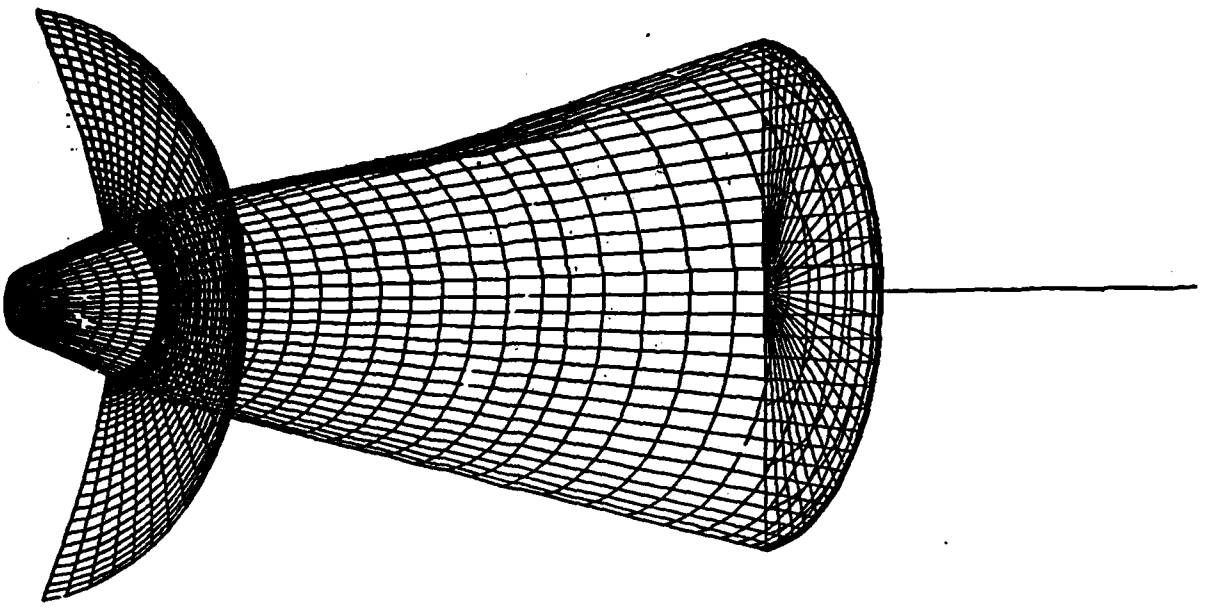

Figure 3. Representative 3-D mesh generated with simplified interactive algebraic procedure.

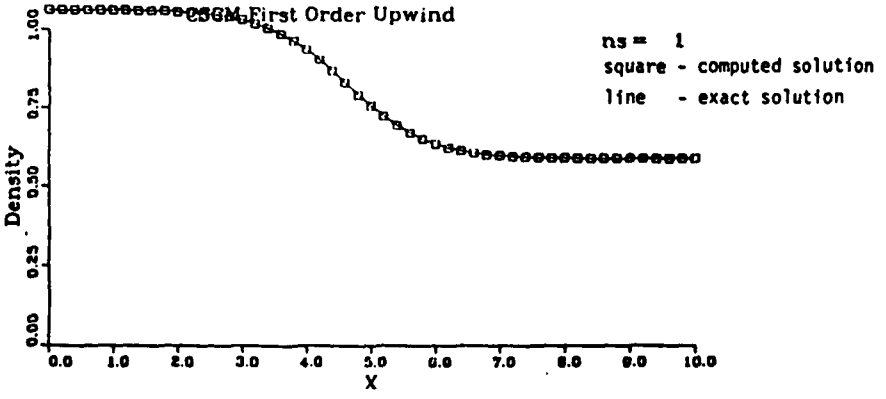

Figure 4. Shubin's diverging nozzle supersonic flow solution developed in one forward sweep from supersonic initial data.

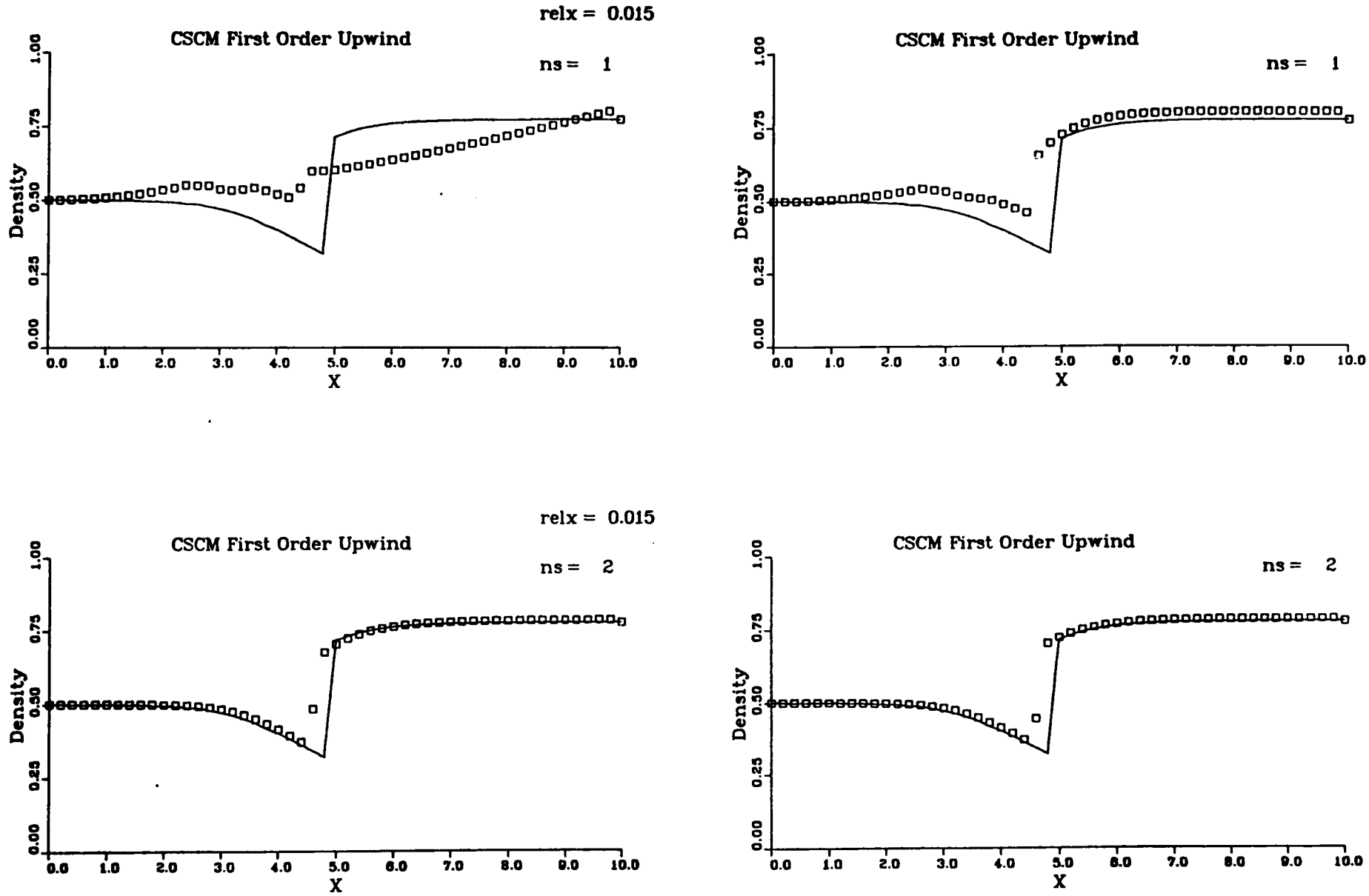

Figure 5. Shubin's diverging nozzle flow solution developed in alternating forward and backward sweeps, one each per global iteration step for five steps. square - computed results , line - exact solution

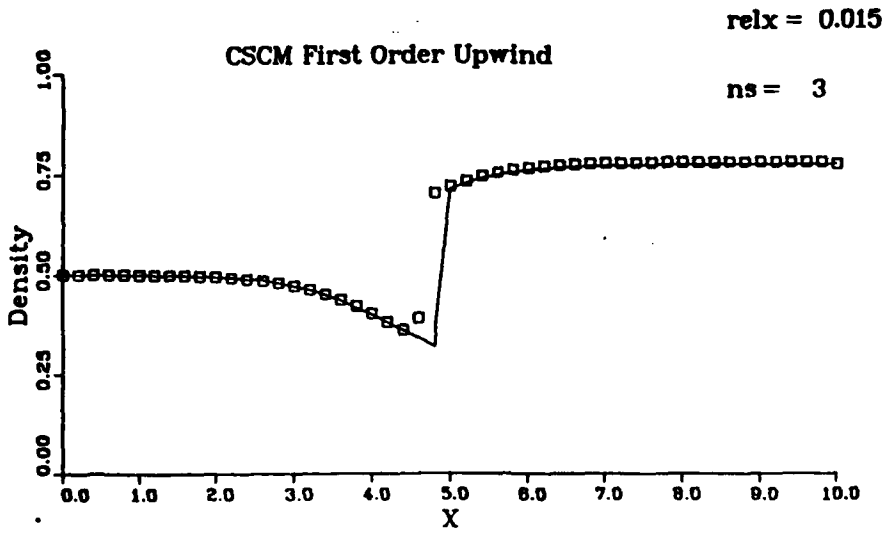

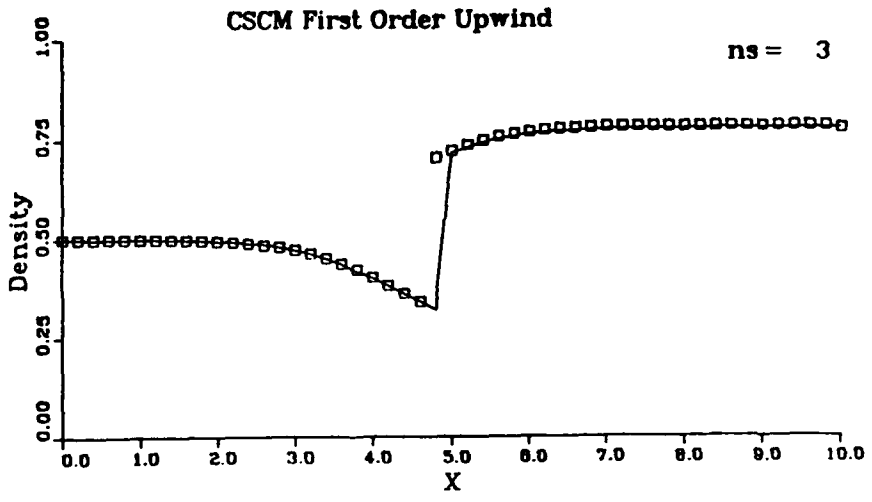

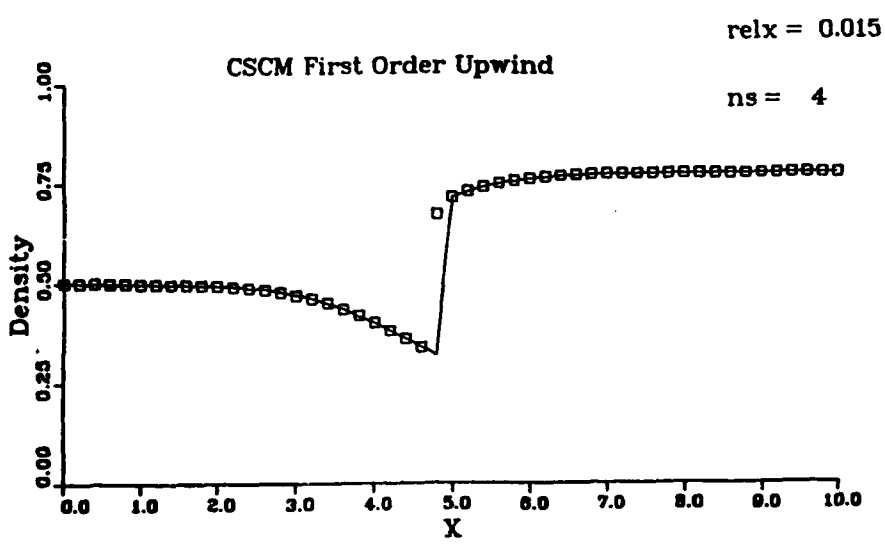

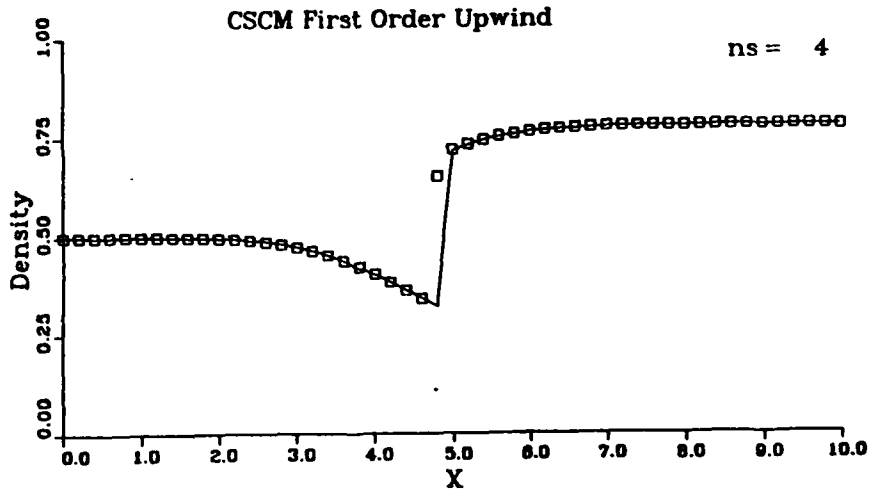

Figure 5. continued

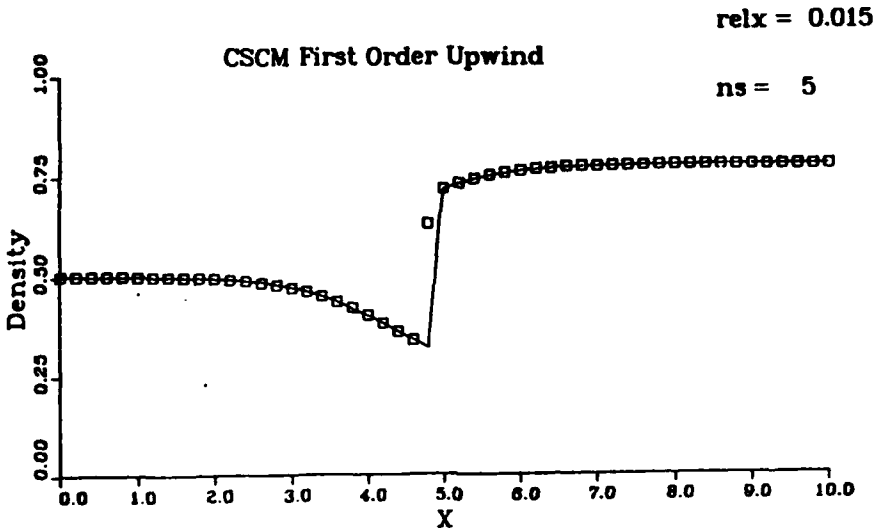

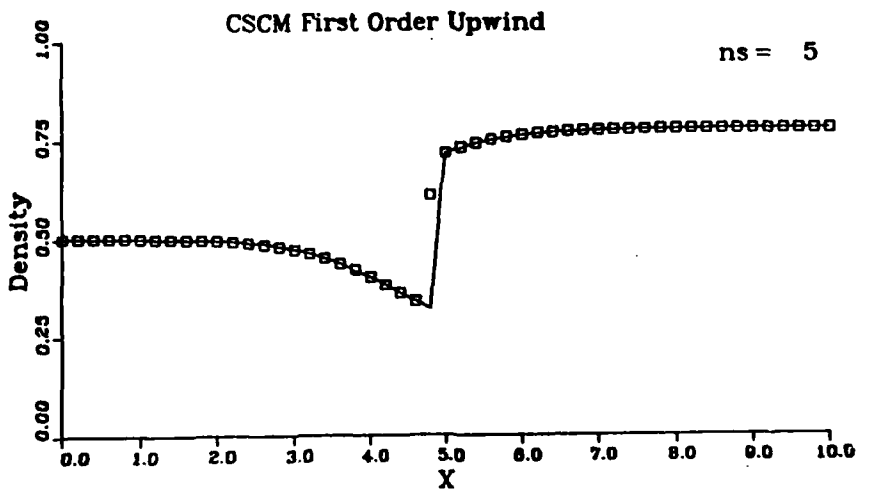

Figure 5. continued

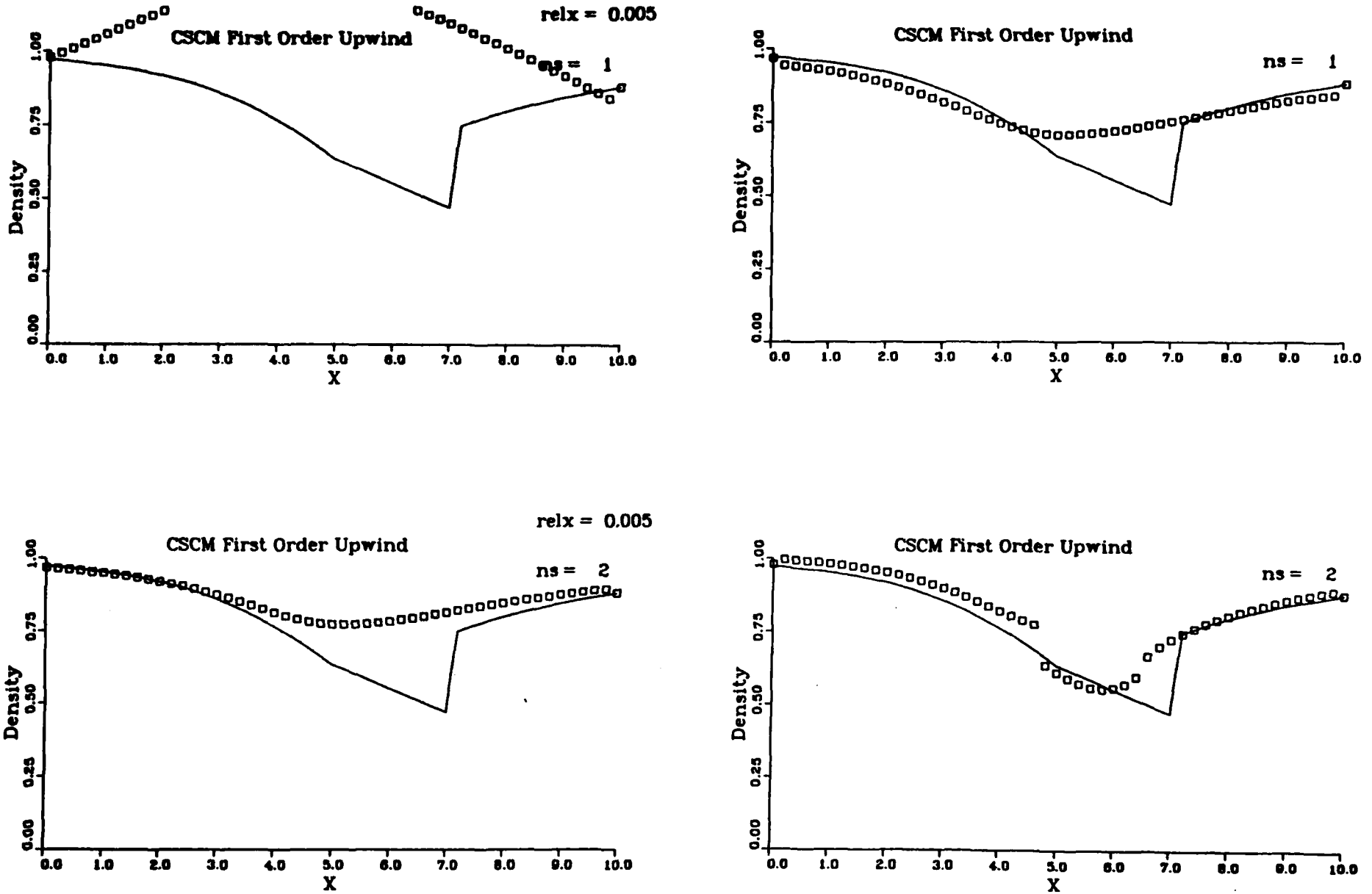

Figure 6. Blottner's converging-diverging supercritical nozzle flow solution developed in alternating direction sweeps for ten global iteration steps. square - computed results , line - exact solution

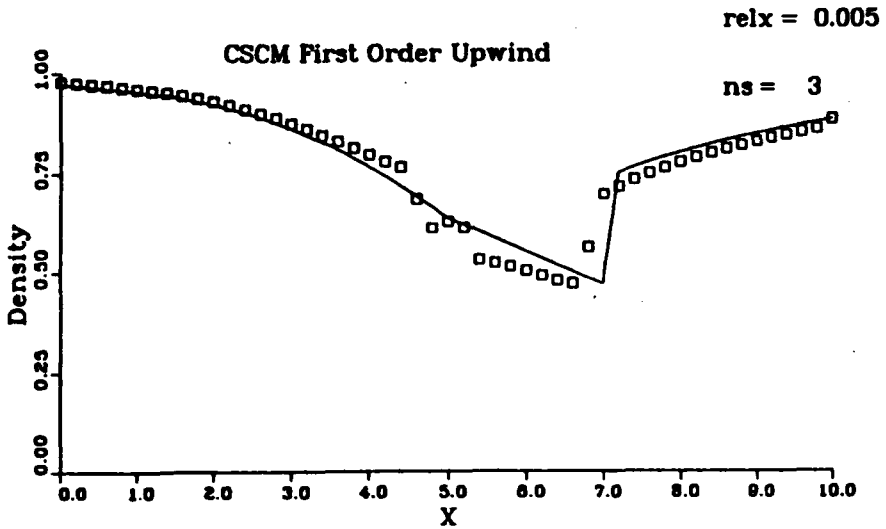

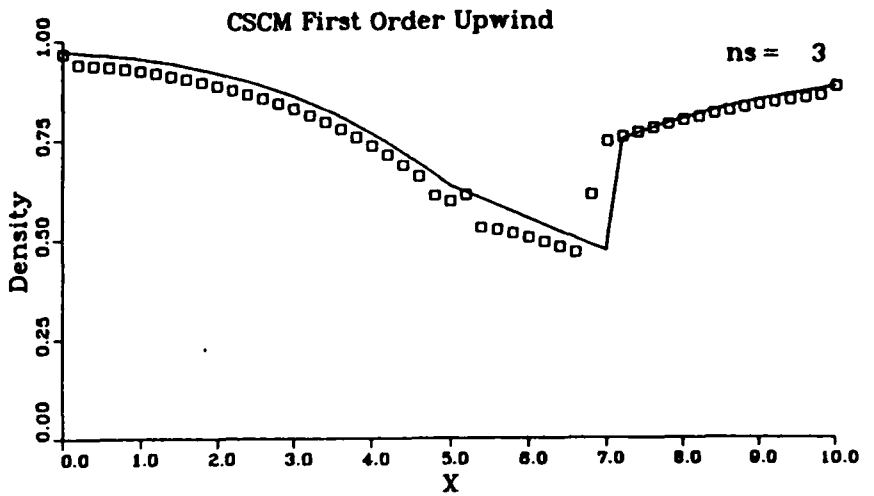

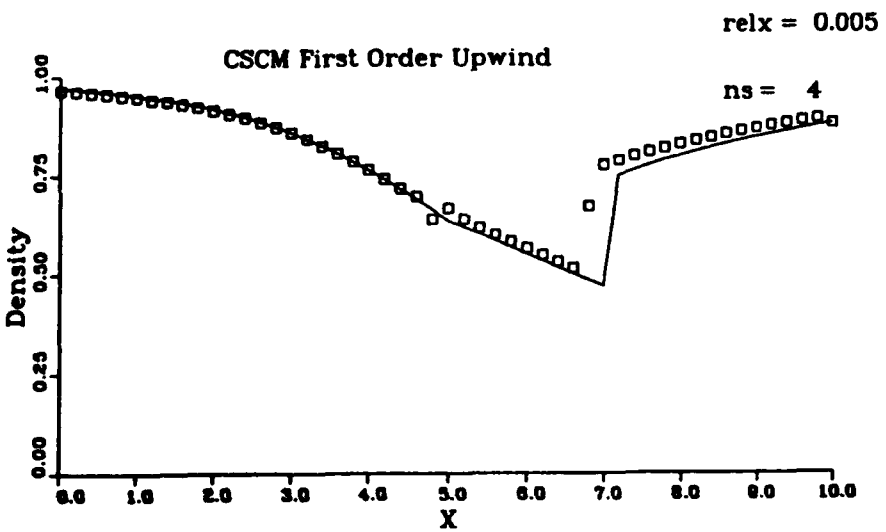

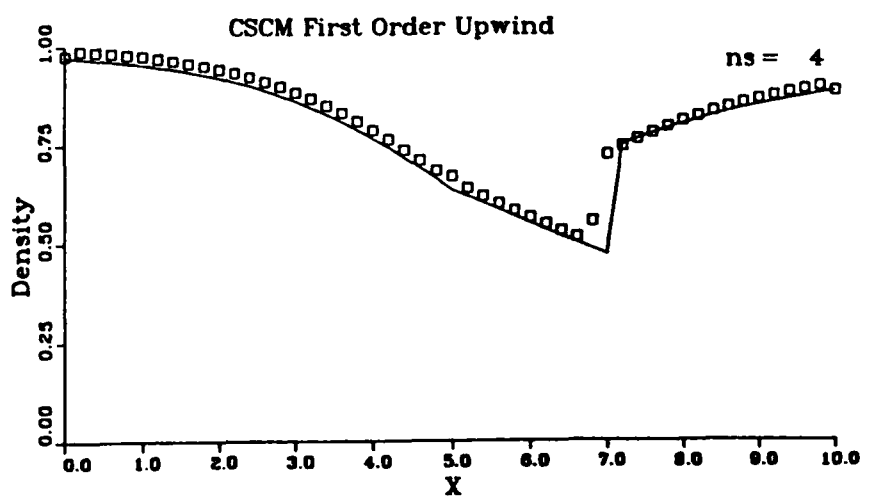

Figure 6. continued

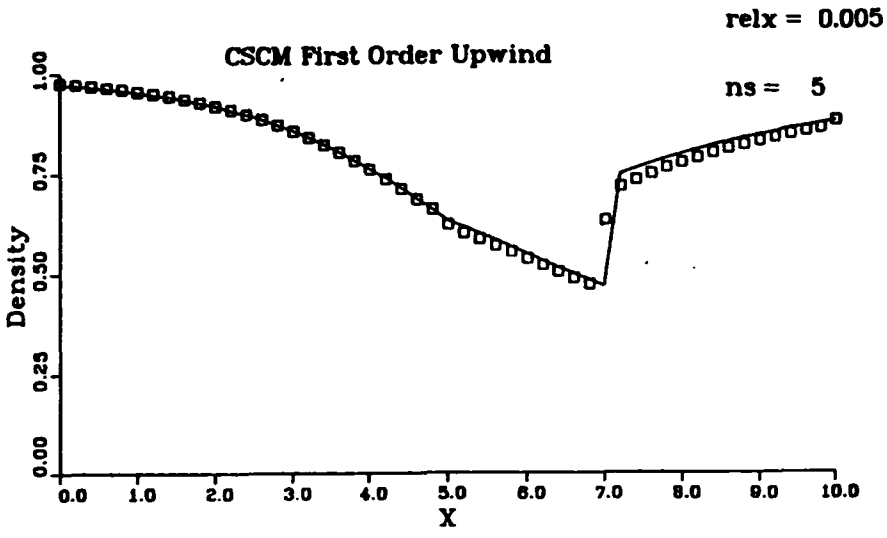

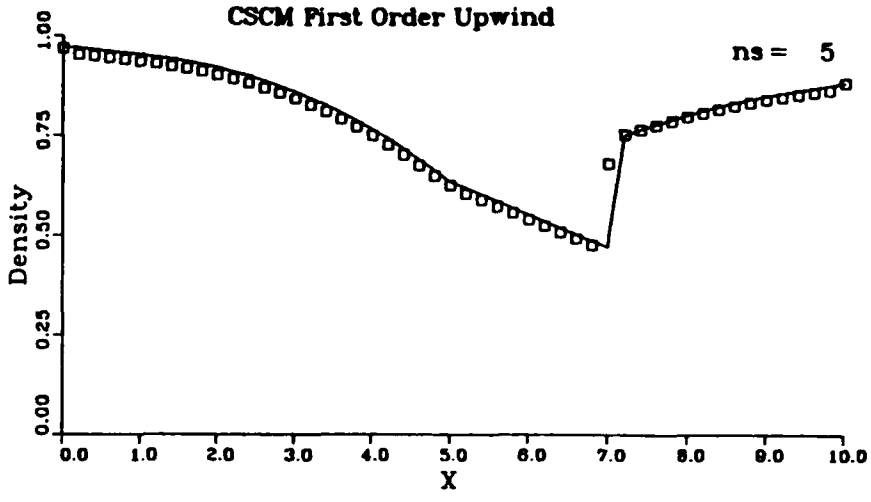

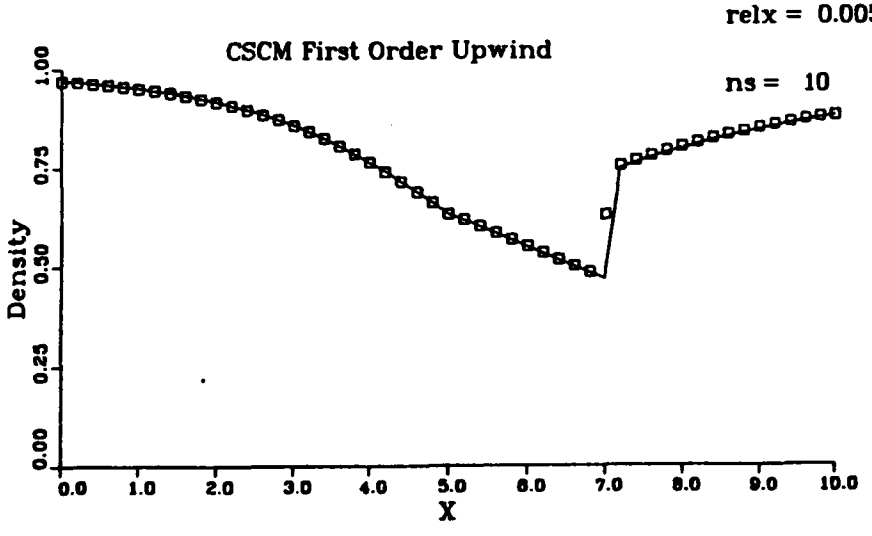

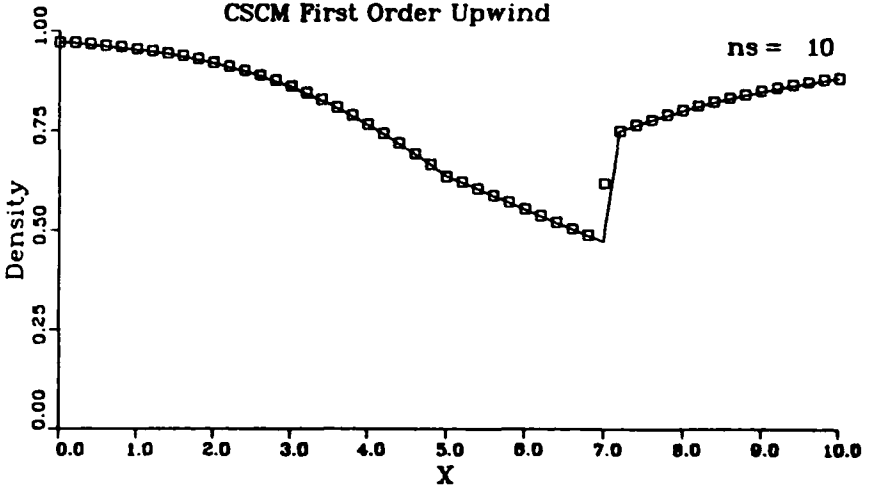

Figure 6. continued

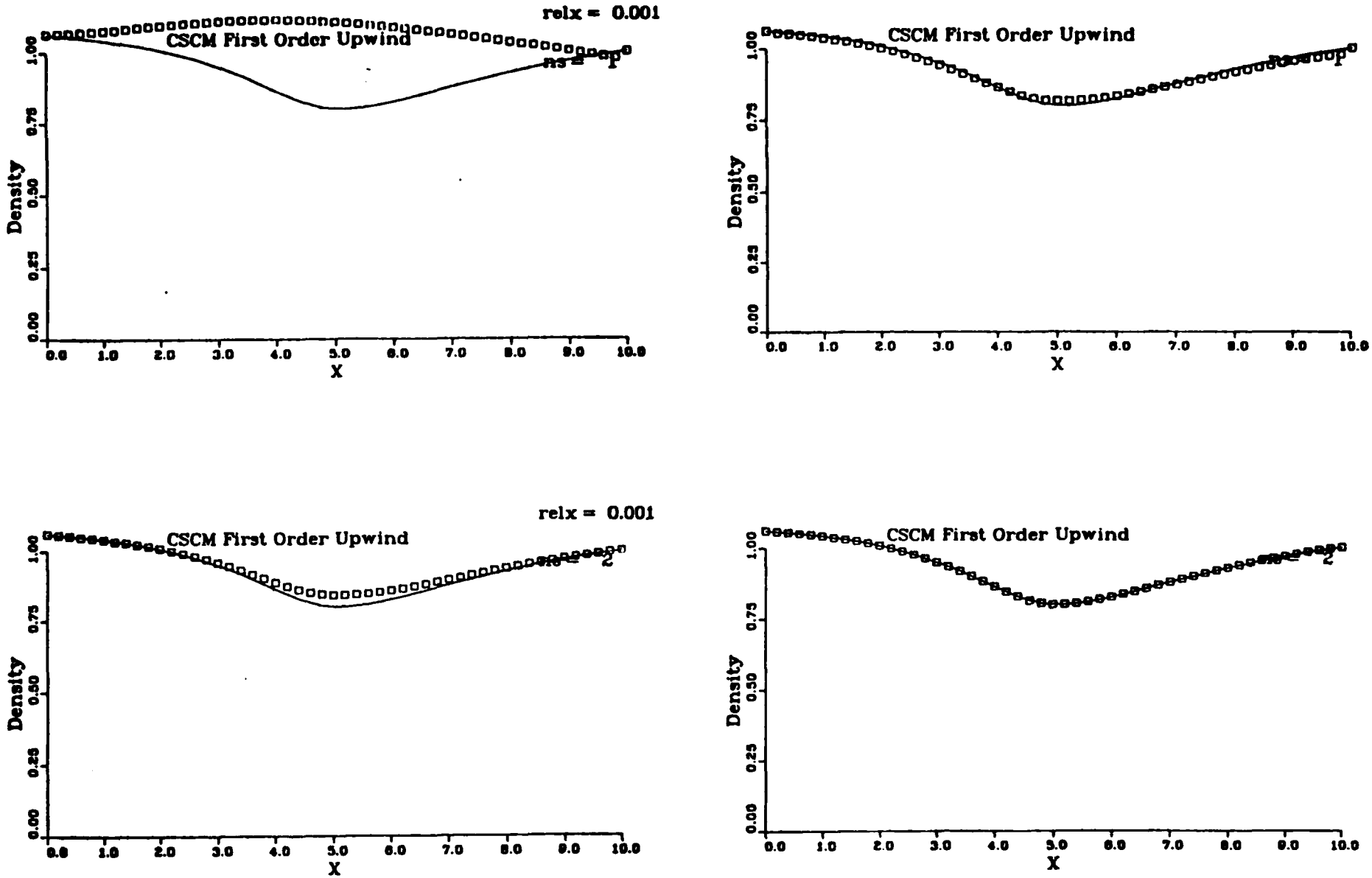

Figure 7. Subcritical solution to Blottner's converging-diverging nozzle developed with alternating sweeps in two global iteration steps. square - computed results , line - exact solution

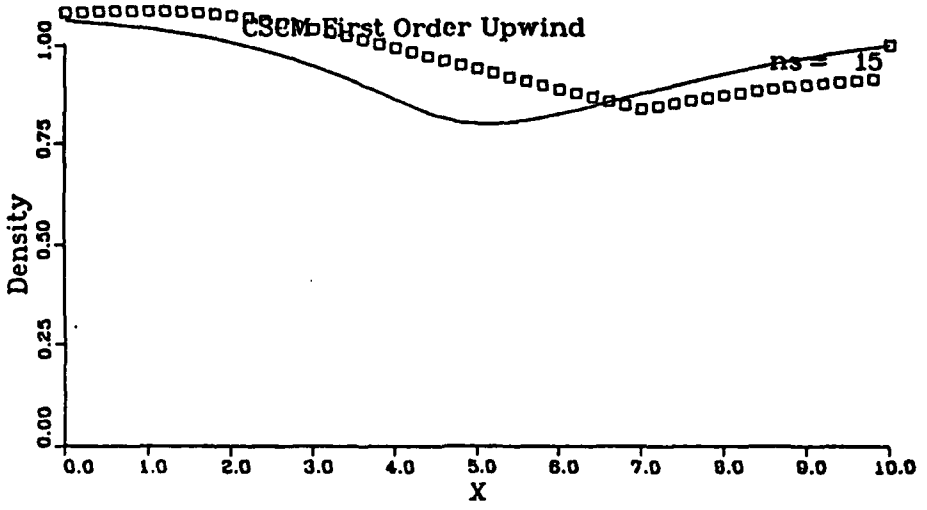

Figure 8. Solution to subcritical nozzle problem after 15 global iterations with forward marching sweeps only.

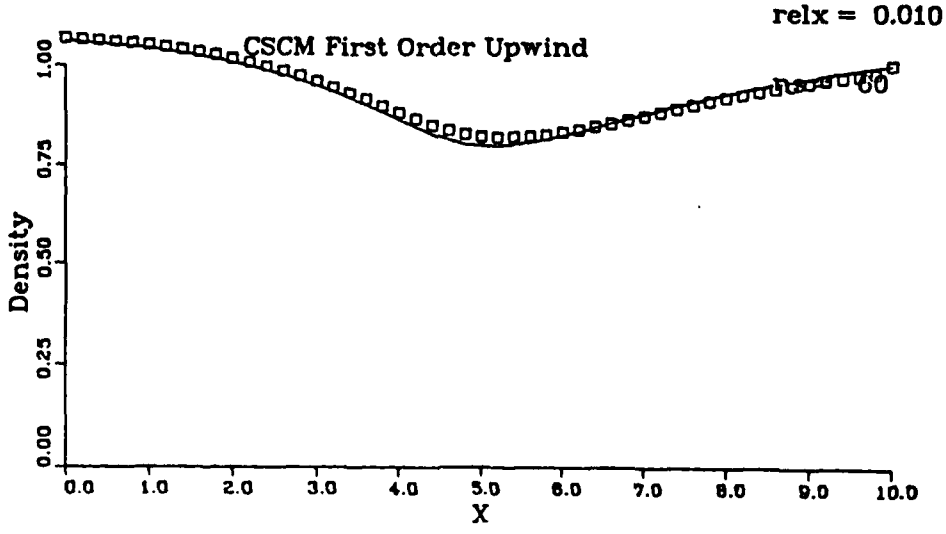

Figure 9. Solution to subcritical nozzle problem after 60 global iterations with forward marching sweeps only.

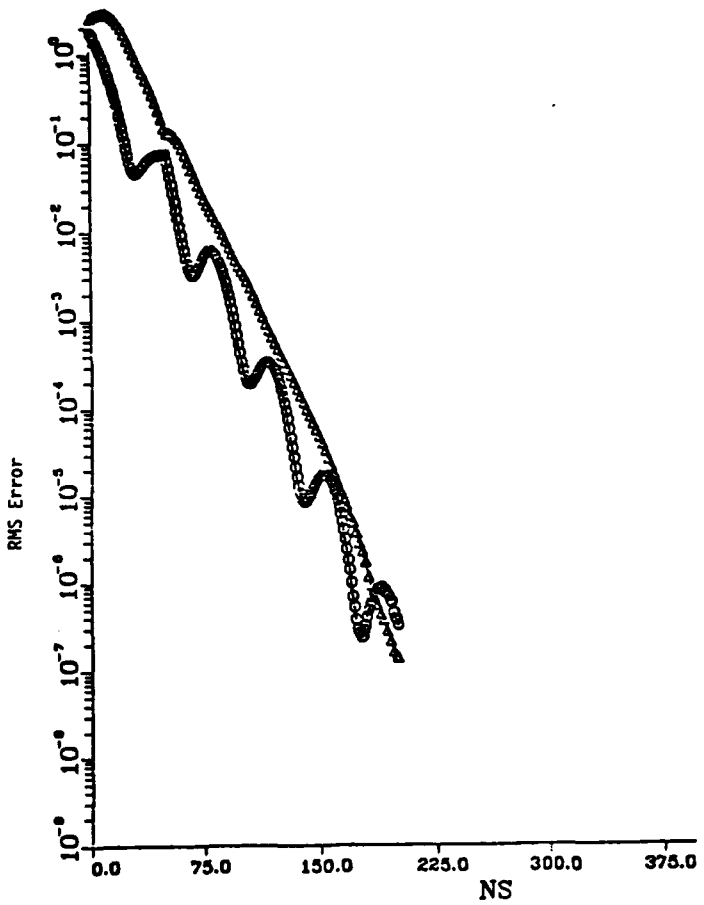

Figure 10. Convergence history of RMS error based on the exact steady solution for the subcritical nozzle flow solved with forward sweeps only.

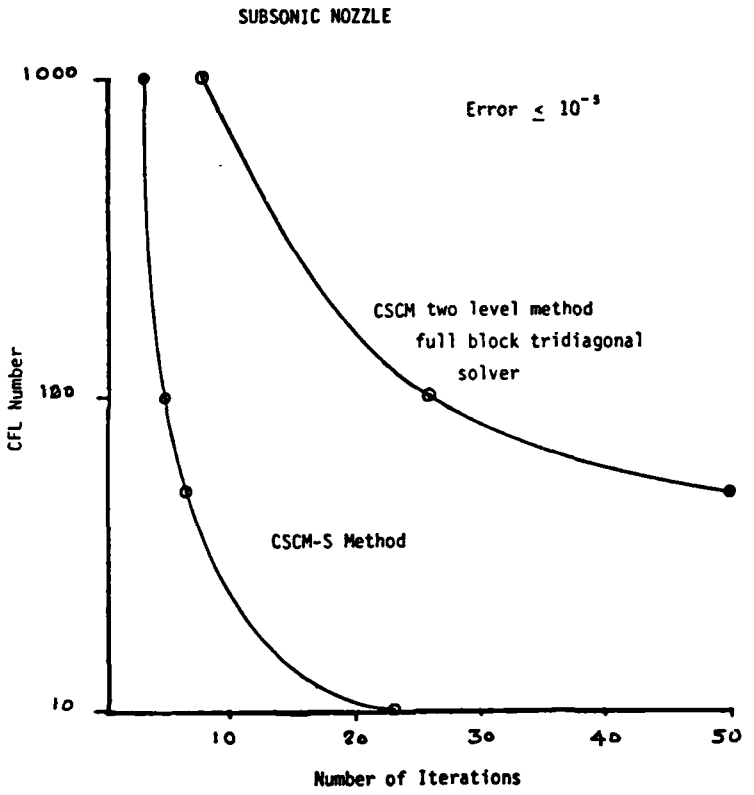

Figure 11. Convergence history comparison between the full block tridiagonal CSCM Solver and the CSCM-S method. The solutions have reached an RMS error less than 1×10^{-5}.

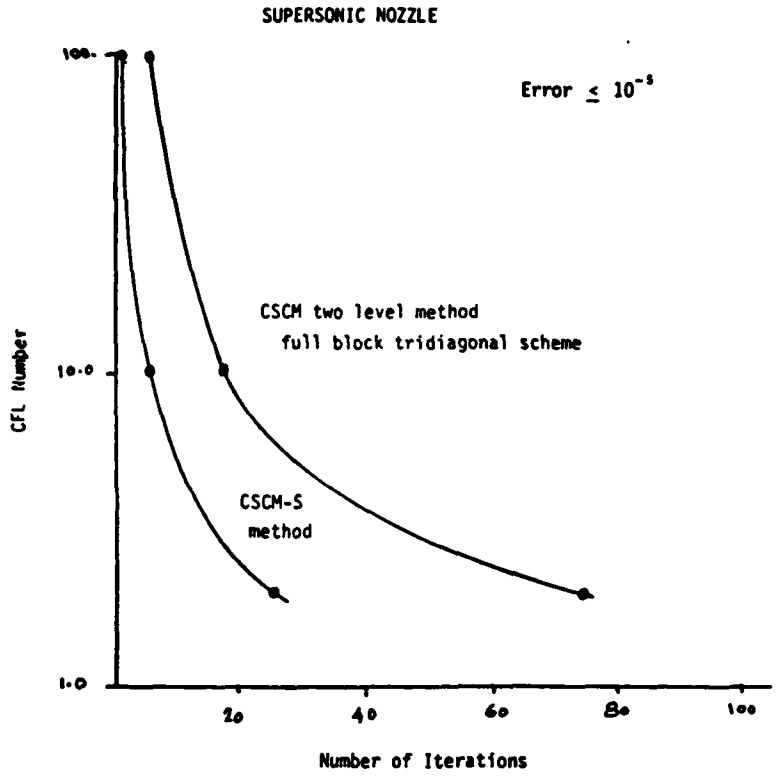

Figure 12. Convergence history comparison between the full block tridiagonal CSCM Solver and the CSCM-S method. The solutions have reached an RMS error less than 1×10^{-5}.

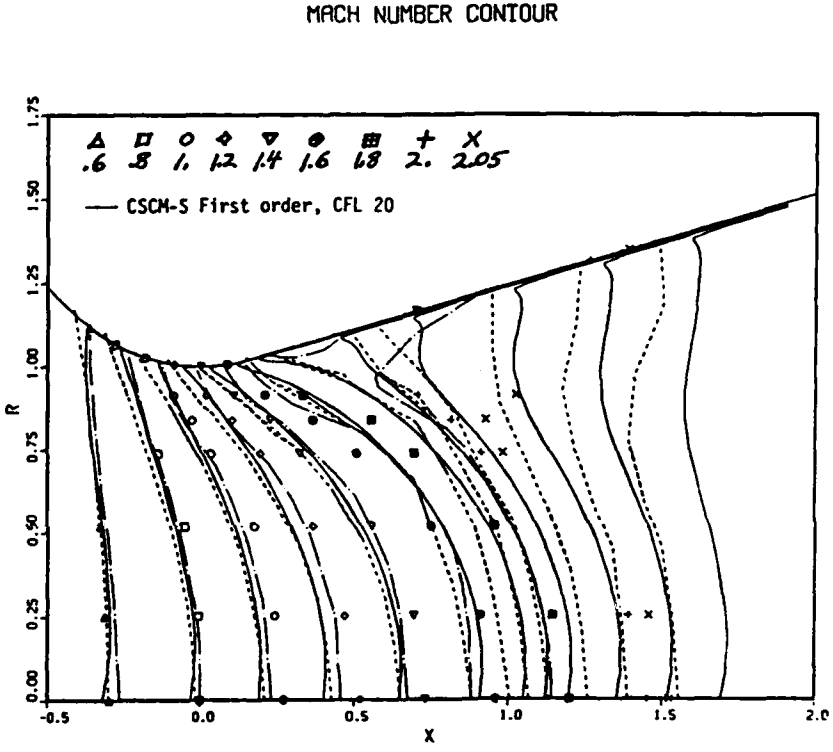

Figure 13. Mach number contours in vicinity of the throat for the axisymmetric transonic nozzle problem solved in ten global iterations. Other computed results of Cline (dashed line) and Prozan (chain dot) and experiment of Cuffel, et al (symbols) are discussed in reference 21.

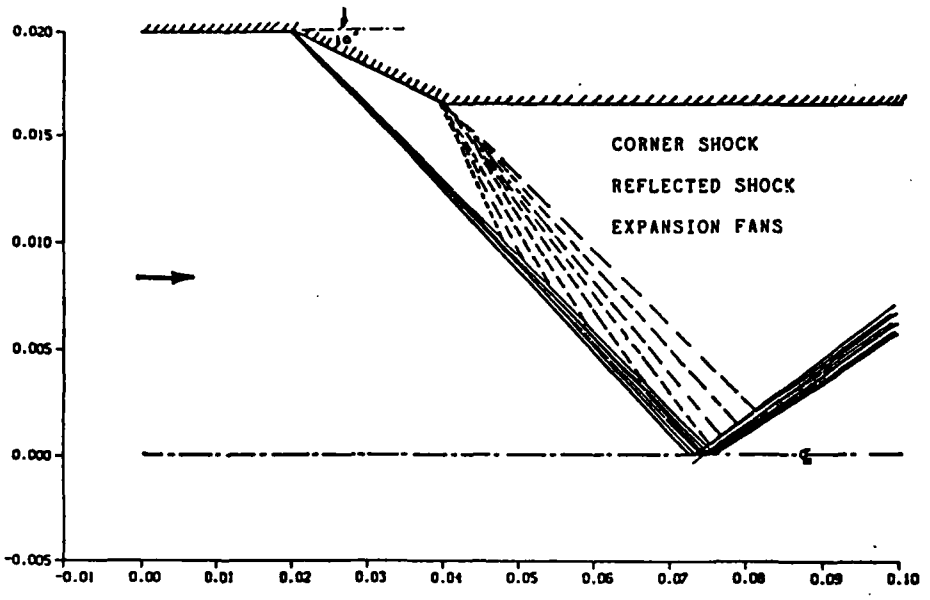

Figure 14. Schematics of the supersonic inlet flow problem.

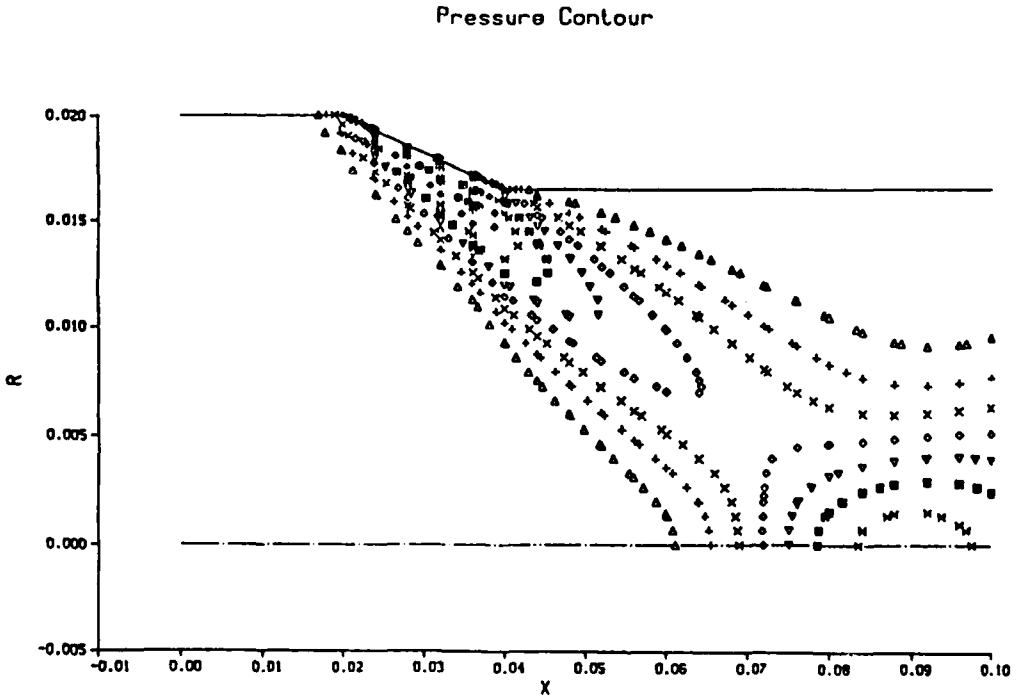

Figure 15. Pressure contours from the first order inviscid solution for the inlet problem after 10 forward sweeps with a 26 x 26 unstretched grid.

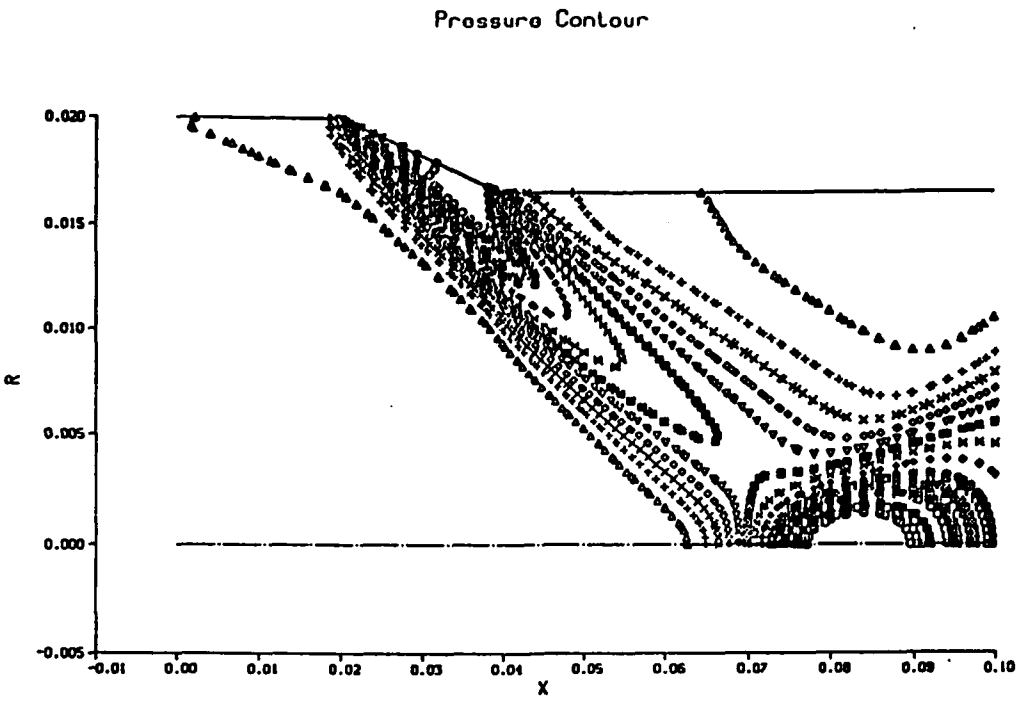

Figure 16. Pressure contours from the first order viscous solution for the inlet after 20 global sweeps with a 51 x 51 stretched mesh. Note the leading edge shock.

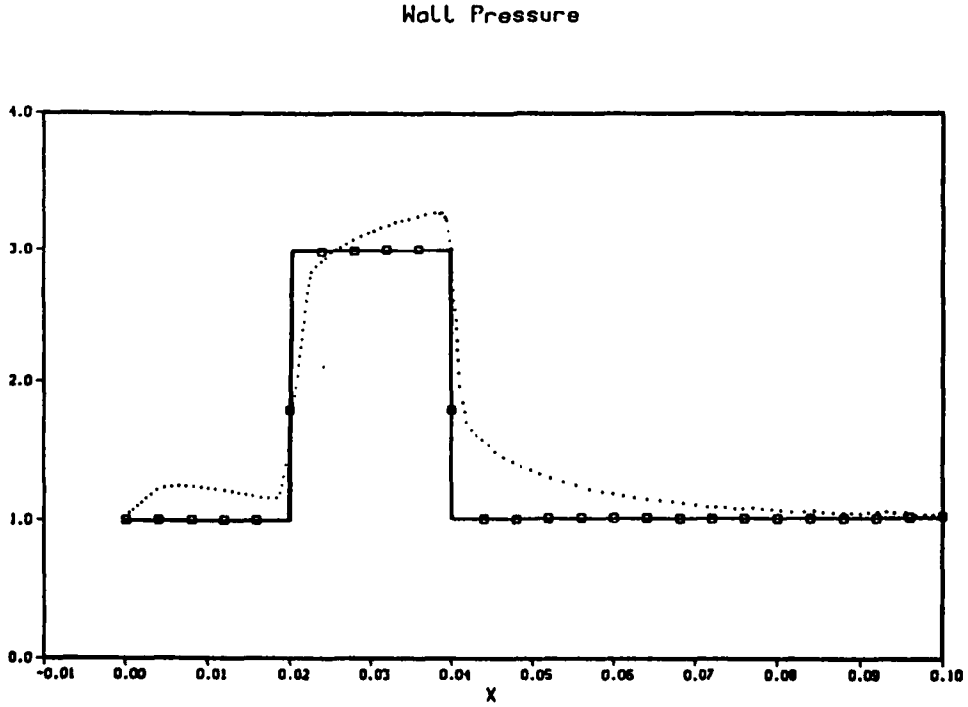

Figure 17. Wall pressure comparison. Line - exact inviscid solution, square - first order inviscid solution, dot - first order viscous solution.

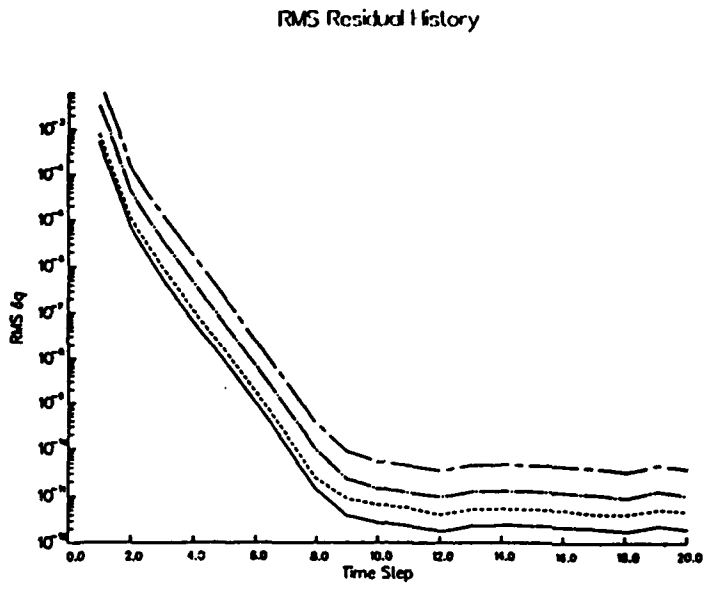

Figure 18. Convergence history of the RMS of the residuals for the inviscid first order inlet problem with 4 inner iterations per global sweep. Note at the end of the first sweep the residual has reduced and the solution has converged for all practical purposes.

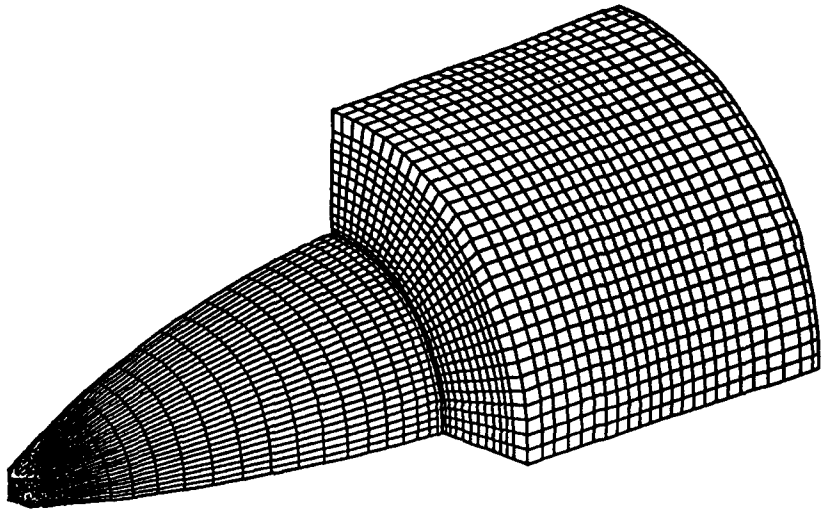

Figure 19. Perspective view of the wall surface mesh for the quarter sector computational domain of an RL-10 rocket nozzle exhausting over a backward step into a cylindrical shroud.

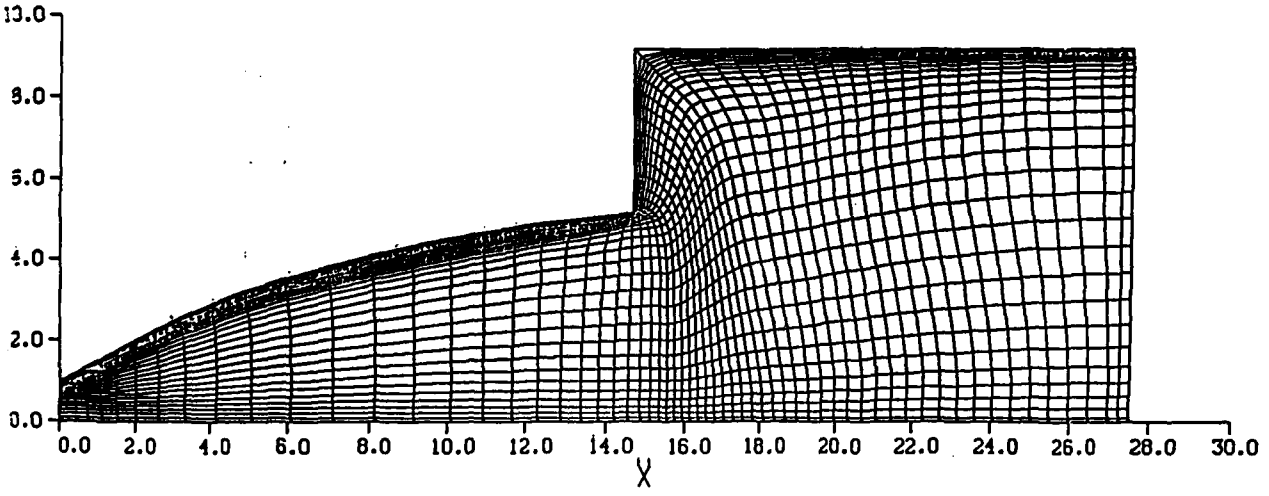

Figure 20. Longitudinal mesh plane for the problem of Figure 19.

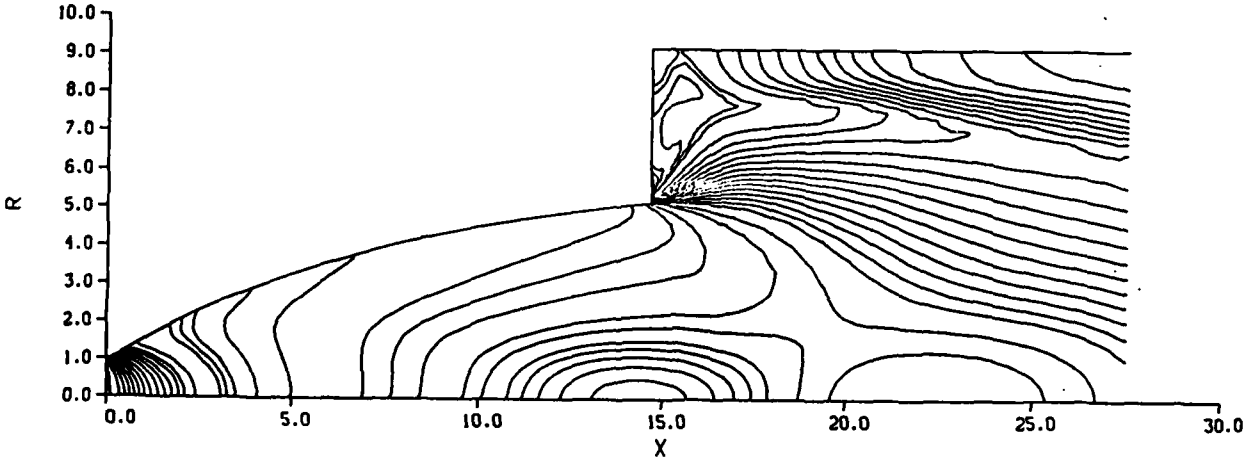

Figure 21. Pressure contour plot for the mesh plane of Figure 20.

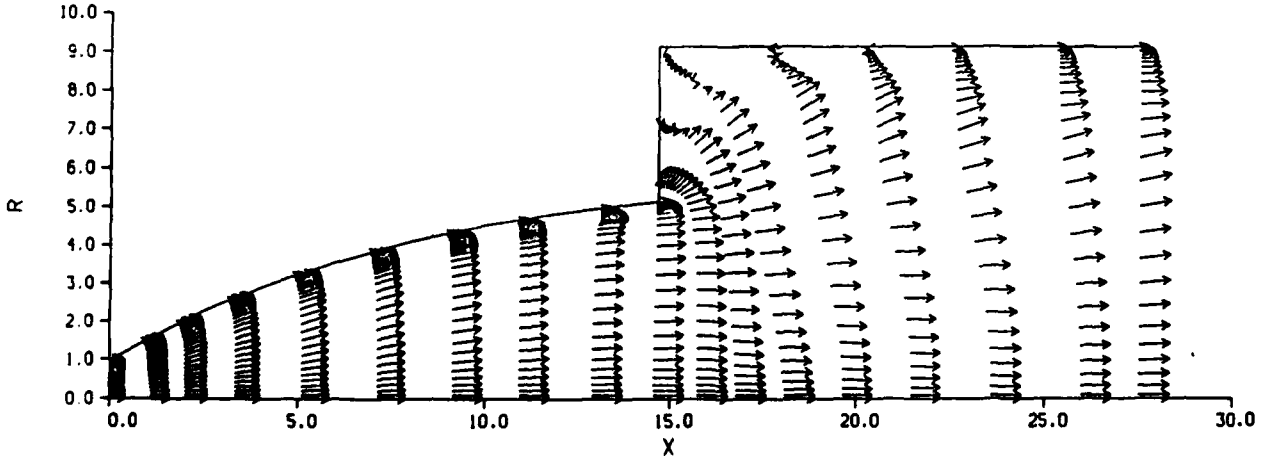

Figure 22. Velocity vector plot for the mesh plane of Figure 20.

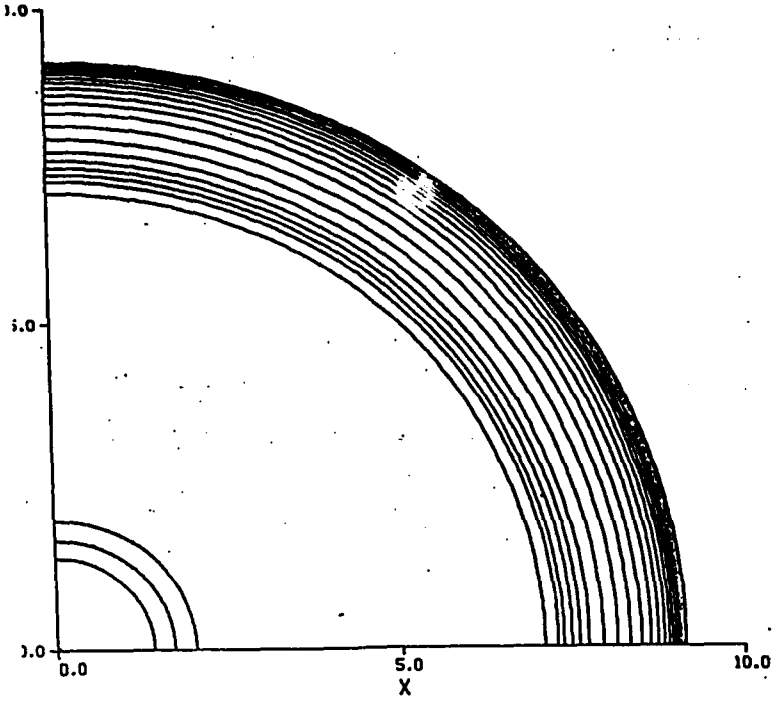

Figure 23. Mach contour plot for a cross flow mesh plane in the shroud.

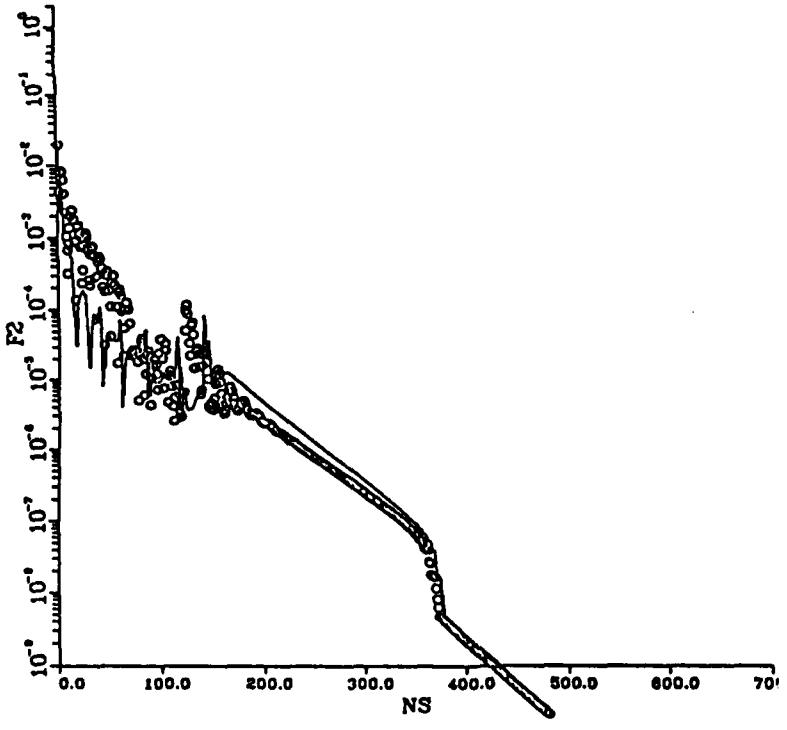

Figure 24. Test on three patches of implicit stability and rate of convergence of (circles) computed boundary point operator differencing to frozen data in adjacent patches; (solid line) effectively continuous grid method.

Figure 25. Boundary condition interpolation procedures. Solution points O , interpolation points X , interpolant data points □ .

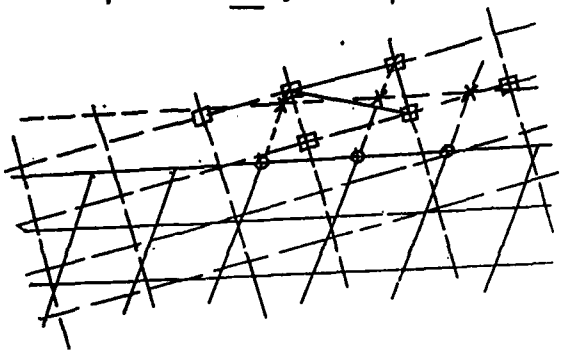

25a. Triangle interpolation for overset mesh.

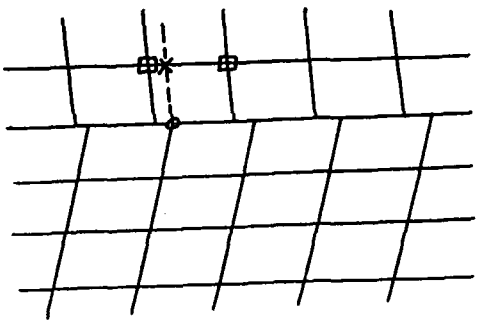

25b. Line interpolation for composite mesh.

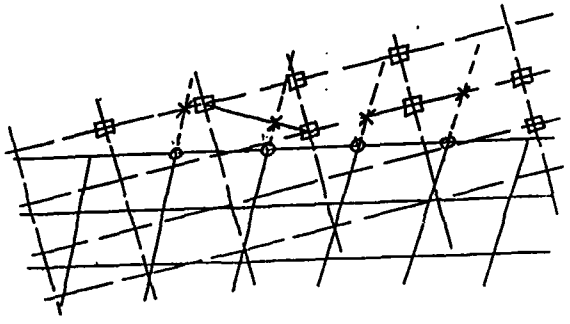

25c. Line interpolation for overset mesh. Straight line extrapolation.

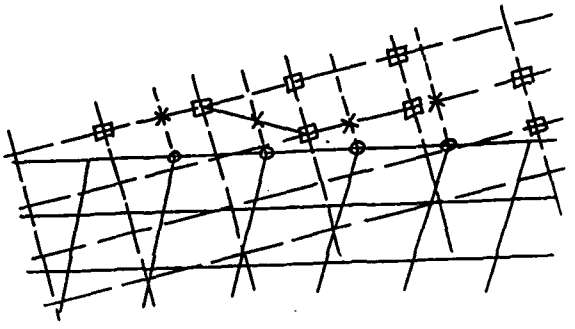

25d. Line interpolation for overset mesh. Extrapolated lines turned in composite mesh analog.

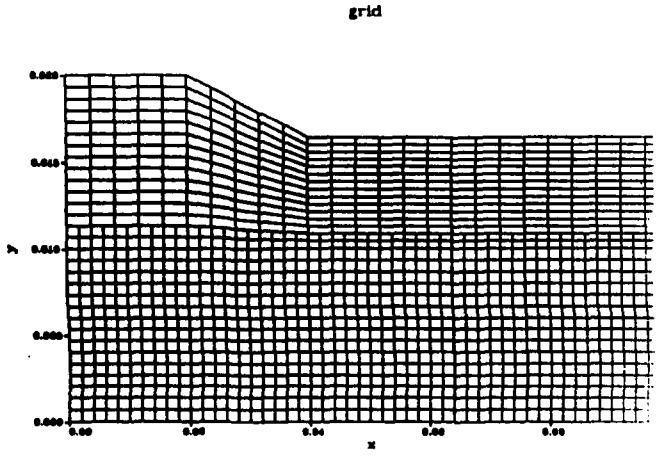

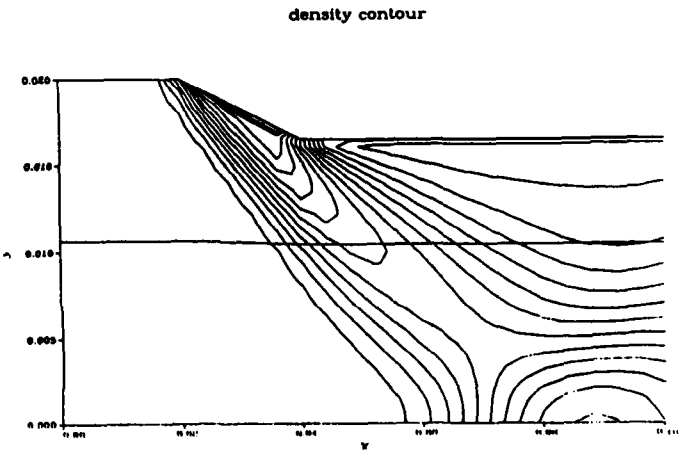

Figure 26. Test of stability of implicit numerical procedure exchanging frozen boundary point data between patched grids.

26a. Two patch computational mesh, line interpolation.

26b. Density contours for mesh 26a.

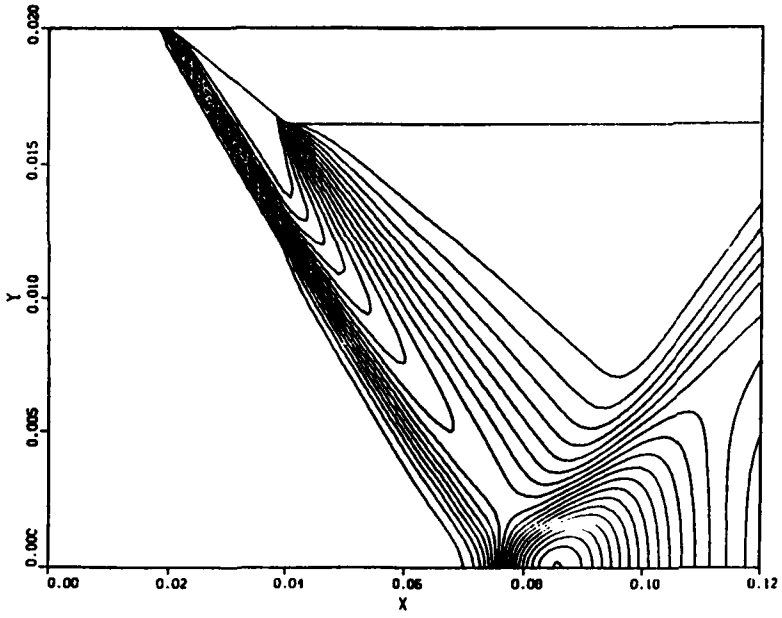

Figure 27. Pressure contours computed on 101 x 101 point uniform mesh.

27a. First order.

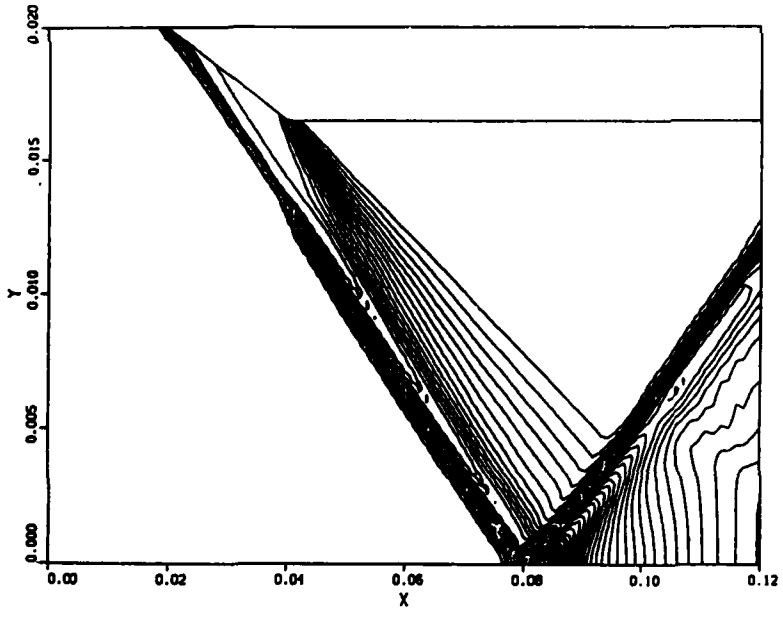

27b. Second order.

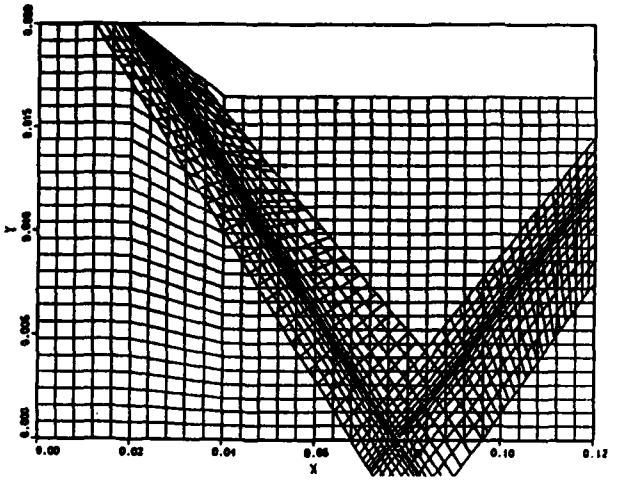

Figure 28a. Shock aligned patched grids for the inlet problem.

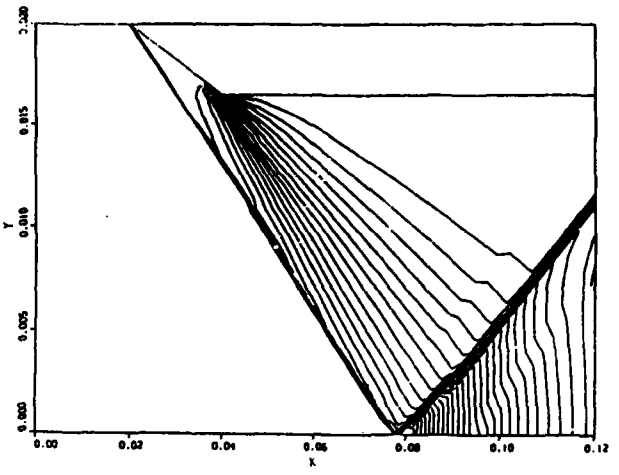

Figure 28b. Pressure contours from first order solution on patched grid.

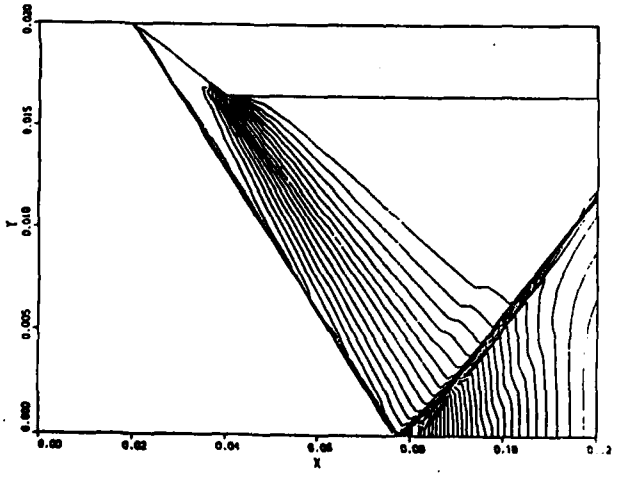

Figure 28c. Pressure contours from second order solution on patched grid.

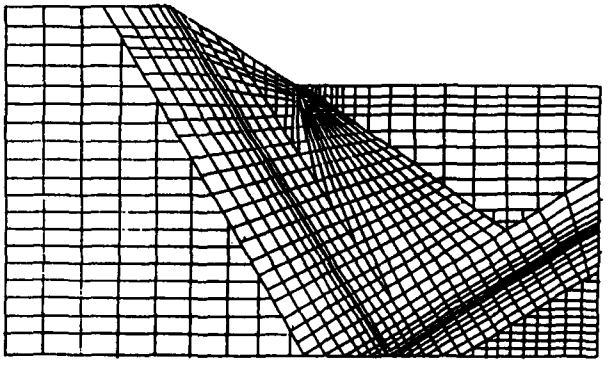

Figure 28d. Sketch of patched adaptive mesh topology concluded from present results to be effective for capture of flow structure of the inlet problem.

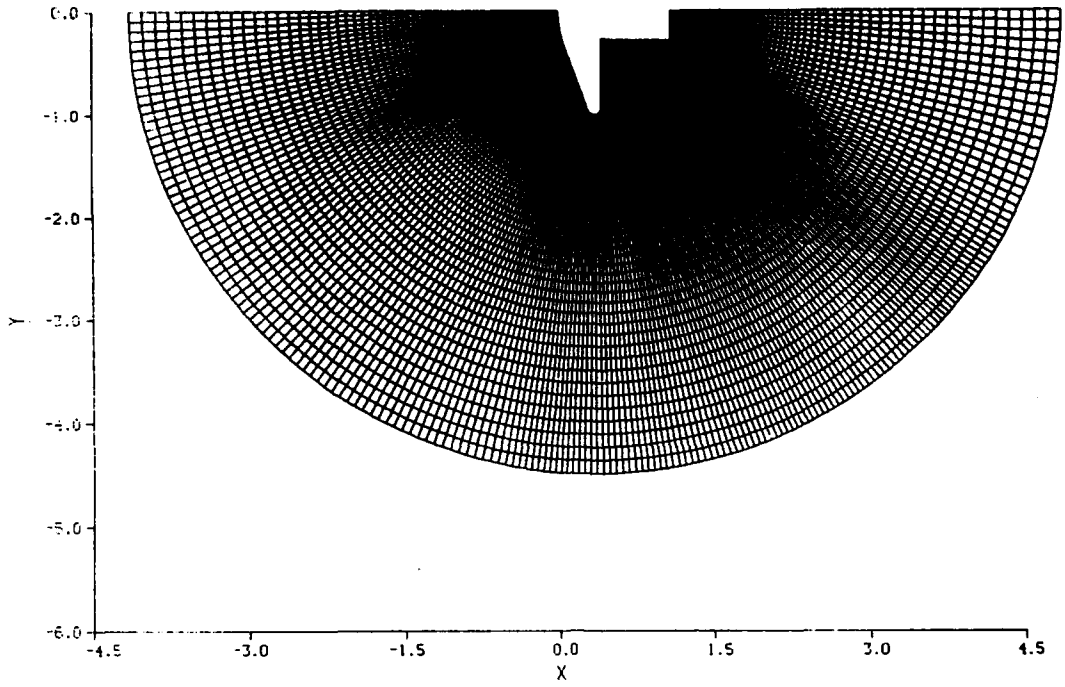

Figure 29. Computational mesh for NASA-Ames model drag brake AOTV.

Figure 30. Contour plots for unsteady shock diffraction solutions around the model AOTV.

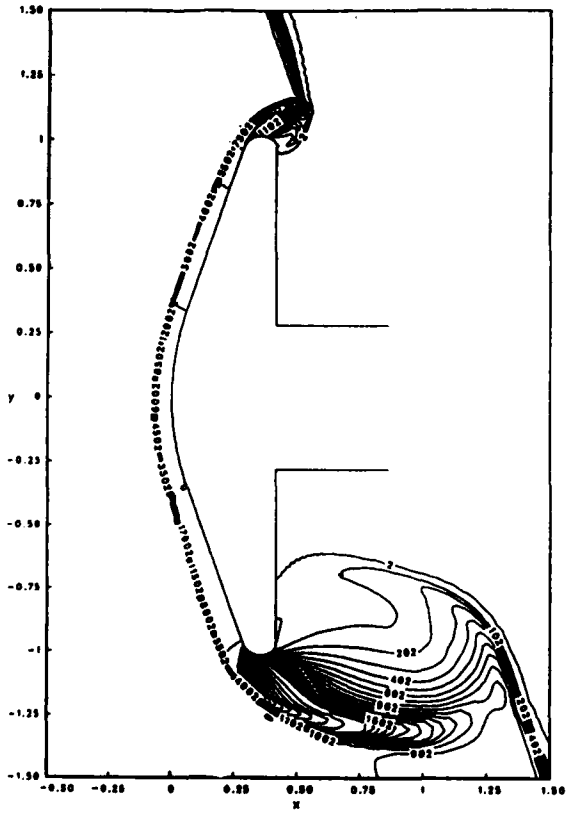

a. Pressure

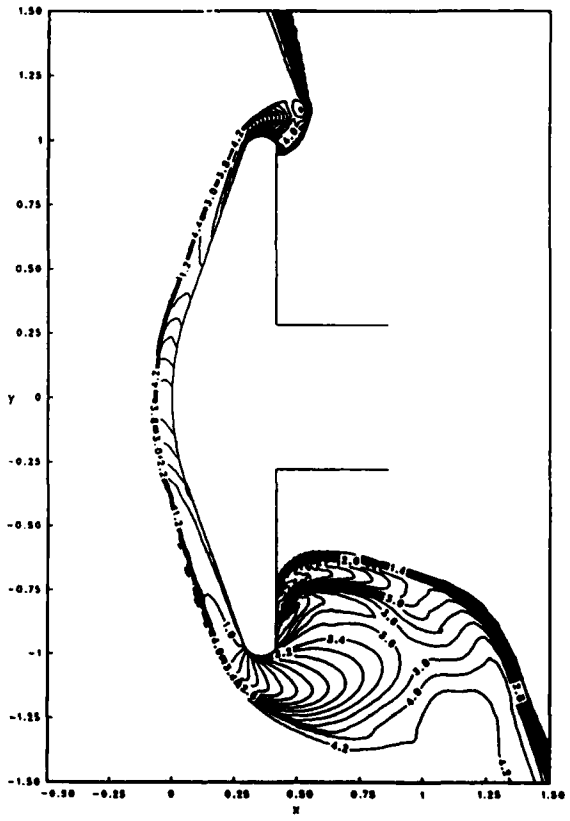

b. Mach

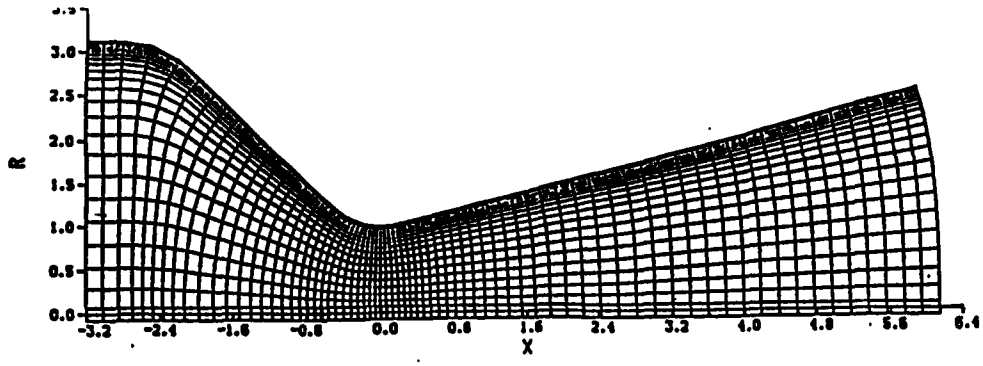

Figure 31. Computational mesh for the Cuffel-Back 45° - 15° transonic nozzle

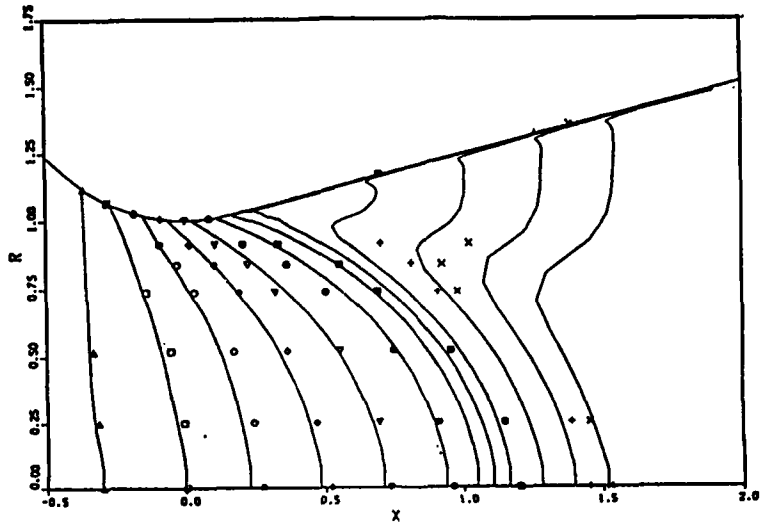

Figure 32a Mach contours in vicinity of throat for unlimited second order upwind method.

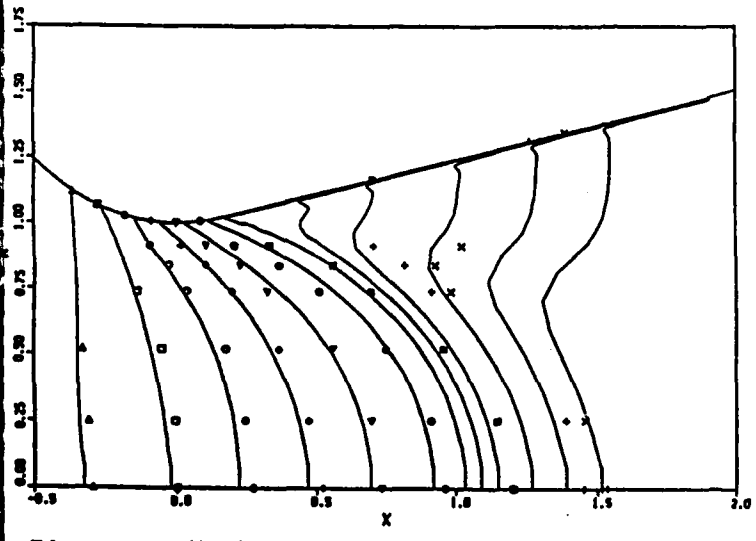

Figure 32b Mach contours for Fromm's scheme with adapted Chakravarthy-Osher limiter, Scheme IIIa.

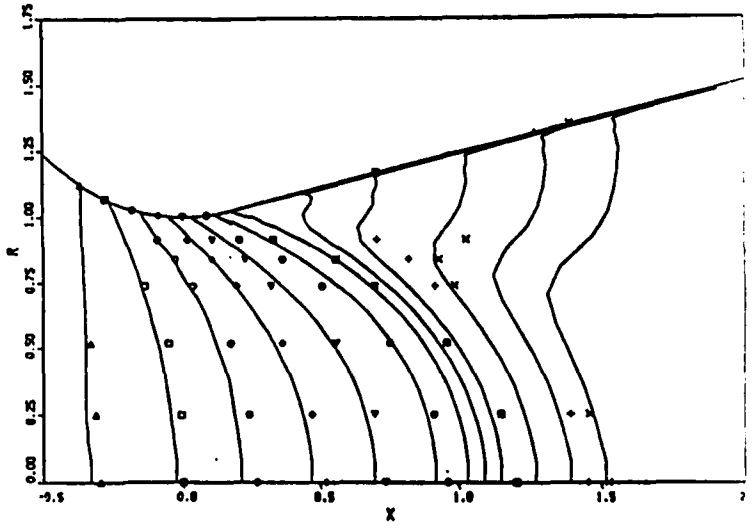

Figure 32c Mach contours for Fromm's scheme with limiter in split partial flux differences, Scheme IIIb.

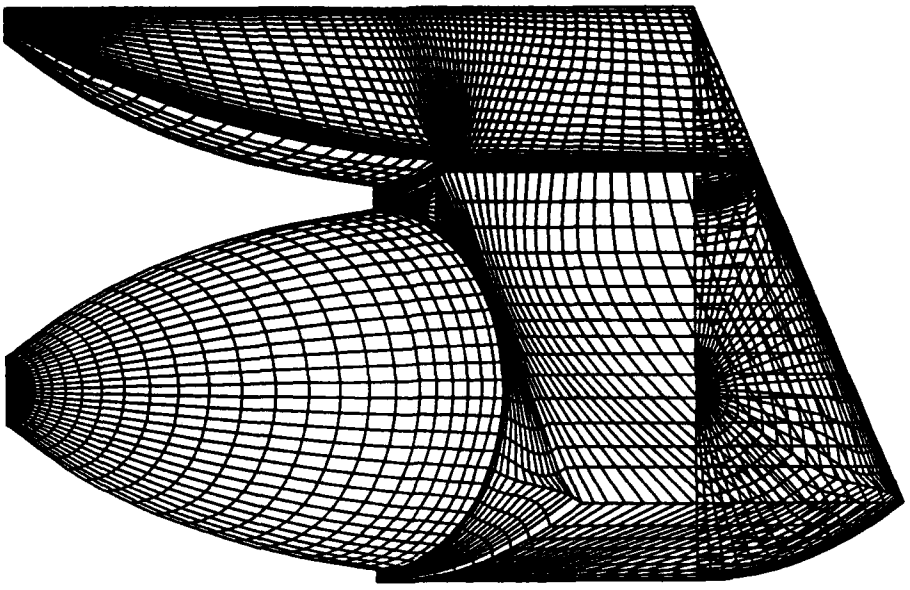

Figure 33a. Perspective view of 3-D surface mesh for the computational domain of the multiple nozzle jet exhaust problem.

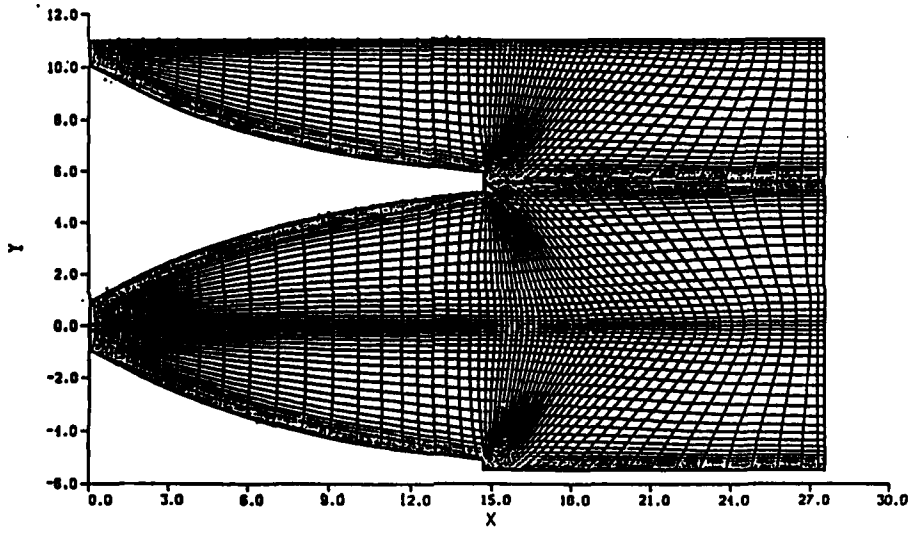

Figure 33b. Computational mesh in the symmetry plane through the center and outer engines.

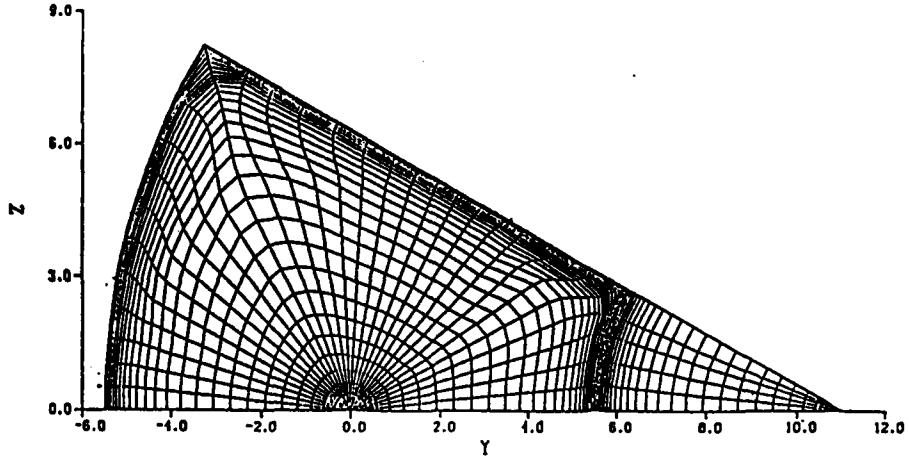

Figure 33c. Computational mesh projected onto a cross flow plane in the shroud.

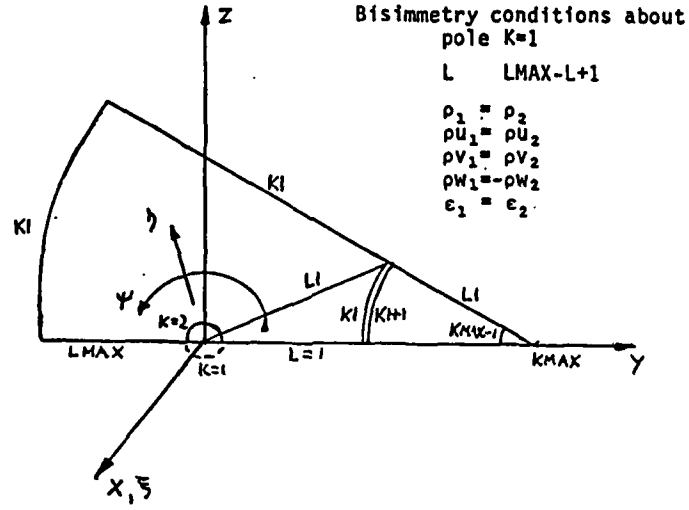

Figure 34. Segmented composite mesh coordinate topology.

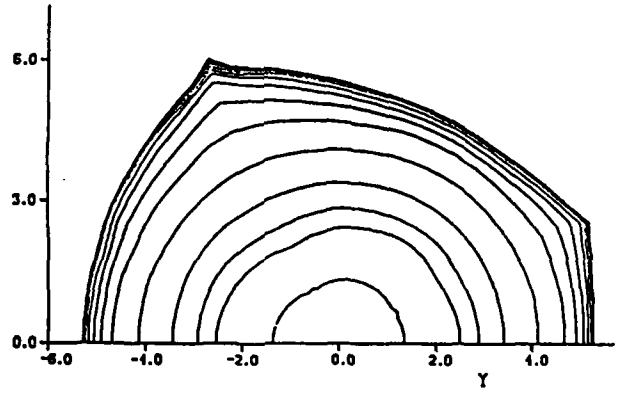

Figure 35. Mach contours on a crossflow coordinate surface intersecting the backward facing step outside the outboard engine nozzle.

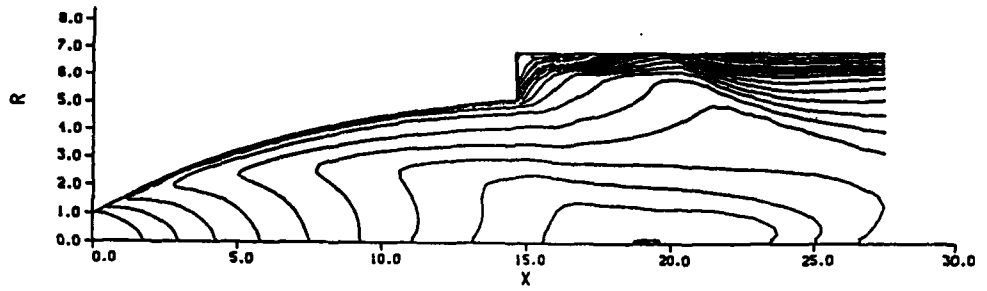

Figure 36a. Mach contour plots in the (outboard engine) azimuthal coordinate plane intersecting the L1 corner (Figure 34).

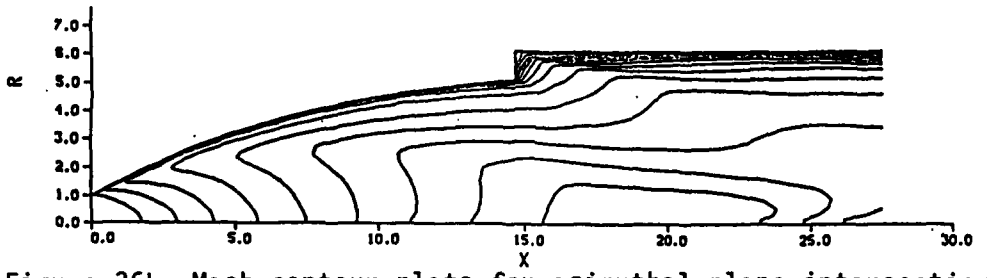

Figure 36b. Mach contour plots for azimuthal plane intersecting the small step at the upper symmetry plane.

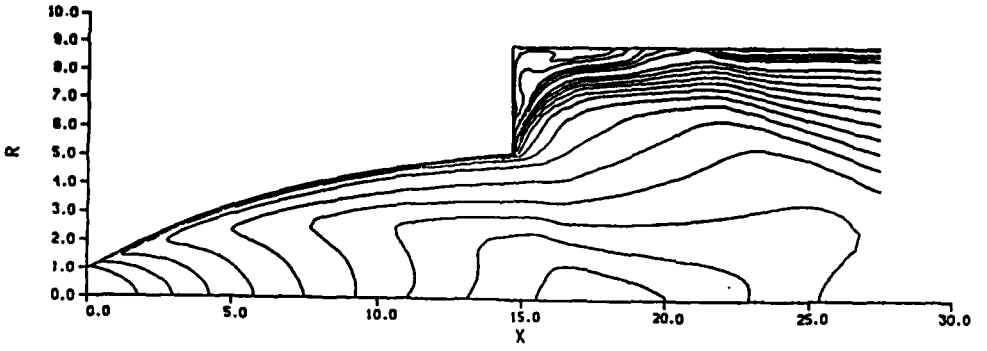

Figure 36c. Mach contour plots for azimuthal plane intersecting the maximum backward facing step at the intersection of the shroud wall and the upper symmetry plane.

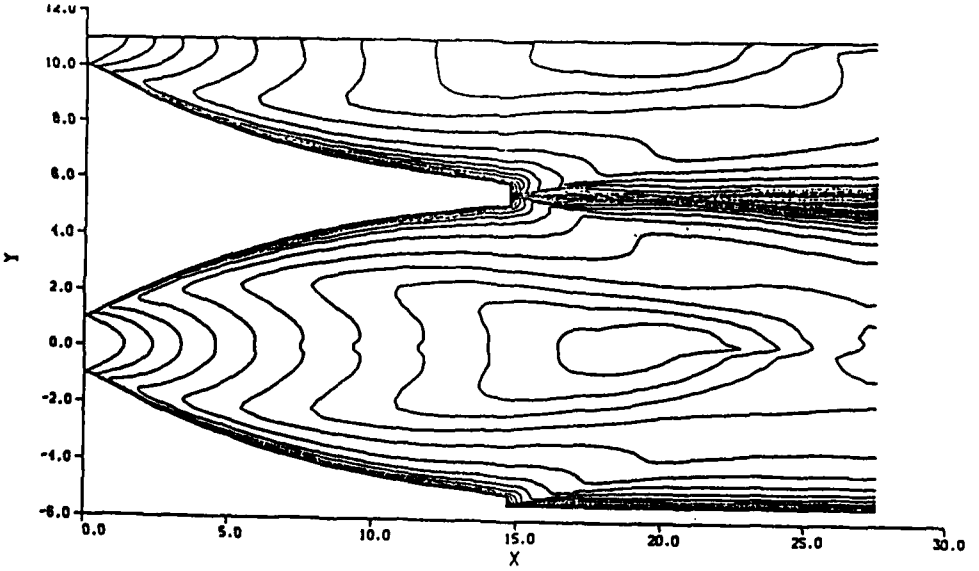

Figure 36d. Mach contour plot in the symmetry plane through the inner and outer nozzle centers.

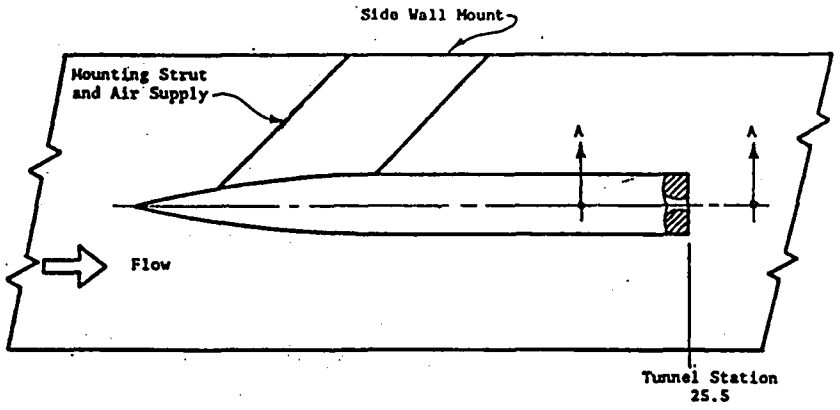

Figure 37. Micom tactical missile model.

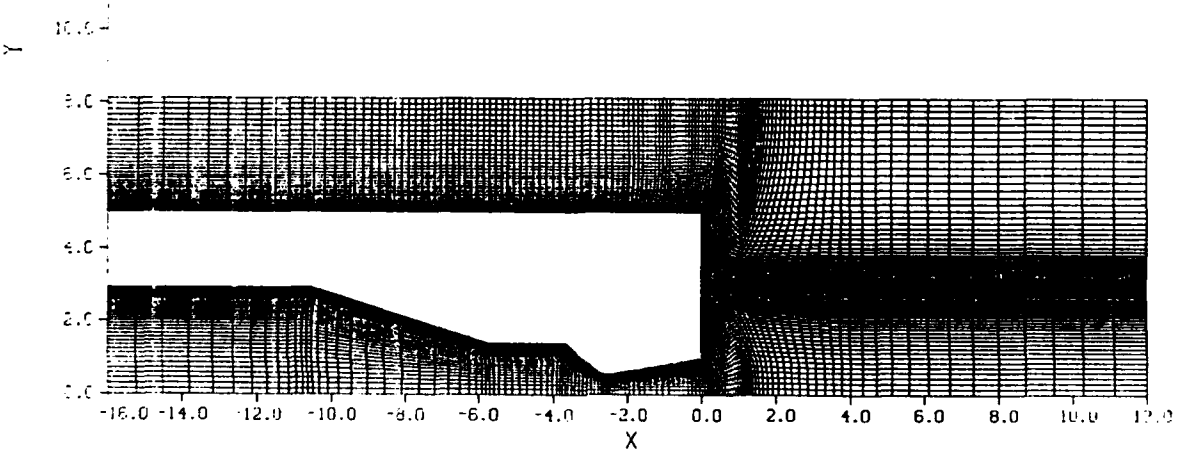

Figure 38a. Double wrap-around mesh for inner and outer flows.

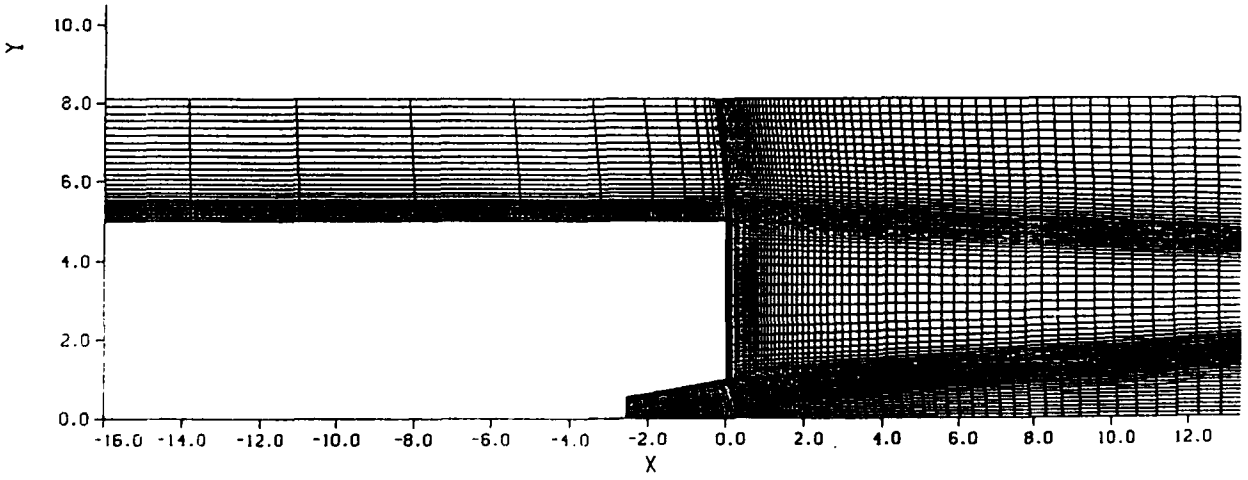

Figure 38b. Segmented composite step mesh.

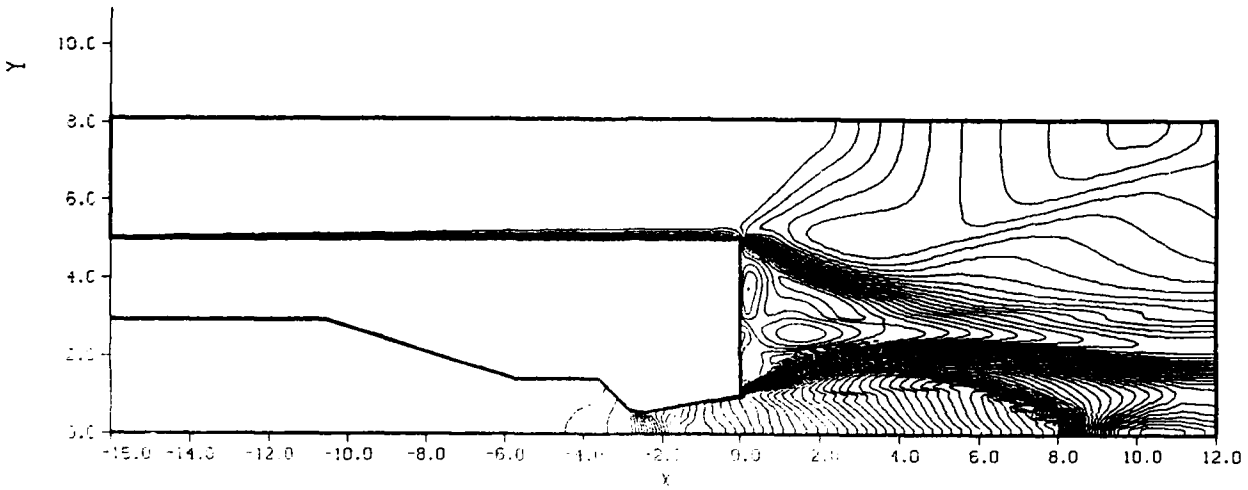

Figure 39a. Mach contour plot for the double wrap-around grid.

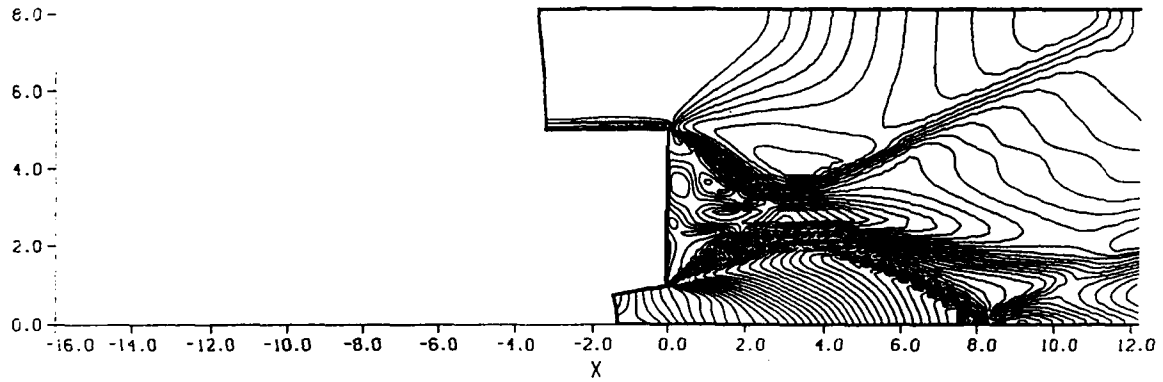

Figure 39b. Mach contour plot for the step mesh.

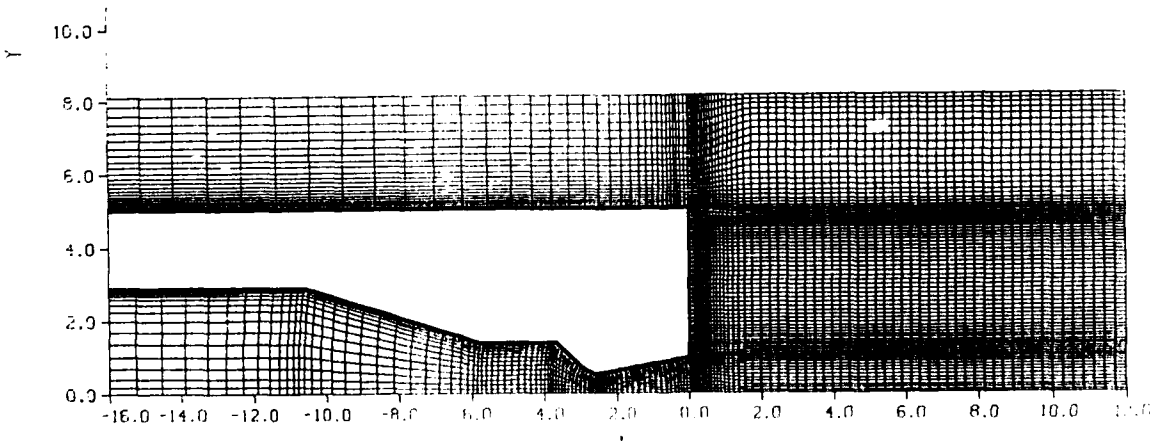

Figure 40a. Hybrid wraparound and composite step grid with overlapping blocks.

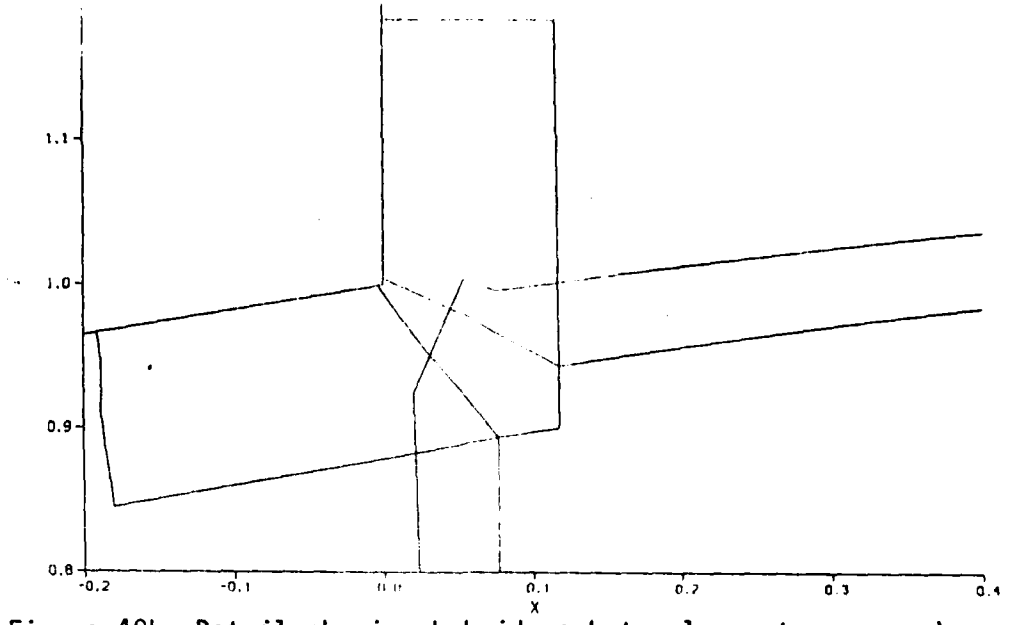

Figure 40b. Detail showing hybrid mesh topology at corner where an overset wraparound patch provides continuity of the viscous boundary layer communication to the base region.

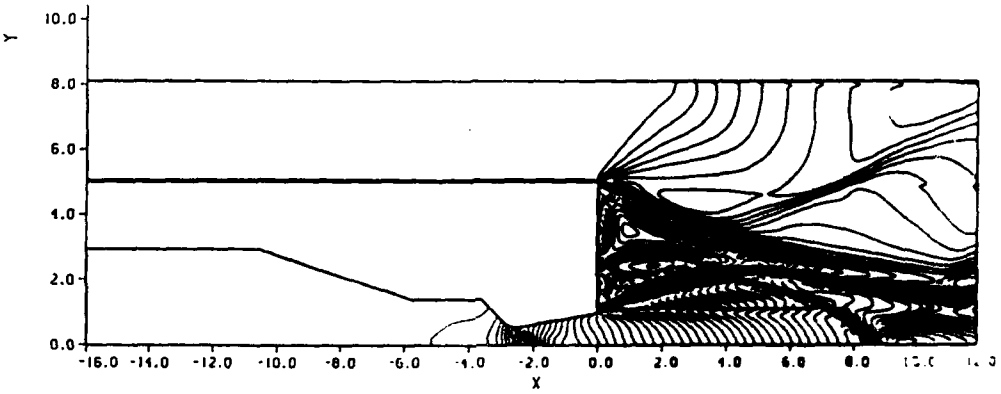

Figure 41. Mach contour plot for the solution on the hybrid mesh.

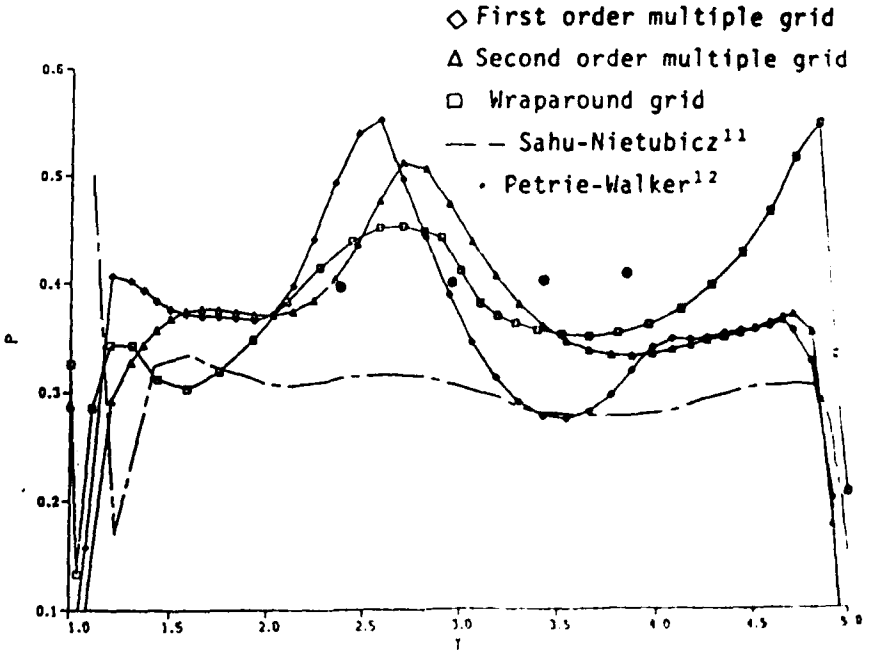

Figure 42. Comparison of experimental measurements and computed base pressure distributions for the micom tactical missile model.

END

7-87

DTIC